INFORMATION TO USERS

The most advanced technology has been used to photograph and reproduce this manuscript from the microfilm master. UMI films the original text directly from the copy submitted. Thus, some dissertation copies are in typewriter face, while others may be from a computer printer.

In the unlikely event that the author did not send UMI a complete manuscript and there are missing pages, these will be noted. Also, if unauthorized copyrighted material had to be removed, a note will indicate the deletion.

Oversize materials (e.g., maps, drawings, charts) are reproduced by sectioning the original, beginning at the upper left-hand corner and continuing from left to right in equal sections with small overlaps. Each oversize page is available as one exposure on a standard 35 mm slide or as a 17″ × 23″ black and white photographic print for an additional charge.

Photographs included in the original manuscript have been reproduced xerographically in this copy. 35 mm slides or 6″ × 9″ black and white photographic prints are available for any photographs or illustrations appearing in this copy for an additional charge. Contact UMI directly to order.

Accessing the World's Information since 1938

300 North Zeeb Road, Ann Arbor, MI 48106-1346 USA

Order Number 8821084

A study of isosinglet meson resonances with $J^{PC} = 0^{++}$, 2^{++}, and 4^{++} below 2 Gev

Goo, Jamyeung A., Ph.D.

City University of New York, 1988

U·M·I
300 N. Zeeb Rd.
Ann Arbor, MI 48106

PLEASE NOTE:

In all cases this material has been filmed in the best possible way from the available copy. Problems encountered with this document have been identified here with a check mark __✓__.

1. Glossy photographs or pages _____
2. Colored illustrations, paper or print _____
3. Photographs with dark background _____
4. Illustrations are poor copy __✓__
5. Pages with black marks, not original copy __✓__
6. Print shows through as there is text on both sides of page _____
7. Indistinct, broken or small print on several pages __✓__
8. Print exceeds margin requirements __✓__
9. Tightly bound copy with print lost in spine _____
10. Computer printout pages with indistinct print _____
11. Page(s) _____ lacking when material received, and not available from school or author.
12. Page(s) _____ seem to be missing in numbering only as text follows.
13. Two pages numbered _____. Text follows.
14. Curling and wrinkled pages _____
15. Dissertation contains pages with print at a slant, filmed as received __✓__
16. Other _____

_____

_____

A Study of Isosinglet Meson Resonances With $J^{PC}=0^{++}$, 2^{++}, and 4^{++} Below 2 Gev

by

Jamy Goo

A dissertation submitted to the Graduate Faculty in Physics in partial fulfillment of the requirements for the degree of Doctor of Philosophy, The City University of New York.

1988

This manuscript has been read and accepted for the Graduate Faculty in Physics in satisfaction of the dissertation requirement for the degree of Doctor of Philosophy.

4/27/88
Date

Chair of Examining Commitee

4/29/88
Date

Executive Officer

Prof. N.P. Chang
Prof. Hiram Hart
Prof. Martin Kramer
Prof. Carl Shakin
Supervisory Committee

The City University of New York

Abstract

A Study of Isosinglet Meson Resonances

With $J^{++}=0^{++}$, 2^{++}, and 4^{++} Below 2 Gev

by

Jamy Goo

Adviser: Professor S. J. Lindenbaum

A large number of data sets on meson-meson system became available including those from a high statistics experiment of π exchange production of the $K_S^0 K_S^0$ system in which the author participated. These data on the $\pi\pi$, $K\bar{K}$, $\eta\eta$, and $\eta\eta'$ systems come from fixed-target(hadronic) experiments. These data which have been obtained using the OPE hypothesis, along with other data for $J/\psi \to MM\gamma$ and $pp \to pp\pi^+\pi^-$, are studied in detail. A re-analysis of the $\pi\pi$ data of the type B-solution which is the only consisent solution relating the $\pi^+\pi^-$ and $\pi^0\pi^0$ data sets shows outstanding inconsistencies among the S-wave amplitudes. The average of the $\pi\pi$ data was derived using the adiabatic averaging method. The data

on the $K\bar{K}$ from the hadronic production experiments(with π beam) are consistent. We then perform a coupled-channel analysis based upon the K-matrix formulation of the S matrix to study processes $\pi\pi \rightarrow MM$. The results indicate that a unitary description of the 2^{++} mesons is achieved. In particular the $f_2(1720)$ is not seen in the hadronic channels. The $f_2(1810)$ is established in the hadronic channels. Only preliminary work on the unitary description of the 0^{++} mesons has been done. We require at least seven resonances to roughly understand the scalar meson spectra.

Acknowledgements

The author would like to express his appreciation to Dr. S. J. Lindenbaum and Dr. R. S. Longacre for their support during this research. Special thanks go to several friends with whom the author spent some substancial amount of time discussing the fundamental issues in meson spectroscopy.

This research was supported by the Department of Energy and the Natinal Science Foundation through the Research Foundation of City University of New York.

This work is dedicated to S. J. Lindenbaum, on the occasion of his 35th anniversary. His passion for and dedication to experimental physics are to be remembered and admired.

TABLE OF CONTENTS

LIST OF TABLES

LIST OF FIGURES

Chapter 1 Motivation for Studies of Meson-Meson Systems

1.1 Introduction

The success of the standard model is so overwhelming that we can now regard the model as the established model of the electro-weak interactions. Unless some drastic discrepancy between experimental results and theoretical predictions including higher order corrections shows up, the electro-weak theory based upon a gauge group $SU(2) \times U(1)$ will be regarded as the correct theory.

A natural extension of the theory based upon a larger group $SU(5)$ has not been established yet, although it is very difficult to doubt correctness of the group $SU(3)$. Without color degrees of freedom, it is virtually impossible to understand various things, three examples are: a)the relative hadron production cross section (R ratio), b)the decay rate of $\pi^0 \rightarrow \gamma\gamma$[1], c)cancellation of triangle anomalies[2]. On the other hand it is to be noted that it is very difficult to implement the color degrees of freedom in the Monte Carlo programs that are used to study hadron productions in e^+e^- or $p\bar{p}$ collisions, although the effective coupling constant used in their algorithm has a behavior of asymptotic freedom as prescribed by Quantum Chromodynamics(QCD). In particular, processes related to the soft gluon emission(and exchange) are exceptionally difficult to deal with. Therefore, the claimed agreements between the experimental results and the Monte Carlo predictions are not necessarily direct verification of the gauge group $SU(3)$.

Substantial progress has been made toward understanding of mesons in the past both experimentally and theoretically as it is attested in numerous review papers, yet it is reasonable to say that many problems are still unsolved in meson spectroscopy below 2 Gev. This is to be compared to the state of affairs in the studies

of mesons that belong to the J/ψ and Υ families. The difficulty is, of course, rigorous perturbative pictures from the first principles are not available below 2 Gev especially in strong interactions. Above 3 Gev, one can choose not to take a perturbative approach and rely on a model of quarks in an effective potential, since often perturbative calculations become exceedingly complex upon introduction of QCD. The successes of the potential models are sufficient to make us state that meson spectroscopy above 3 Gev is understood. These successes are further supported by the fact that the lattice Monte Carlo simulation also gives a potential of one of the desired forms(Coulobmic and linear)[3]. Efforts are being made to study non-perturbative aspects of the gauge theory, however satisfactory pictures of light mesons have not emerged yet. For those who study light-meson spectroscopy, this is clearly unfortunate and frustrating. Theorists created many phenomenological models, their predictions challenged experimental findings. In many cases, only qualitative agreements have been seen, and sometimes even qualitative understanding of experimental results was difficult to achieve. There are still a large volume of data that has not taught us much about light mesons unless we take highly phenomenological viewpoints. It is hoped that the Monte Carlo simulation of the lattice gauge theory will produce the detailed description of mesons in terms of Quantum Chromodynamics. This might take a long time for two reasons: a)current limitations in computational power; b)difficulties in treating fermion fields on the lattice.

Having stated that meson spectroscopy below 2 Gev is unclear, an experimentalist might ask the following question : Do we really understand the available data on meson resonances ?

In order to answer this question, it was decided to do systematic studies of the available meson spectra in a particular sector.

1.2 Motivation

Many hadronic meson-meson production experiments had been performed in the past. This was perhaps motivated by the fact that mesons that decay into two identical mesons are relatively easy to study. Availability of such two- meson production data is generally good. Indeed several meson resonances had been seen after rigorous analysis of the data. Since a given resonance has more than one decay mode as kinematics and the conservation of quantum numbers dictate, it is important to establish branching ratios with reasonable accuracy. From analysis of the data, determinations of mass and width of a given resonance in a compatible and consistent way dealing with different data sets become possible. This sort of parameter determination is highly significant to establish a consistent picture of the meson resonance. Thus we are naturally compelled to consider the necessity of a multi- channel analysis of the data.

Tools that can be used to do such a global study of the meson production data are available.

One-particle-exchange(O.P.E.) mechanism makes it possible to extract interaction amplitudes from the raw data. Thus data from a reaction,

$$\pi^- p \rightarrow \pi^+ \pi^- n$$

can be studied to extract the amplitudes for the reaction,

$$\pi^- \pi^+ \rightarrow \pi^- \pi^+.$$

Similarly one can obtain the amplitudes for other reactions such as,

$$\pi^- \pi^+ \rightarrow K^- K^+$$

$$\pi^- \pi^+ \rightarrow \eta\eta.$$

Obviously two mesons can come to interact with each other and form a resonance state and then decay into two mesons. The ideal is to do experiments on meson-meson productions simultaneously using the same π-beam and the same detector. This is, of course, technically very difficult in the fixed-target setting. Problems that arise from this difficulty are numerous, one of which is the difference in the beam momenta among experiments. Fortunately this problem is not severe since the beam momentum dependence is known in the expression for a cross section derived in the one- particle-exchange model. Another problem is systematics coming from the acceptance of detectors, but here one assumes that experimentalists carefully studied the characteristics of their detectors and the acceptance calculations had been relibably done to make needed corrections to the data.

It should be noted that this O.P.E. mechanism has been rigorously applied to many reactions with mostly satisfactory results.

The S-matrix is unitary, this is most simply realized by defining a new matrix K through the T-matrix. Thus by performing a coupled-channel analysis one can directly determine each element of the matrix from which a consistent and compatible set of parameters of resonances may be obtained. As it is discussed later, implementation of this unitarity will lead us to complicated non-linearity which makes fits time-consuming. Also introduction of the K-matrix requires that one appropriately extract resonance mass and width. Finally this non-linearity makes error estimates even more time-consuming.

Problems to be investigated are numerous.

The scalar sector seems to be in the darkest part of meson spectroscopy below 2 Gev. One can make a separate study on scalar mesons if problems can be reasonably solved. History of light meson spectroscopy tells us that nobody has achieved such

a goal. A conventional argument is that scalar mesons have quantum numbers same as those for vacuum and vacuum effects are not understood well. The scalar sector of the J/ψ and Υ families seems relatively problem-free. This is a good contrast if one remembers that some of these states are classified as $^{2s+1}L_J = ^3P_0$ according to the quark model.

Among the scalar mesons the most difficult one is the f_0 (1300). Parameters of this state are not yet accurately known. The reported values for the parameters of this state appear to be split into two sets: 1) around m=1.25 Gev/c^2, Γ=300 Mev/c^2, 2) around m=1.45 Gev/c^2, Γ=150 Mev/c^2. Other states recently claimed such as the $f_0(1240)$ or the $f_0(1730)$ have not been confirmed yet.

Mesons with $J^{PC} = 2^{++}$ are better understood. Yet there are problems to be extensively investigated. One state, the $f_2(1720)$ discovered at SLAC, has never been observed in the hadronic meson production experiments. One does not necessarily need to do partial wave analysis to establish highly narrow objects. Unfortunately the $f_2(1720)$ is as wide as any ordinary hadronic states, the phase motion that is important to study this state as a resonance(or other) has never been observed although its spin-parity assignment is fairly definite. accepting the fact that the "bump" seen at SLAC is a particle or at least a meson resonance, the crucial problem to be studied is to establish with confidence that this state is seen in the hadronic data. This is not a trivial problem, since resonances can exhibit interferences. A resonance seen in one hadronic channel as a "bump" may not be seen in another channel. A well-known example is the $f_2(1525)$ which is clearly seen in the K^+K^- spectra from experiments using incident K beams, this state does not appear as a clear peak in other hadronic channels. Another state $f_2(1810)$, regarded as a radial excitation of the $f_2(1270)$, is yet to be established.

Finally we may ask if we have seen a strange partner of the $f_4(2030)$.

In short, unsolved problems in meson spectroscopy below 2 Gev are many and much work should be done.

In the present work, the meson systems in the sector of $J^{PC} = 0^{++}$, 2^{++}, and 4^{++}, are systematically studied.

1.3 Organization of the Work

The present work is organized in the following manner.

Two chapters(Chapter 2 and Chapter 3) are devoted to the studies of the data on the two important systems, namely the $\pi\pi$ and the $K\bar{K}$ systems. Since a substantial amount of time was spent to study the $\pi\pi$ system, Chapter 2 is somewhat long. But it contains an important description of a new averaging procedure along with the results of a re-analysis of the existing $\pi\pi$ data carried out by the author (in some cases re-analysis was necessary).

Chapter 5 contains discussions on various data sets available to the present author. Among these the most important is the data on the $\eta\eta$ system that became available only recently. Other data sets form auxiliary data sets in a sense since our primary objectives are to understand the meson-meson systems seen in hadronic production experiments. These auxiliary sets are the $\pi\pi$ and $K\bar{K}$ data from the SLAC experiments on the radiative decay of the J/ψ and the $\pi\pi$ data taken from the $p\bar{p}$ collision experiment performed at CERN.

Throughout these three chapters, the author's emphasis is upon observation of the details of the data and inference from the facts. The experimental details on each experiment, in particular on the subject such as apparatus, are not included. The only exception is the $K_s^0K_s^0$ production experiment performed at the BNL MPS II facility in which the present author has participated, this experiment forms a major part of the basis of this work. A description of the experiment and analysis procedures is given in Chapter 4.

Chapter 6 describes the details of the method we used in this analysis. The K-matrix has been around for a long time, rigorous discussions on the subject can

be found in many textbooks and papers. Therefore discussions on the K-matrix are kept minimum in the chapter. The detailed results of this investigation are presented and discussed in Chapter 7 along with tables of the parameters obtained in the fit. Some of these results have been already published.

Chapter 8 contains general comments and summary of this work.

Chapter 2 The $\pi\pi$ Data

2.1 Introduction

Traditionally the $\pi\pi$ scattering has been an excellent testing ground for theorists and experimentalists as well. The model of Lovelace-Shapiro-Veneziano[4] was one of the earliest attempts to verify fundamental ideas in the theories of strong interactions such as duality and trajectories. At the moment there is no rigorous way to understand the $\pi\pi$ interactions directly from QCD. In this chapter, we review the currently available sets of the $\pi\pi$ amplitudes. Discussions on the experimental details and theoretical interpretation will be kept to minimum. Our primary goal is to construct the world averages of these amplitudes.

2.2 The Data Sets

We have chosen the following sets of amplitudes available to us, these are all from the (unpolarized) fixed-target experiments.

(1) Cason *et al.*[5]

(2) Apel *et al.*[6]

(3) Corden *et al.*[7]

(4) Martin-Pennington, β-solution[8]

(5) Martin-Pennington, β'-solution[8]

(6) Estabrook-Martin [9]

(7) Hyams *et al.*[10]

The $\pi\pi$ scattering in hadronic reactions are known to be dominated and sufficiently described by the one-particle-exchange (OPE) mechanism in the region of

a small t, the four-momentum transfer to the nucleon squared. Usually the events distributed in t are selected by introducing a cut in $|t|$. The π-exchanged amplitudes can be obtained by extrapolating the raw data to the π pole in the OPE expression, this is to be discussed in the next section in more details. *One important thing is that these are extracted quantities, not real data.* But these will be called the data. The data sets (3) through (7) come from the reaction

$$\pi^- p \to \pi^+ \pi^- n,$$

whereas the sets (1) and (2) come from the following reactions

$$\pi^+ p \to \pi^0 \pi^0 \Delta^{++}$$

$$\pi^- p \to \pi^0 \pi^0 n$$

respectively, and these data determine the amplitudes for the process,

$$\pi^+ \pi^- \to \pi^0 \pi^0.$$

Differences in the beam momenta have been corrected in the process of the amplitudes extraction through the use of the OPE expression. One should note that the features of the total cross section for the $\pi\pi$ production, especially those in the t distributions, predicted by the OPE model are generally valid up to 175 Gev/c incident beam momentum[12].

The set (3) is the so-called B-solution. The observation of the $\rho(1600)$ which is now regarded as a radial excitation of the $\rho(770)$ in the recent $\pi\pi$ production experiment[13] in a reaction,

$$\gamma p \to \pi^+ \pi^- p$$

demonstorated that the G-solution favored by Corden *et al.* is a wrong solution, the origin of which can be traced to their choice of an inappropriate combination of the

Barrelet zeroes for the amplitude construction, this solution can now be regarded as a good example of the well-known problems of ambiguities which manifest itself in the process of decomposing the moments into the partial waves. The validity of the B-solution in the analysis of Corden *et al.* and the variant β and β' solutions obtained by Martin and Pennington and separately by Estabrook and Martin is established by the analysis of the $\pi^0\pi^0$ data[5,6]. We have reconstructed the B-solution from the G-solution of Corden *et al.* by following the usual steps to derive the amplitudes from the moments in a reverse order, correctness of these procedures and consistency of the results with the original data were checked by requiring that the optical theorem be satisfied. This direct application of the theorem is based upon the fact that the total cross section should be the same no matter which solution one chooses. The application of the theorem is, in this sense, a strong constraint on the phases of the individual waves. This extensive re-analysis was motivated by the fact that the only data sets that extend to the important mass region above 1.8 Gev/c^2 are the sets (1) and (3). The observation of a radial excitation of the $f_2(1270)$ at around 1.8 Gev/c^2 in the analysis of Cason *et al.* justified our choice of the B-solution. There are two other independent sources of evidence for this state $f_2(1810)$:

(a) the D-wave spectrum found in the analysis of the $\eta\eta$ data from the reaction,

$$\pi^- p \rightarrow \eta\eta n$$

shows this state(to be discussed in chapter 5).

(b) the mass spectrum of the 4π system obtained in the reaction,

$$\pi^+ d \rightarrow \pi^+\pi^+\pi^-\pi^- pp$$

shows a modest enhancement on top of a background, the mass and width determined by fits are consistent with those of $f_2(1810)$[11].

The $\pi\pi$ amplitudes have to satisfy a set of constraints derived from analyticity and unitarity. The solution β was obtained in this manner. In the process, another solution was discovered almost accidentally, "in a seemingly distant part of a parameter space"[8]. It turned out that this solution, the β' solution, was equally good except in the minor details[8].

Our primary interest is the I=0 part of the S-,D-, and G-waves. Both of the $\pi^+\pi^-$ and the $\pi^0\pi^0$ amplitudes contain the isospin 2 part. These amplitudes are decomposed in the following way,

$$A_{\pi^+\pi^-} = \frac{1}{3}I_2 + \frac{2}{3}I_0$$

$$A_{\pi^0\pi^0} = \frac{1}{3}I_2 - \frac{1}{3}I_0$$

where I_0 and I_2 are the isospin 0 and isospin 2 parts respectively. A simple subtraction has to be performed to obtain the isospin 0 components. The results from numerous experiments on the reaction,

$$\pi^+ p \rightarrow \pi^+\pi^+ n$$

provided a useful parametrisation of the amplitudes of the I=2 components[14], we have used this parameterization to determine the I=0 amplitudes.

The phases of the I=2 component are negative and small both for the S- and D-waves. Typically at 0.9 Gev/c^2, the $S-$ and $D-$phases are around -20 degrees with errors of 5 degrees and -2 degrees with errors of 0.5 degrees respectively. The phases stay approximately constant above 1.0 Gev/c^2, and do not greatly influence phases of the I=0 parts when subtractions are performed.

The I=2 component of the G-waves is not known, this makes the isospin assignment uncertain. This will be discussed in section 2.4.

2.3 The OPE Model and Amplitude Ambiguities

In this section the most fundamental aspects of the O.P.E. model and the amplitude ambiguities are briefly discussed. Procedures to obtain scattering amplitudes are mostly empirical, since general methods to find a unique set of amplitudes do not exist.

Historically the One-Particle-Exchange model is a product of: a)the original suggestion by Yukawa that strong force is mediated by π, b)the Feynman diagrammatic way of viewing the strong interactions.

In many simple processes such as $NN' \rightarrow NN'$ (nucleon-nucleon interactions) the scattering amplitudes satisfy dispersion relations defined on a complex plane of the kinematic variables(Mendelstam variables),

$$T(s,t) = T_{Born}(s,t) + T_c(s,t),$$

where $T_{Born}(s,t)$ is the Born amplitude and $T_c(s,t)$ is the remaining amplitude in a contour integral form defined on the same complex plane. In a certain kinematic region, the Born amplitude dominates strongly. Because of this dominance of the Born amplitudes, Chew suggested a method to determine the magnitude of the strong coupling constant which is the residue of the Born amplitude. The π pole in the Born amplitude is located in an unphysical region if one has a t-channel exchange of π. One can evaluate the following quantities which are free from π pole(which is the nearest t channel pole),

$$\lim_{t \rightarrow m_\pi^2} (t - m_\pi^2)^2 \frac{d\sigma}{d\Omega},$$

where $\frac{d\sigma}{d\Omega}$ is the measured differential cross section. This method was later generalized by Chew and Low[15] in order to study more complex processes. The outcome is the method to determine the cross section for the $\pi\pi$ scattering from the cross sections for $\pi N \rightarrow \pi\pi N$. For the reaction $\pi^- p \rightarrow \pi^+\pi^- n$, the expression for the cross section is,

$$\frac{d^3}{dt dm_{\pi\pi} d\Omega} = \frac{1}{2\pi m_N^2 p^2} \frac{g^2}{4\pi} \frac{-t}{(t-m_\pi^2)^2} q m_{\pi\pi}^2 \frac{d\sigma_{\pi\pi}}{d\Omega},$$

where m_N is the nucleon mass, p the incident π^- laboratory momentum, $g^2/4\pi$ the π-nucleon coupling constant, q the π^+ momentum in the $\pi\pi$ center of mass system, $m_{\pi\pi}$ the dipion effective mass, and $d\Omega$ is the differential solid angle. The $\pi\pi$ differential cross section has the following familiar expression,

$$\frac{d\sigma_{\pi\pi}}{d\Omega} = \frac{1}{q^2} |\sum_l (2l+1) a_l P_l(\cos\theta)|^2.$$

This expansion in terms of Legendre polynomials give the scattering amplitudes,

$$f(\cos\theta) = \sum_{l=0}^{l_{max}} (2l+1) a_l P_l(\cos\theta).$$

The fact that we only measure the absolute modulus squared of the amplitude $|f(\cos\theta)|^2$ is the source of the problems of the amplitudes ambiguities. The above amplitude is a polynomial in $\cos\theta$ when Legendre polynomials $P_l(\cos\theta)$ are expressed in terms of $\cos\theta$. Extending $\cos\theta$ into the complex plane, we can write $z = \cos\theta$. It is elementary to show that the amplitude can also be written down in a factorized form,

$$f(z) = c \prod_{l=1}^{l_{max}} (z - b_l),$$

where c is an over-all coefficient and b_l are the zeroes of the polynomials. Also we can rewrite the above factorized form into the following form,

$$f(z) = f(1) \prod_{l=1}^{l_{max}} \frac{(z-b_l)}{(1-b_l)},$$

where $f(1)$ is the forward scattering amplitude. The differential cross section is proportional to,

$$|f(z)|^2 = |c|^2 \prod_{l=1}^{l_{max}} (z - b_l)(z - b_l^*),$$

obviously complex zeroes appear in conjugate pairs in the expression. If one of zeroes in the expression for the amplitude is replaced by its complex conjugate,

$$f(z)_m = c \prod_{l=1, l\neq m}^{l_{max}} (z - b_l)(z - b_m^*),$$

we obtain an amplitude $f(z)_m$ entirely different from the original amplitude $f(z)$. But this amplitude gives the same differential cross section. There are $2^{l_{max}}$ ways of making different amplitudes that give the same differential cross section. As it was mentioned in the previous section, if one amplitude set is given, one can reconstruct the rest of the amplitude sets by numerically exploring the amplitude polynomial on the complex plane. The partial amplitudes, $(a_l, l = 0, l_{max})$, change as a function of energy, the invariant mass of $\pi\pi$ in our case. This is equivalent to stating that an amplitude vector a_l moves inside an Argand circle as energy changes. As this change takes place, complex zeroes $(b_l, l = 1, l_{max})$ move on the complex plane making complicated trajectories. The choice of complex zeroes is made to make these trajectories continuous. And each set of continuous trajectories defines a solution set of partial amplitudes. These trajectories themselves do not give clear physical pictures, instead one studies Argand plots of the amplitude vectors that resulted from the sets of trajectories. A large number of possibilities can be eliminated by this method. Particular difficulties arise when a higher wave is added to the amplitude. When this takes place, ambiguities become twice larger. Also noteworthy is a factor $2l+1$ in front of the l-th partial wave amplitude. Higher wave amplitudes are magnified by this factor, in the expression for the cross section this

appears as a factor of $(2l+1)$. Therefore differential cross section is particularly sensitive to the higher wave amplitudes. This makes the choice of l_{max} important in any analysis. However the dynamics is such that below 2 Gev reasonable choices of l_{max} can be made.

The optical theorem constraint which was used takes the following form,

$$\sigma_{\pi\pi} = \frac{4\pi}{q^2}\sum_l (2l+1)\mathrm{Imag}(a_l).$$

2.4 The General Features of the Data Sets

The general features of the data sets are now discussed. All the plots of the amplitudes modulus squared are those of $(2l+1)|a_l|^2$. Figures 2.1 show the S- and D-waves of the set (1). These were obtained by re-analyzing the published moments. This re-analysis was motivated by the unavailability of the D-wave phases in their publication. They give only 7 sets of data points between 1.5 Gev/c^2 and 2.1 Gev/c^2. In this mass region, one half of the data shown here were obtained by linear interpolation between the mass bins. The $f_0(1300)$ and the $f_2(1270)$ are unmistakable in the spectra. A region around 1.80 Gev/c^2 of the S-wave in which we expect the $f_0(1720)$ will require a careful analysis, whereas the $f_2(1810)$ is easily seen. The elasticity of the S-wave around the $f_0(1300)$ is slightly large, this is one outstanding problem shared by the amplitudes that belong to the class of the the B-solution. We notice that a minimum of $|S|^2$ around 1.6 Gev/c^2 is not small , this is a consequence of the fact that S-phase of $\pi^0\pi^0$ is not canceled by the isospin subtraction, this is a feature also noticeable in the $\pi^+\pi^-$ phases of the β'-solution.

Figures 2.2 come from the second set. The over-all features agree with those of (1). The D-phases of the sets (6) and (7) were used to obtain the S-phases of this set. A discontinuity at 1.18 Gev/c^2 comes from the fact that we connected two

solutions one with $\phi_s - \phi_d \geq 0$ and the other with $\phi_s - \phi_d \leq 0$ so that we could minimize violation of unitarity while maintaining reasonable error bars. The bin at 1.18 Gev/c^2 is an appropriate one to make this connection.

Figures 2.3 are the B-solution. Large error bars in the S-phases around 1.6 Gev/c^2 are the unavoidable features shared by these solutions. There are two ways to represent amplitudes in an Argand plot. We use one representation in which phases are measured from the positive real axis. In this representation phases carry large error bars when the amplitude vectors stay near the origin. In the other representation phases carry large error bars when the vectors are near the center of the Argand circle. Figures 2.4 to 2.6 are the β-,β'-, and the B- solutions, these are extensively discussed[8,9,10]. The elasticity of the S-waves of the set (4) is slightly smaller. The difference is that the S-wave amplitudes of the β-solution completes an Argand circle from outside, whereas those of the β'- solution stay inside of the circle. This difference manifests itself in the last three mass bins, 1.58, 1.62, and 1.66 Gev/c^2. On the Argand plot one can draw ellipses around data points showing the errors in lengths of the amplitude vectors and the phases. The amplitude vectors in the region around 1.6 Gev/c^2 are all reasonably close to each other in spite of this difference in the phase motion. Between 1.5 and 1.8 Gev/c^2 the thresholds of three important channels($\eta\eta'$, $\rho\rho$, and $\omega\omega$) open. The $\rho\rho$ and $\omega\omega$ systems have been studied[16] in the radiative decays of the J/ψ, at present we have no hadronic data on the $\rho\rho$ and $\omega\omega$ systems. On the other hand it was reported that the $\eta\eta'$ system around 1.6 Gev/c^2 from the reaction $\pi^-p \rightarrow \eta\eta' n$ is purely S-wave. The S-wave of the $\eta\eta$ system does not have a minimum around 1.6 Gev/c^2, instead one observes a resonance in that region.

Figures 2.7 through 2.9 show the behavior of the sets (7), (1) and (2) in a region below 1.2 Gev/c^2. This region has long been plagued by inconsistency among the data from the old $\pi^0\pi^0$ production experiments [5,17]. The elasticities of the S-waves of (1) and (2) show this typical discrepancy below 0.9 Gev/c^2. If one takes the estimated uncertainty reported in the analysis of Apel *et al*, the error bars of $|S|^2$ in the set (2) can be large enough to cover those in (7). And this makes data points of (1) somewhat isolated from the other two. The S-phases of (7) and (2) are consistent enough to make us observe a broad enhancement at around 0.8 Gev/c^2, whereas the set (1) could possibly make the enhancement look like a resonance state. We comment that phase motion of the D-wave of (1) has no significance since $|D|^2$ shows no structure and is negligibly small below 1.0 Gev/c^2, the same observation can be made on the D-wave of (7). Let us note that the processes considered in (1) and (2) are fundamentally different only in one respect, a $pn\pi^+$ vertex is not the same as a $p\Delta^{++}\pi^-$ vertex. But this difference was presumably taken into account when the OPE extrapolation was performed. The $\pi^0\pi^0$ production experiments are advantageous in that the ambiguity of amplitudes is easier to resolve above 1.0 Gev/c^2, but experiments are generally very difficult to perform compared to the $\pi^+\pi^-$ production experiments. Figures 2.10 through 2.11 show the G-waves of the sets (1) and (3). Figures 2.11 show an almost pure Breit-Wigner shape. One wonders why the G-phases of set (1) are different from those of (2) in the low mass region. We have considered a hypothesis that the amplitude that describes the set (1) is a sum of a pure Breit-Wigner amplitude and a background of the form,

$$A = A_1 + A_2$$

$$A_1 = \frac{m_h \Gamma_{\pi\pi}}{m_h^2 - s_{\pi\pi} - i m_h \Gamma_h}$$

$$A_2 = \frac{qB(rq)C}{m_{\pi\pi}}$$

$$\Gamma_{\pi\pi} = qB(rq)\Gamma^2 = D\Gamma_h$$

where Γ_h is the total width of the $f_4(2030)$, $\Gamma_{\pi\pi}$ being its $\pi\pi$ partial width, $B(rq)$ is the Blatt- Weisskopf barrier factor determined by a parameter r and momentum q(the precise form is given in Chapter 6). D and C are real and complex parameters respectively. Γ is another parameter which represents the $\pi\pi$ coupling of the $f_4(2030)$. By fitting the set (1) we could describe its phase motion as an interference between the Breit-Wigner amplitude and a background at a 2σ level with acceptable mass and width of the $f_4(2030)$. The result is that the $|G|^2$ of (1) is systematically smaller than that of (2) as shown in Figures 2.11. We emphasize that there is no assurance that the G-wave of (3) contains no appreciable background. The parameters for the $f_4(2030)$ obtained from a fit without assuming any background could lead to an overestimate of the $\pi\pi$-coupling of this state.

If we exclude the data points below 1.78 Gev/c^2, both results are consistent therefore they can be averaged, without the hypothesis of a background for (1).

The D- and G-waves are consistent and can be readily averaged by the standard method of least-square averaging[18]. Difficulties exist in the region above 1.80 Gev/c^2 of the D-waves and in the above-mentioned region of the G-waves. In the region of the D-wave above 1.80 Gev/c^2 where only two data sets exist, the arithmetic averages with errors reflecting the range of values were used.

2.5 The Averages of the Data

A method we propose here is reasonable and conservative, all the data sets are included. Averages and errors are estimated adiabatically in this method as explained below. Averages and errors are calculated according to the least-square formula with weights. The important assumption we make is that discrepant results had been obtained because some of these values belonged to the tail parts of the Gaussian distribution, one of them could be right near the true mean, this we do not know. When χ^2 is calculated, each datum is reviewed. Only the data points that made large χ^2 contributions are selected, the errors of those that gave χ^2 larger than a specified χ^2 (64 for the first cycle in our case) are scaled by $(\frac{\chi^2}{\chi^2_{cut}})^{1/2}$ where χ^2 comes from the particular data point not from the total χ^2 and χ^2_{cut}=64 in the beginning. The new averages and errors are calculated using the same data including the deviant data points with scaled (larger) error bars. The shift of the new averages due to this scaling is mild because the scaling only applies to the deviant points from the main body of the data defined by the averages and errors. The next cycle is gone through with a smaller χ^2, 16 in our case. The cycles will be repeated till the convergence is achieved, the convergence is achieved when $\chi^2_{tot}/(N-1)$ becomes equal or less than 1 where N is the total number of data sets in each mass bin. One should be careful when the first averages are computed, since deviant points with small errors influence the central values which in turn change χ^2. One can expand errors of those points by hand to see if this occurs. If expansion of an error by 1σ does not change the central values within 1σ, this error expansion is not necessary. The first value of χ^2_{cut} is chosen by looking for the maximum χ^2. The resulting series of values of χ^2_{cut} define a set of σ-hypotheses by which we mean that selected deviant points are away from the estimated mean at least by this specified σ. The result is a quite conservative estimate of averages and errors.

Figures 2.12-2.13 show the results of the averages with errors by this method(see Tables 1 and 2), the points above 1.8 Gev/c^2 including those of the G-wave are the arithmetic averages with errors reflecting the range of values from two sets. For comparison Figures 2.14 show the averages of the G-waves obtained from the standard least- square averaging method without weights(see Table 3). One should note that the errors of the S-wave around the $K\bar{K}$-threshold should be much larger than those shown here due to a rapid phase motion of the $f_0(975)$. The continuity of the phases is generally good. To summarize, we have constructed the world averages of the I=0 $\pi\pi$ amplitudes of the type B-solution. In spite of the difficulties in the S-waves, a resulting picture is satisfactory.

Table 2.1 The averages of the S- and D-waves.

Mass($\pi\pi$)	$\|S\|^2$	$\delta\|S\|^2$	$\|D\|^2$	$\delta\|D\|^2$	ϕ_S	$\delta\phi_S$	ϕ_D	$\delta\phi_D$
0.66	0.803	0.074	0.006	0.005	58.54	8.42	1.76	1.98
0.70	0.897	0.053	0.010	0.005	70.80	6.80	2.49	1.99
0.74	0.964	0.032	0.015	0.005	81.07	5.82	3.46	1.99
0.78	0.975	0.035	0.017	0.018	82.07	6.79	4.21	9.22
0.82	0.991	0.017	0.069	0.057	89.08	5.58	1.97	2.99
0.86	0.997	0.012	0.053	0.028	89.00	5.15	2.23	2.00
0.90	0.979	0.027	0.090	0.024	99.70	3.67	14.22	7.36
0.94	0.881	0.055	0.134	0.057	110.63	4.22	34.45	6.22
0.98	0.710	0.061	0.196	0.069	103.79	4.97	29.78	5.39
1.02	0.622	0.056	0.302	0.068	77.97	5.32	20.78	9.21
1.06	0.581	0.060	0.452	0.052	75.40	3.18	19.59	4.98
1.10	0.716	0.073	0.712	0.055	78.55	2.84	23.96	3.72
1.14	0.966	0.090	0.947	0.069	84.50	3.15	29.36	3.83
1.18	0.855	0.140	1.550	0.108	86.32	1.76	35.45	5.52
1.22	0.783	0.113	2.821	0.152	95.73	6.49	62.82	3.11
1.26	0.912	0.142	3.503	0.057	105.06	7.89	81.31	4.07
1.30	1.091	0.216	2.957	0.104	113.31	14.92	105.19	5.35
1.34	0.944	0.097	2.268	0.095	123.32	10.97	118.54	5.92
1.38	0.878	0.138	1.502	0.073	125.13	16.31	125.20	7.46
1.42	0.690	0.074	1.042	0.064	133.61	17.66	125.84	6.17
1.46	0.455	0.050	0.681	0.087	138.52	16.30	141.00	7.02
1.50	0.273	0.047	0.411	0.048	146.37	16.25	133.52	7.17
1.54	0.082	0.042	0.360	0.030	149.20	15.87	131.01	6.60
1.58	0.075	0.044	0.299	0.053	103.42	28.40	132.81	6.01
1.62	0.039	0.026	0.332	0.044	43.41	76.34	138.60	6.96
1.66	0.071	0.020	0.298	0.128	112.82	28.39	140.26	6.85
1.70	0.196	0.046	0.307	0.077	87.38	29.78	137.01	12.17
1.74	0.492	0.143	0.514	0.096	86.60	16.15	128.64	8.41
1.78	0.516	0.134	0.806	0.281	77.76	16.74	104.03	13.44
1.82	0.512	0.188	0.948	0.278	126.72	19.22	153.83	9.82
1.86	0.523	0.211	0.926	0.267	126.71	8.41	149.91	8.11
1.90	0.523	0.276	0.758	0.223	125.47	7.91	136.88	7.41
1.94	0.459	0.262	0.565	0.195	119.50	10.75	130.90	7.08
1.98	0.490	0.239	0.541	0.062	121.02	13.43	145.00	6.44
2.02	0.464	0.131	0.392	0.060	120.32	17.67	144.39	6.83
2.06	0.448	0.154	0.343	0.052	132.24	14.34	158.28	5.18
2.10	0.682	0.070	0.298	0.056	159.70	33.00	157.00	4.20

Table 2.2 The averages of the G-waves versus the mass of $\pi\pi(\mathrm{Gev/c^2})$. The $|G|^2$ is in the unit of $9\times$ Argand unit squared(unitarity limit is 9).

Mass($\pi\pi$)	$\|G\|^2$	$\delta\|G\|^2$	ϕ_G	$\delta\phi_G$
1.82	0.012	0.007	62.00	17.00
1.86	0.049	0.017	65.65	9.00
1.90	0.186	0.098	73.53	6.74
1.94	0.215	0.103	91.58	5.81
1.98	0.080	0.033	116.24	7.62
2.02	0.136	0.047	121.64	23.10
2.06	0.065	0.018	137.16	11.70
2.10	0.010	0.058	153.20	47.90

Table 2.3 The averages of the G-waves versus mass of $\pi\pi(\mathrm{Gev/c^2})$ using the standard least square averaging method without weight.

Mass($\pi\pi$)	$\|G\|^2$	$\delta\|G\|^2$	ϕ_G	$\delta\phi_G$
1.78	0.064	0.021	36.77	9.40
1.82	0.098	0.033	67.97	16.03
1.86	0.059	0.028	67.74	8.84
1.90	0.172	0.041	67.85	11.61
1.94	0.246	0.049	85.60	13.99
1.98	0.129	0.044	105.69	28.39
2.02	0.219	0.045	89.61	14.85
2.06	0.096	0.017	120.85	10.63

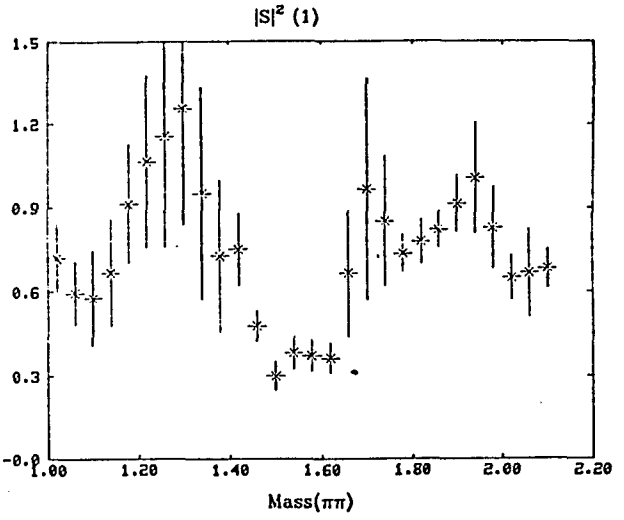

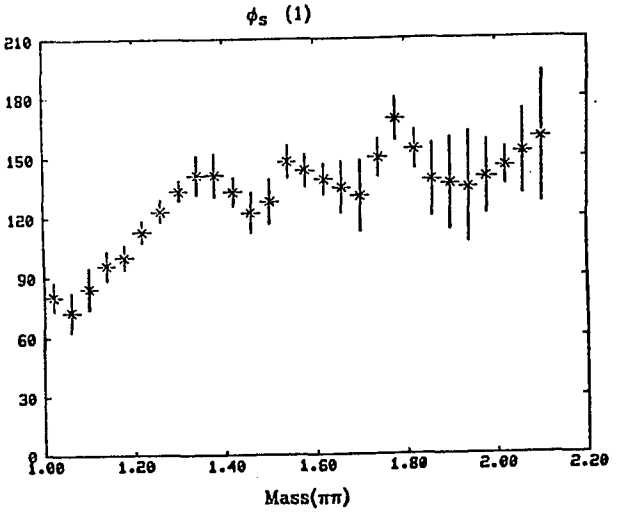

Fig. 2.1 (a) S-wave amplitudes from set (1) as a function of the invariant mass of $\pi\pi$. $|S|^2$ is in the Argand unit, ϕ_S is in the unit of degree and $M_{\pi\pi}$ is in unit of Gev/c^2.

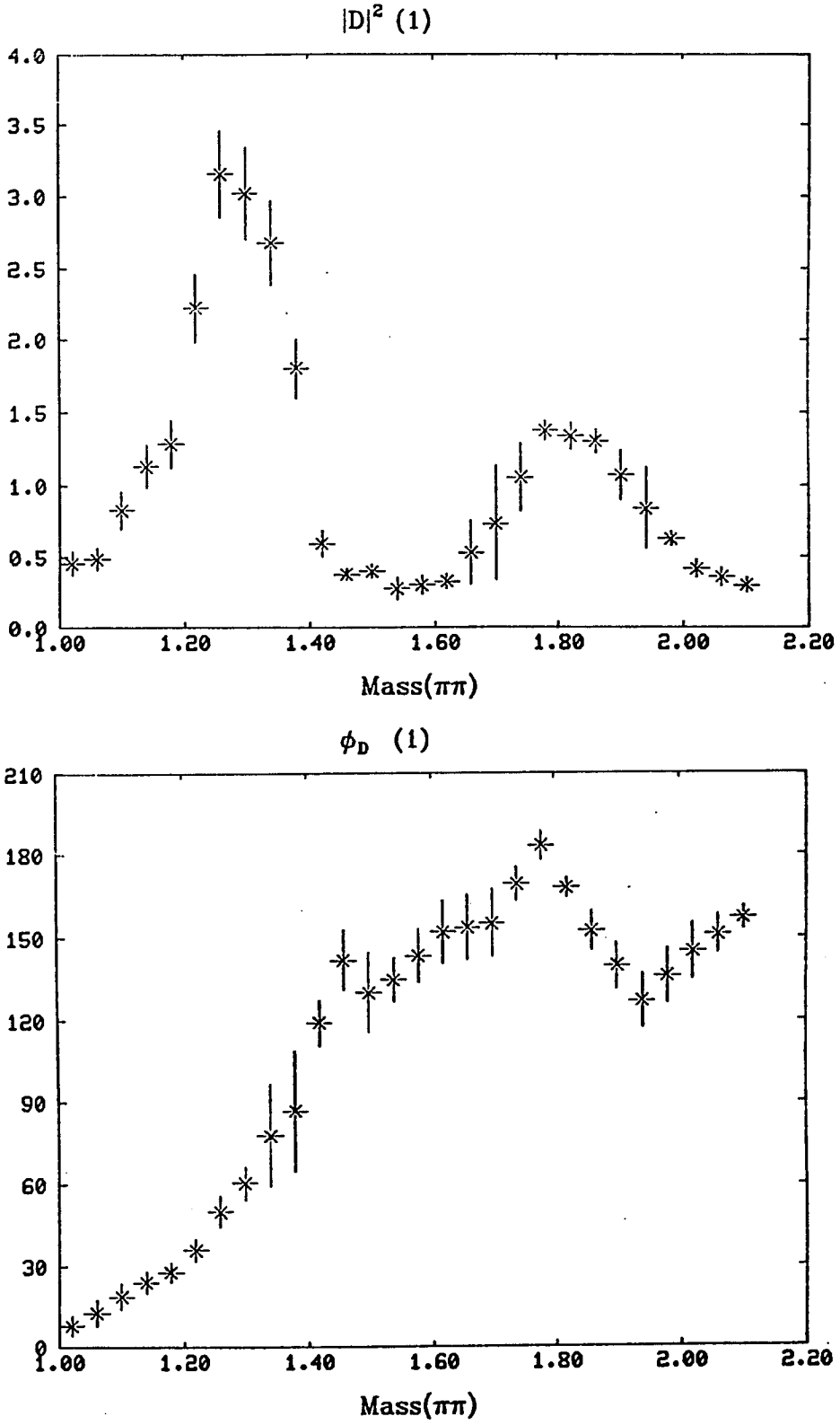

Fig. 2.1 (b) *D*-wave amplitudes from set (1) as a function of the invariant mass, units are the same as in Fig. 2.1 (a) .

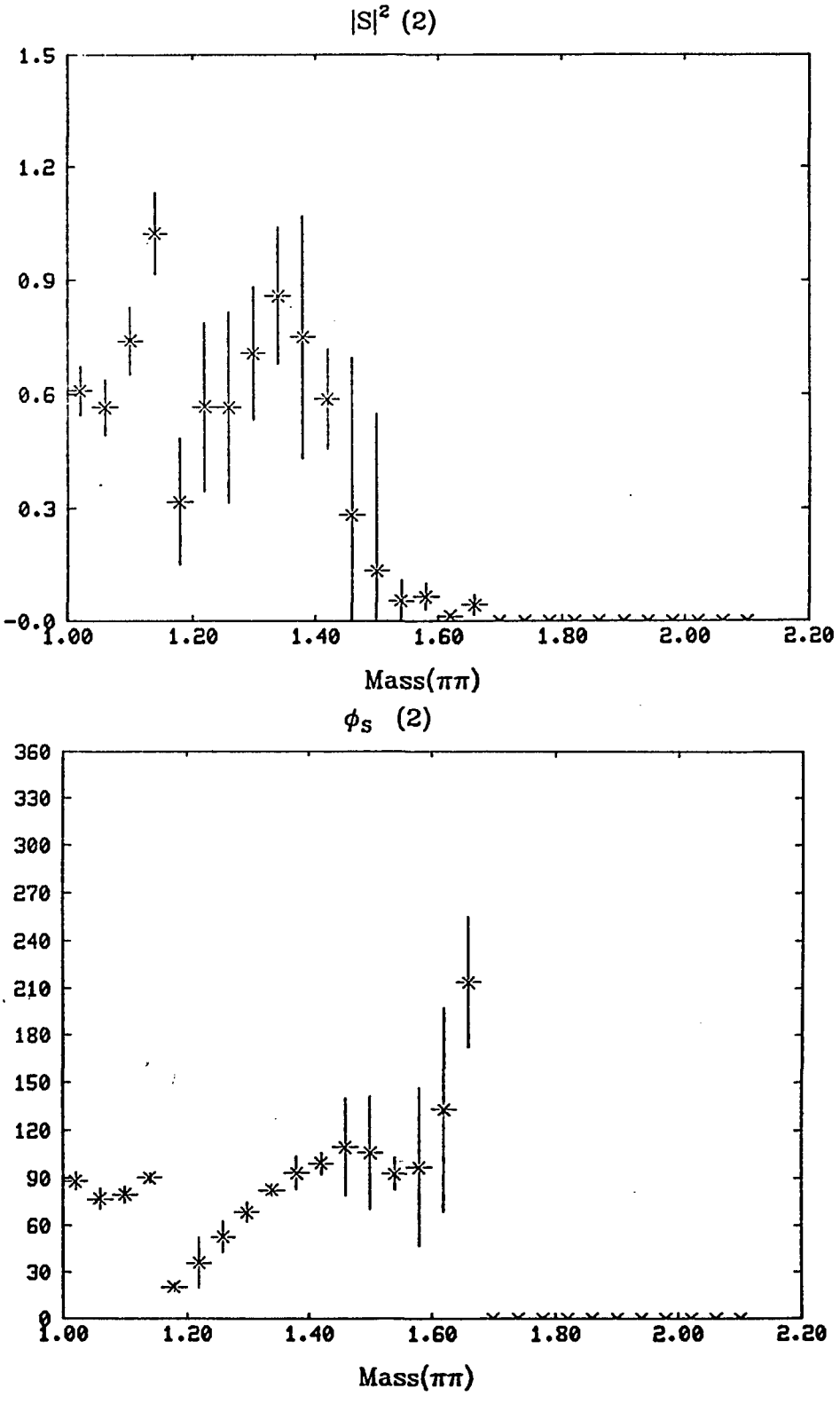

Fig. 2.2 (a) *S*-wave amplitudes from set (2).

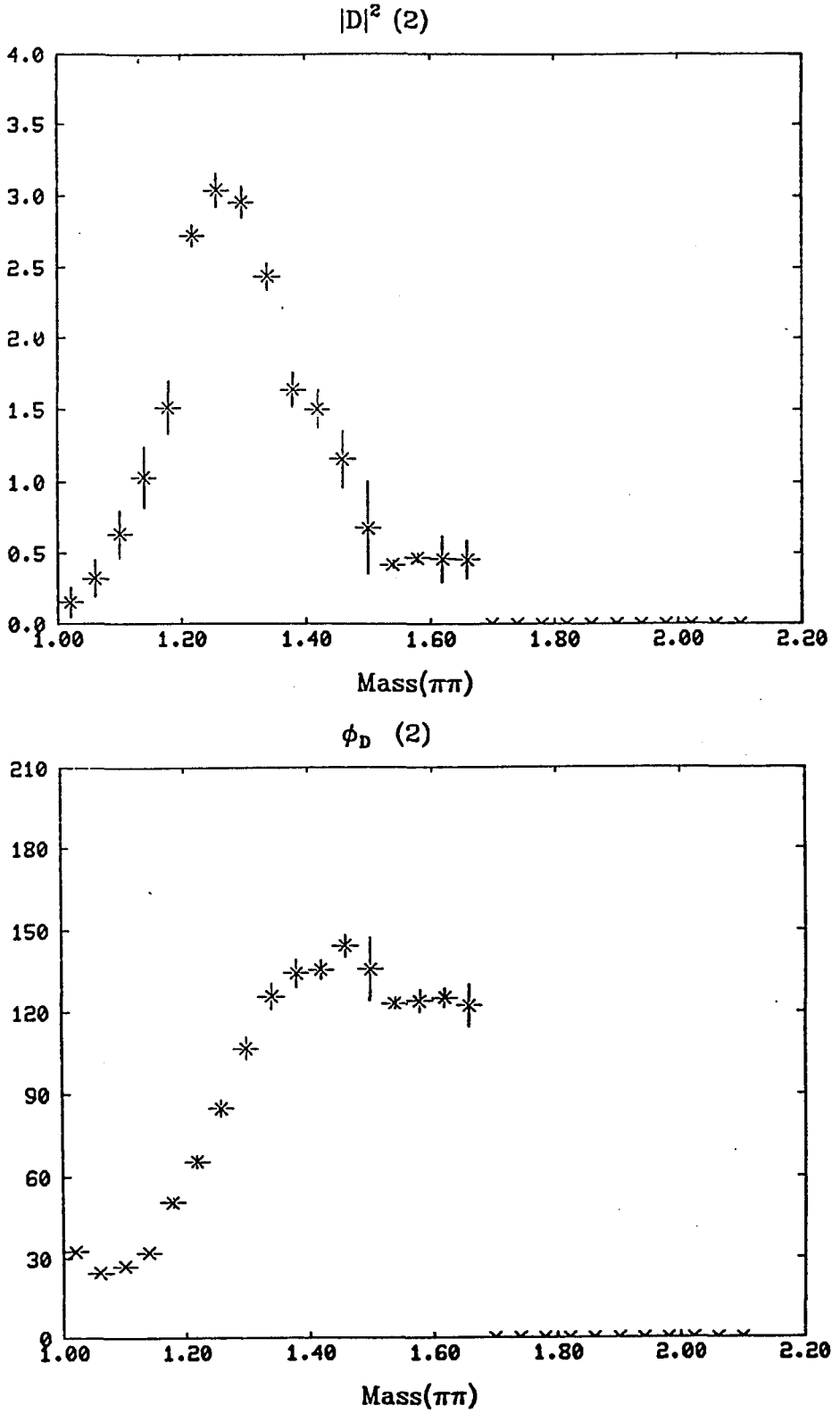

Fig. 2.2 (b) *D*-wave amplitudes from set **(2)** .

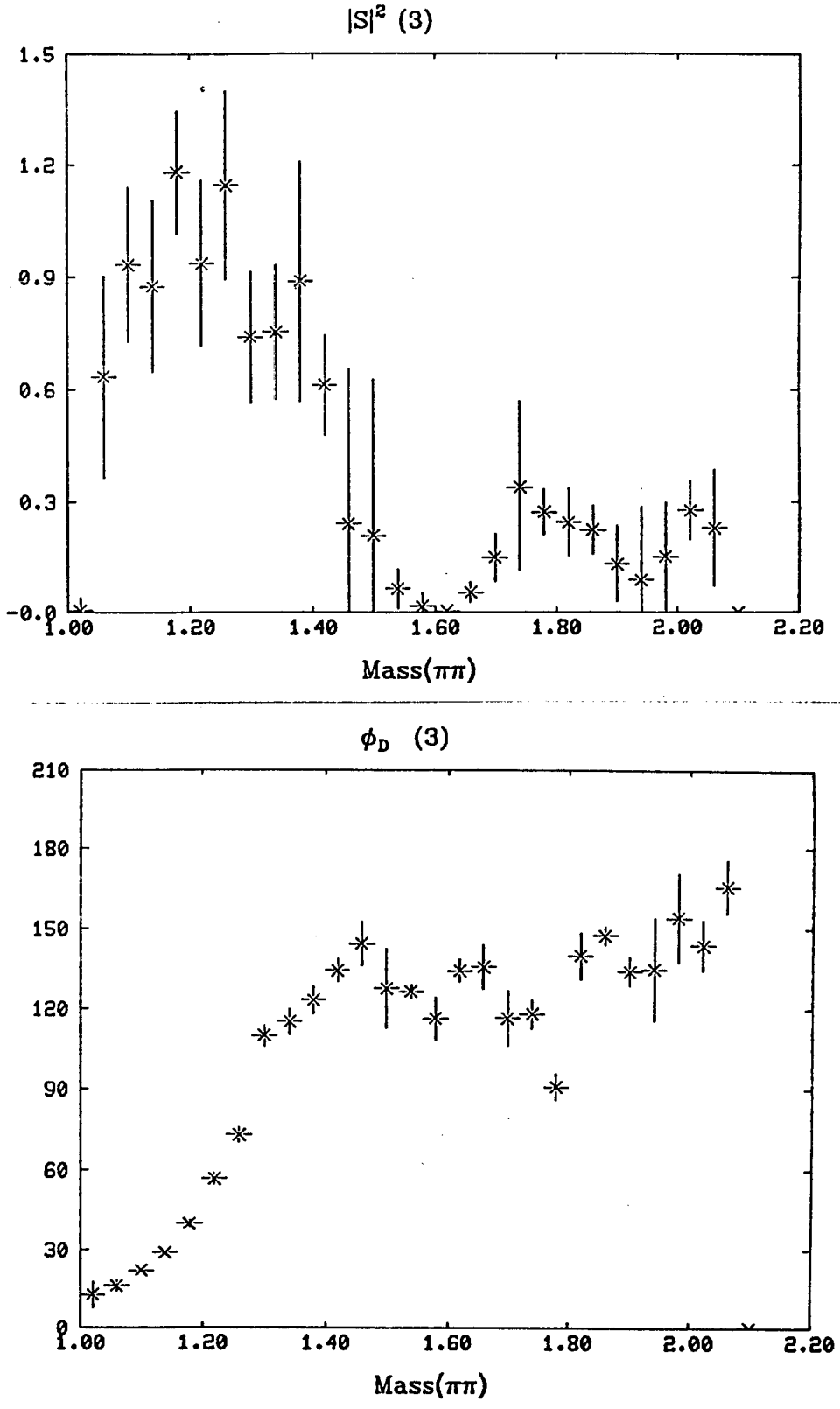

Fig. 2.3 (a) *S*-wave amplitudes from set (3).

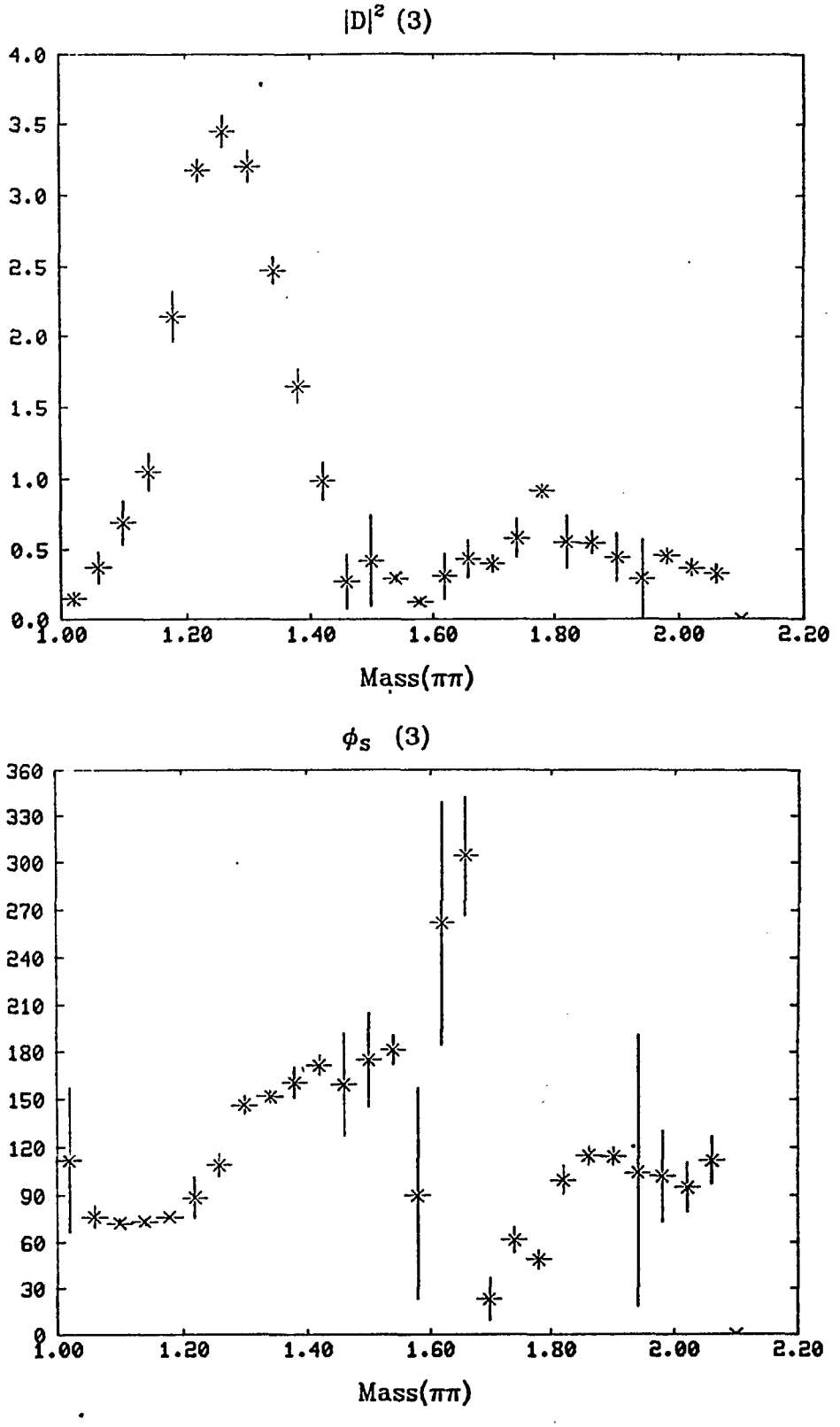

Fig. 2.3 (b) *D*-wave amplitudes from set **(3)**.

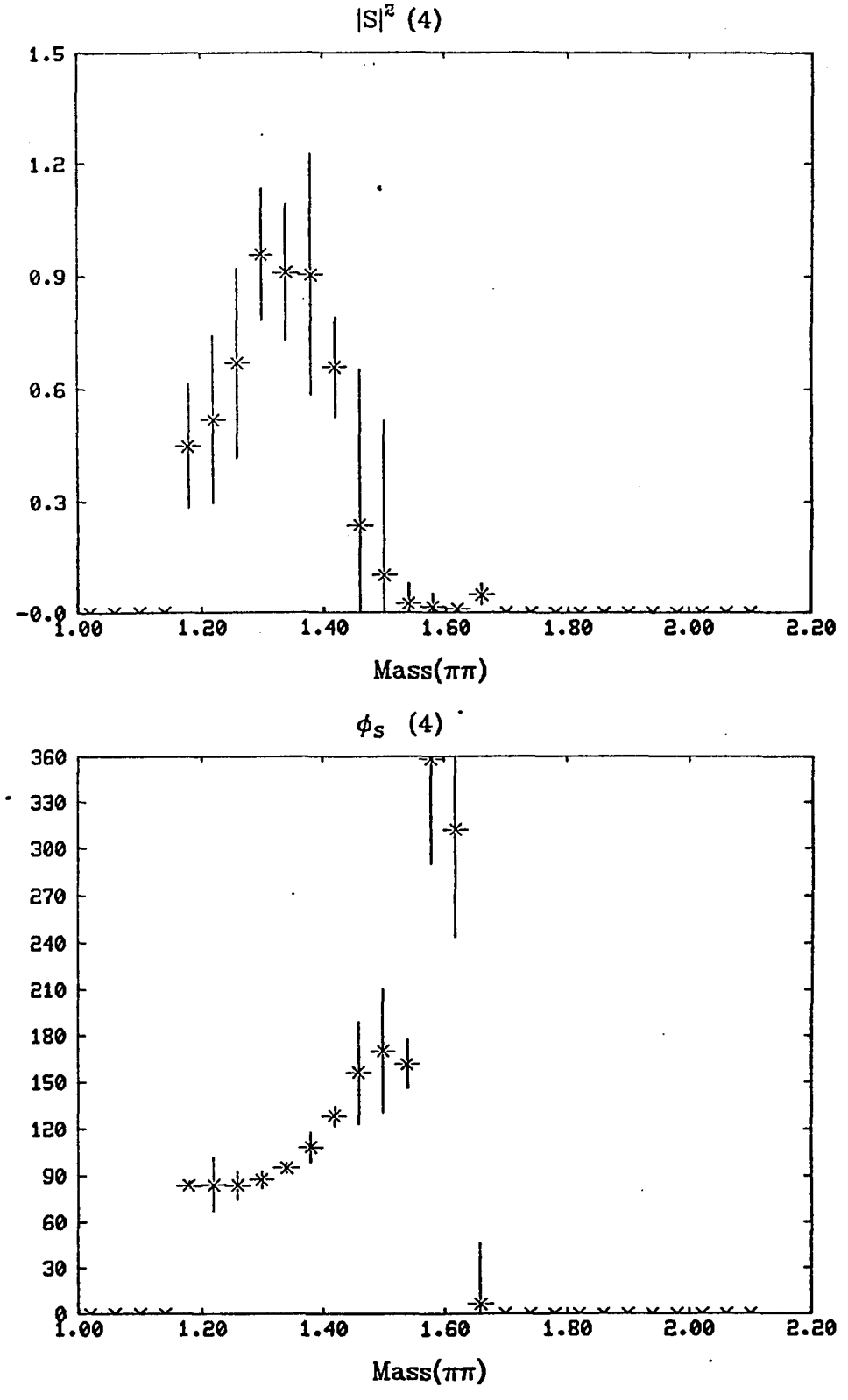

Fig. 2.4 (a) S-wave amplitudes from set (4).

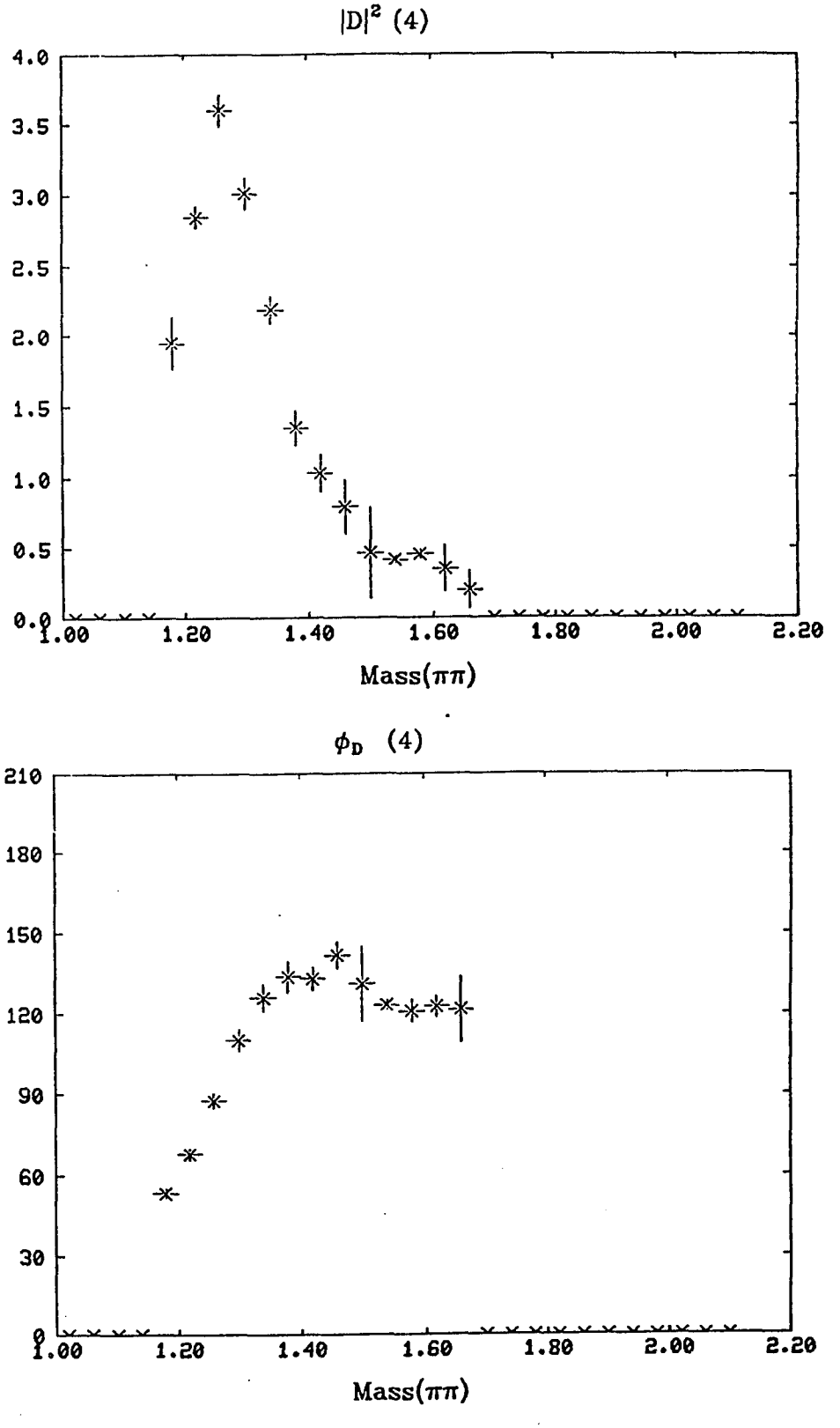

Fig. 2.4 (b) ***D*-wave amplitudes from set (4).**

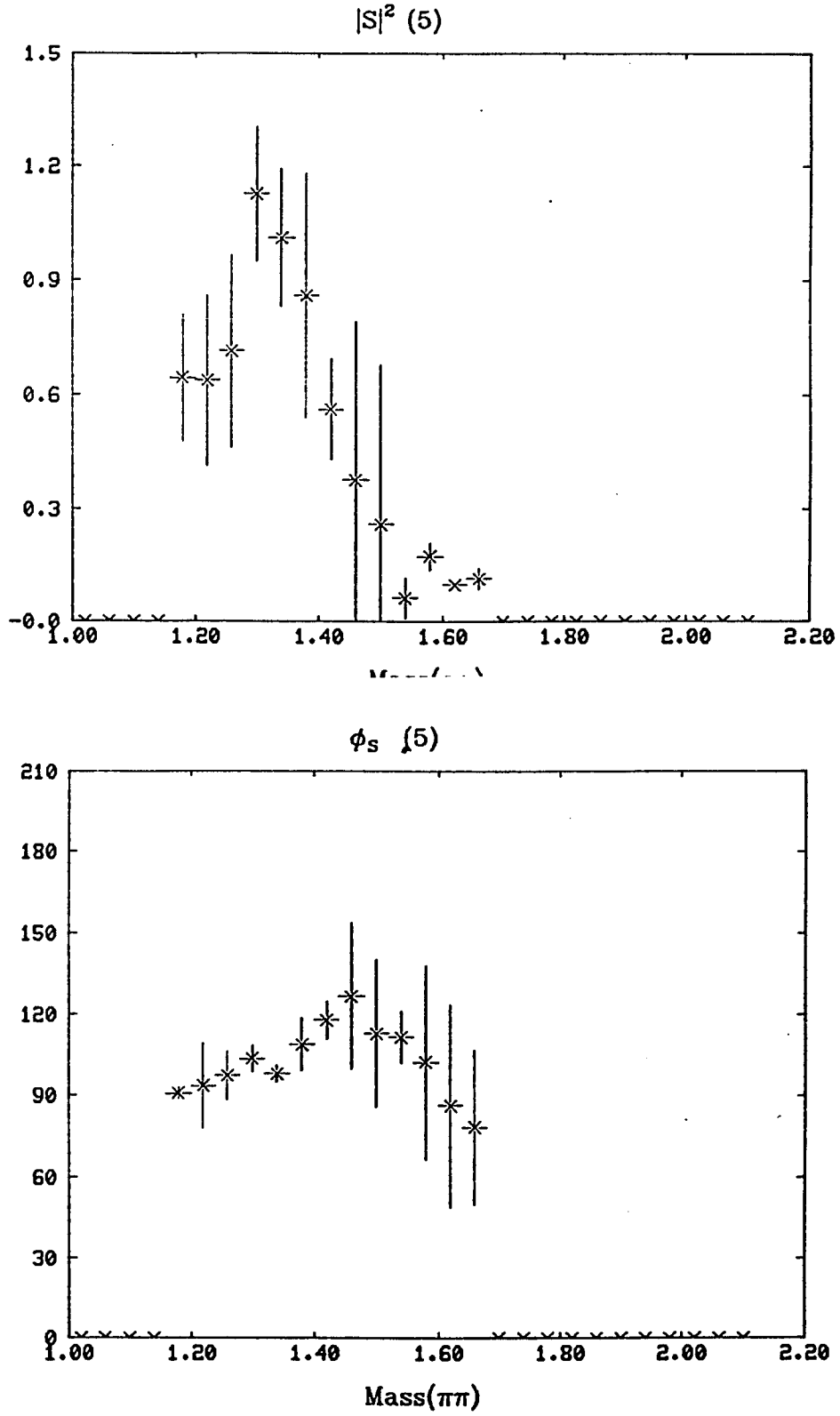

Fig. 2.5 (a) *S*-wave amplitudes from set (5).

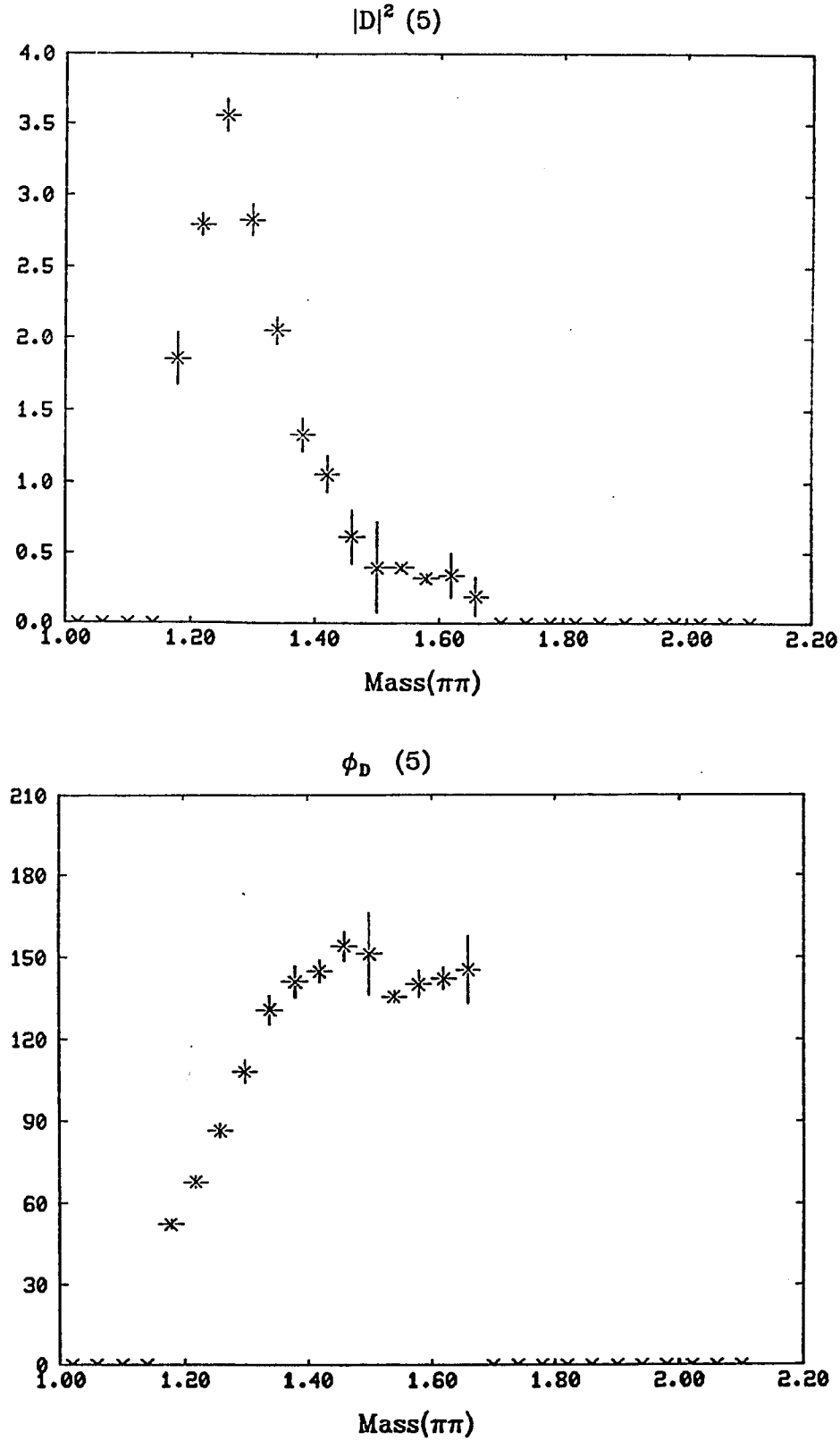

Fig. 2.5 (b) *D*-wave amplitudes from set (5) .

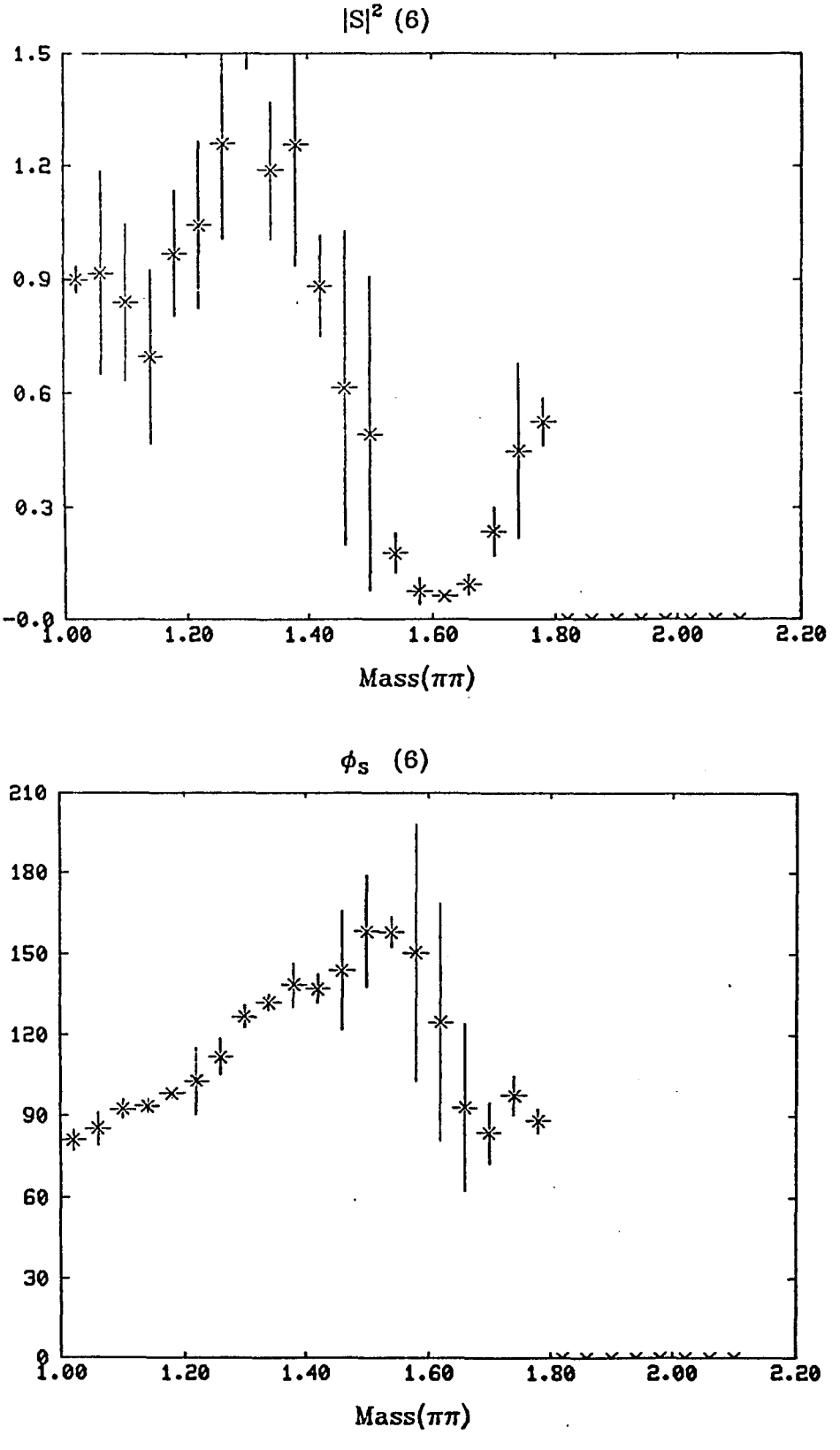

Fig. 2.6 (a) *S*-wave amplitudes from set (6).

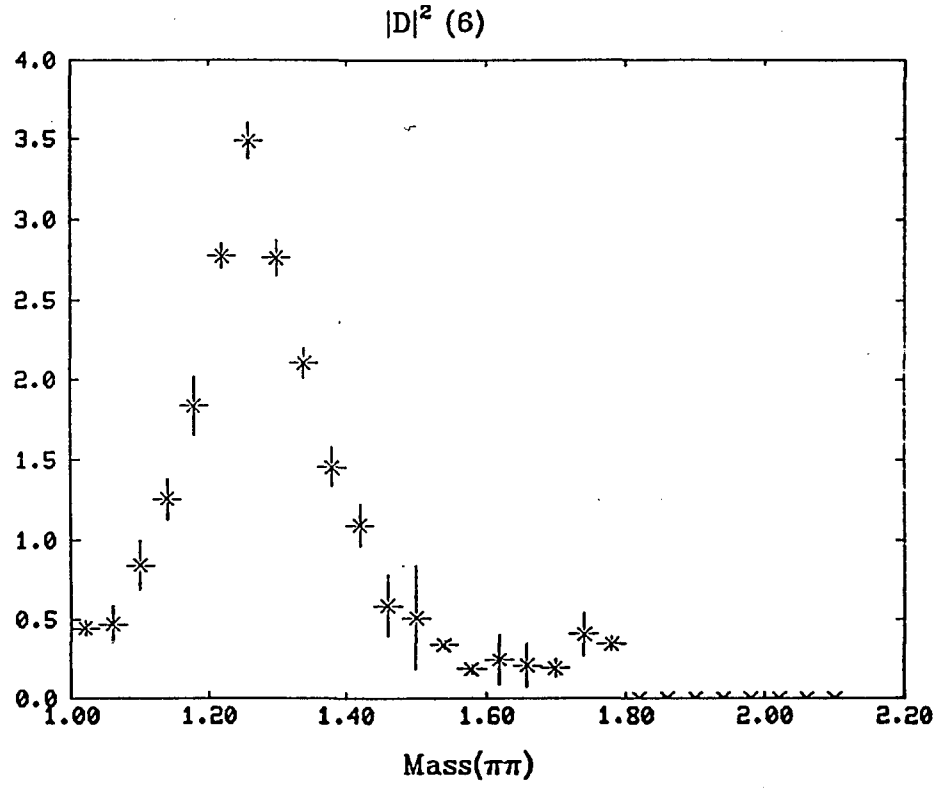

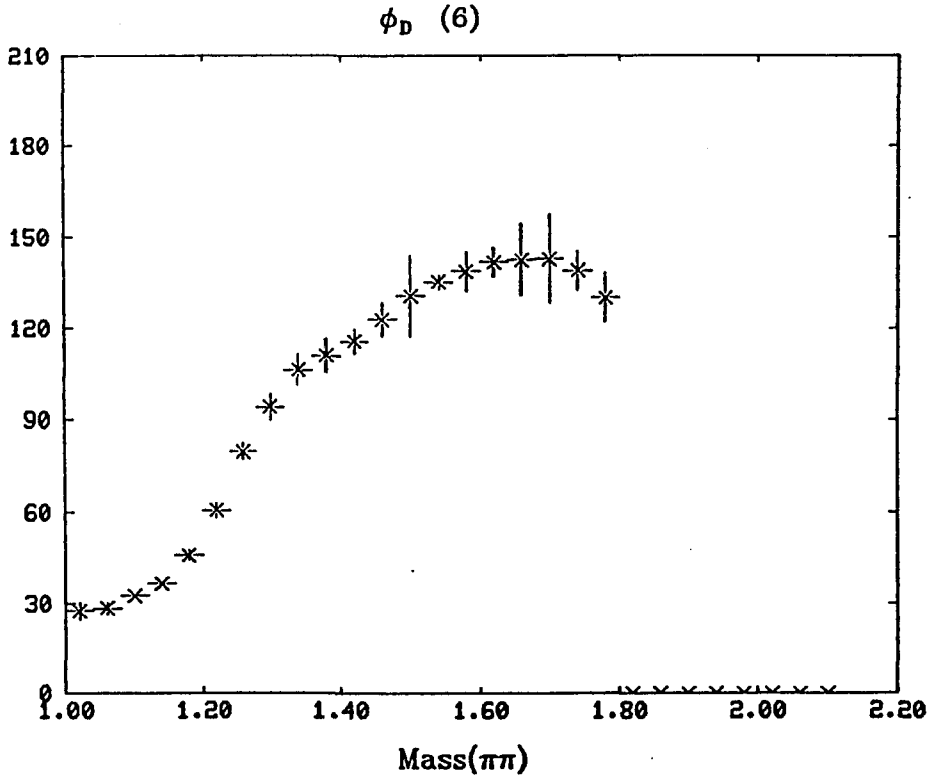

Fig. 2.6 (b) *D*-wave amplitudes from set (6)

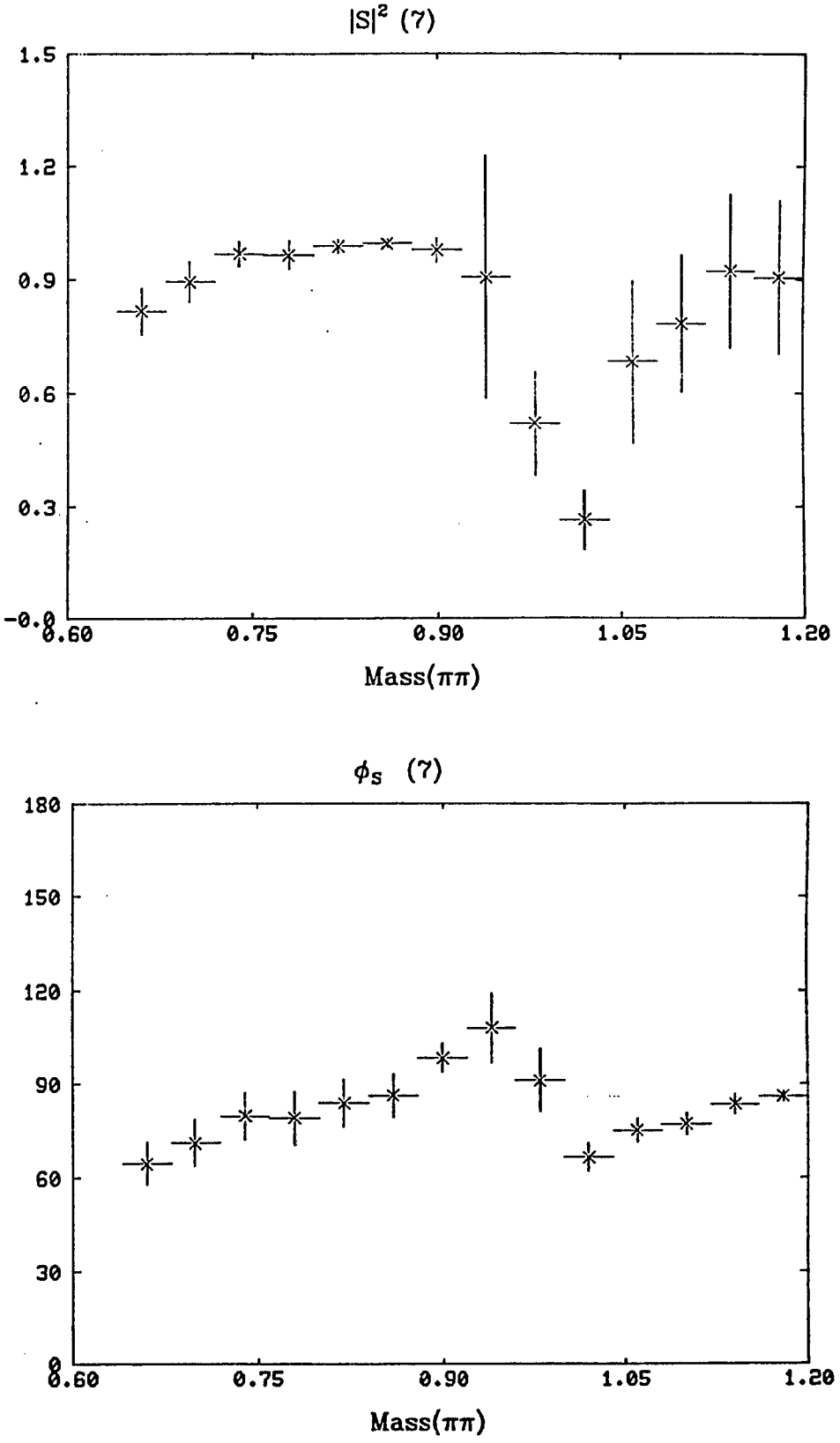

Fig. 2.7 (a) *S*-wave amplitudes from set (7).

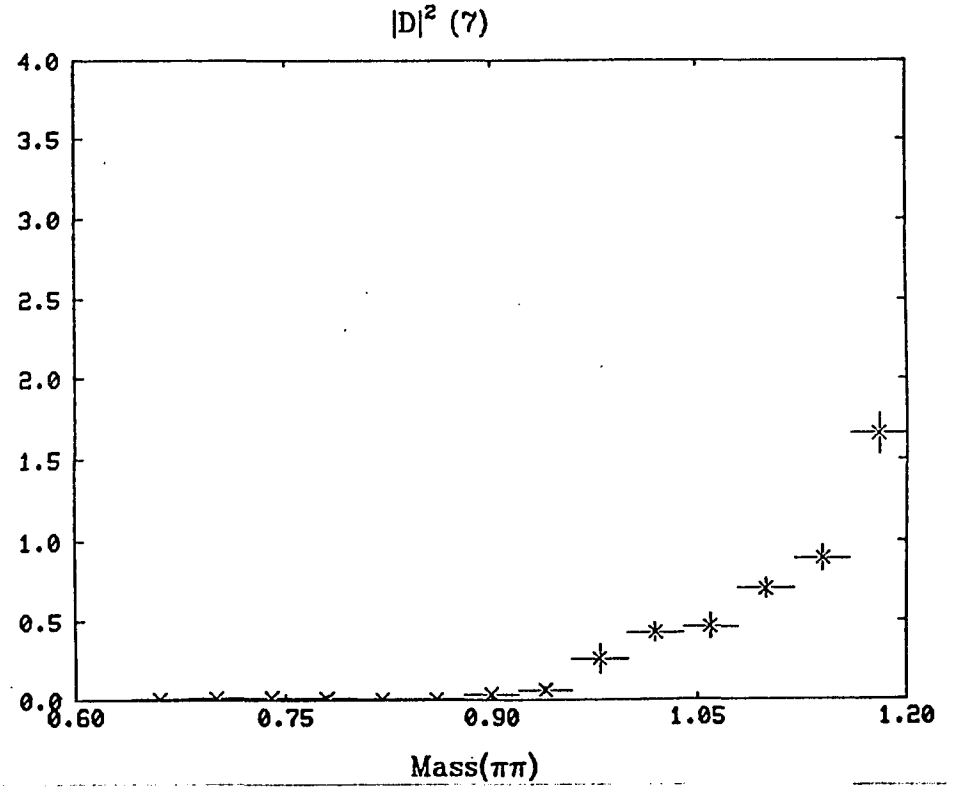

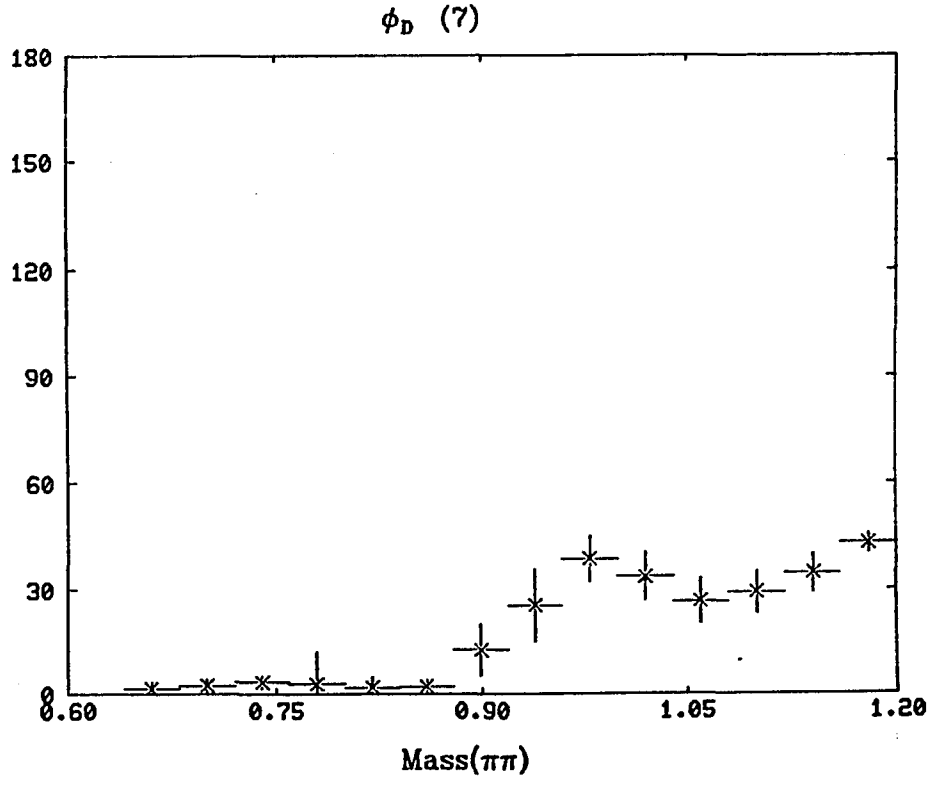

Fig. 2.7 (b) *D*-wave amplitudes from set (7).

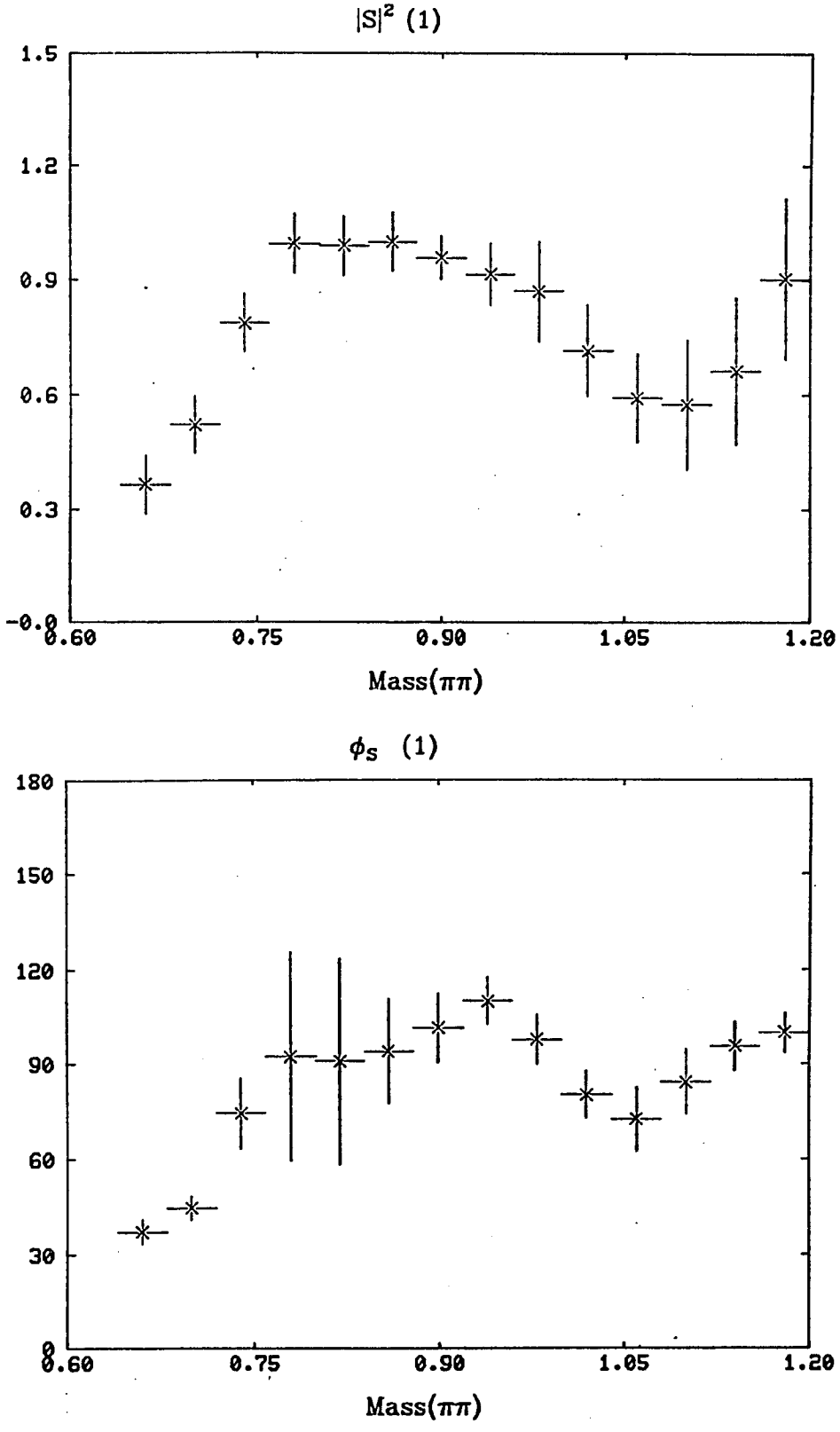

Fig. 2.8 (a) *S*-wave amplitudes from set (1) below 1.2 Gev/c^2.

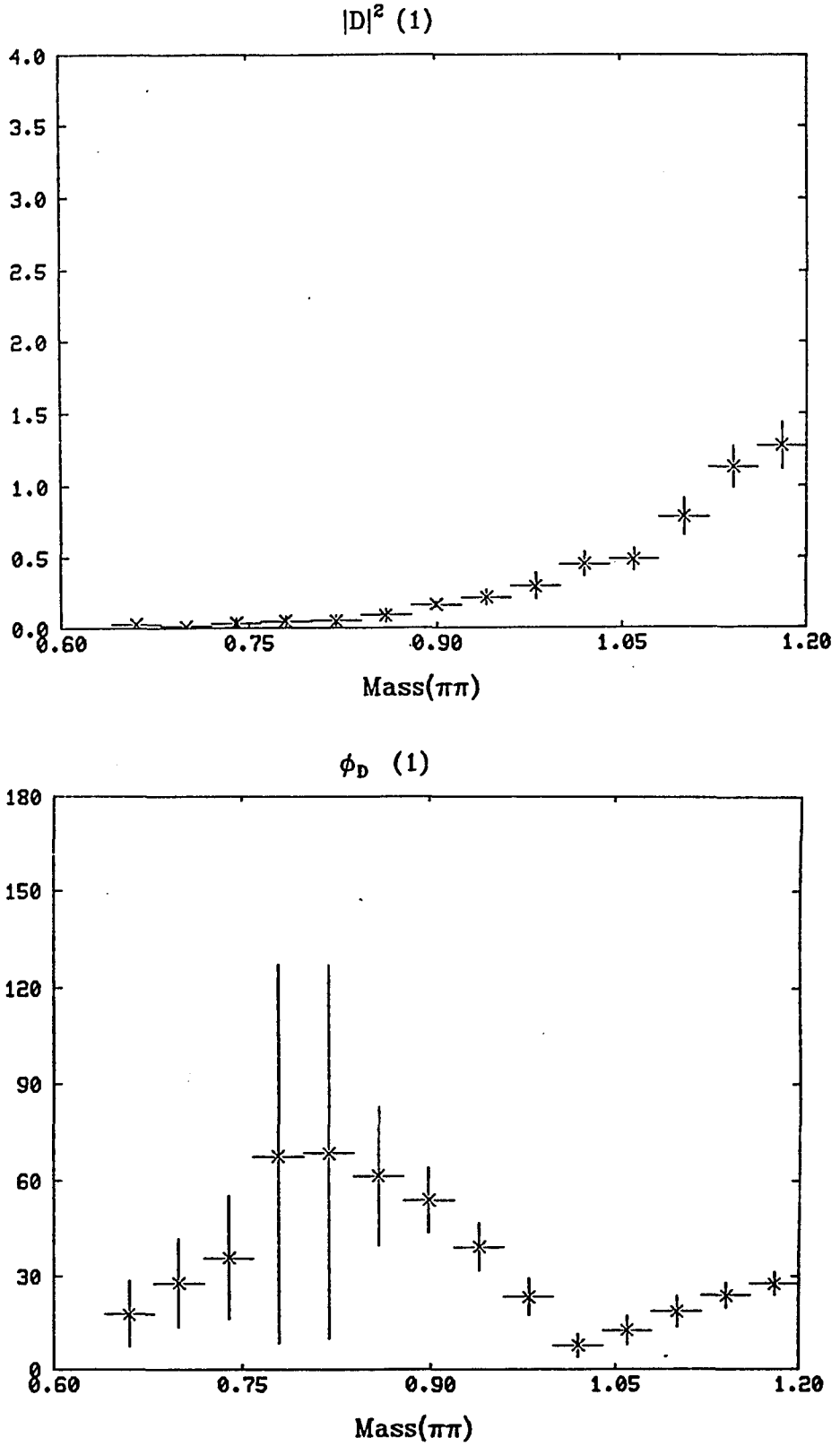

Fig. 2.8 (b) *D*-wave amplitudes from set (1) below 1.2 Gev/c^2.

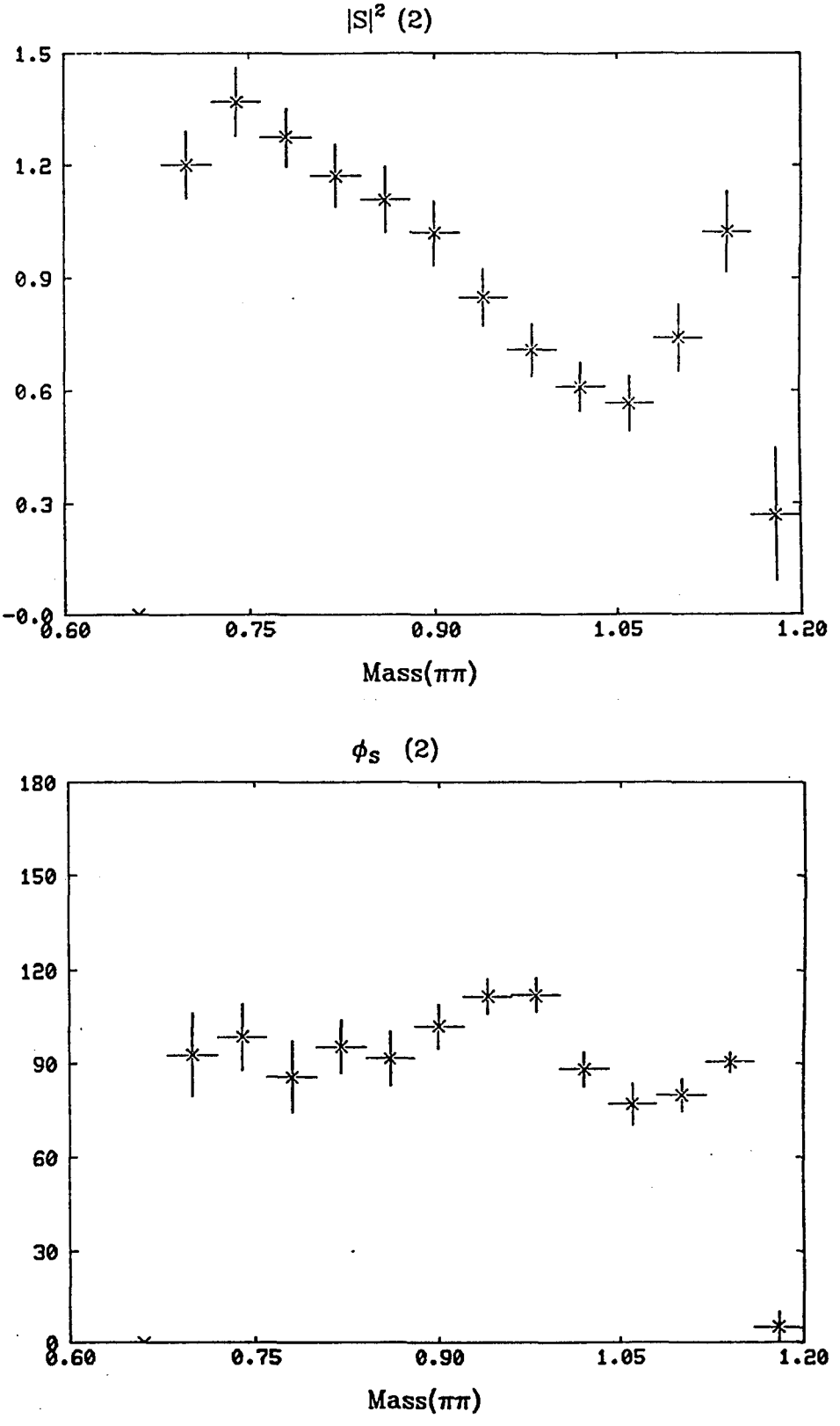

Fig. 2.9 (a) S-wave amplitudes from set (2) below 1.2 Gev/c^2.

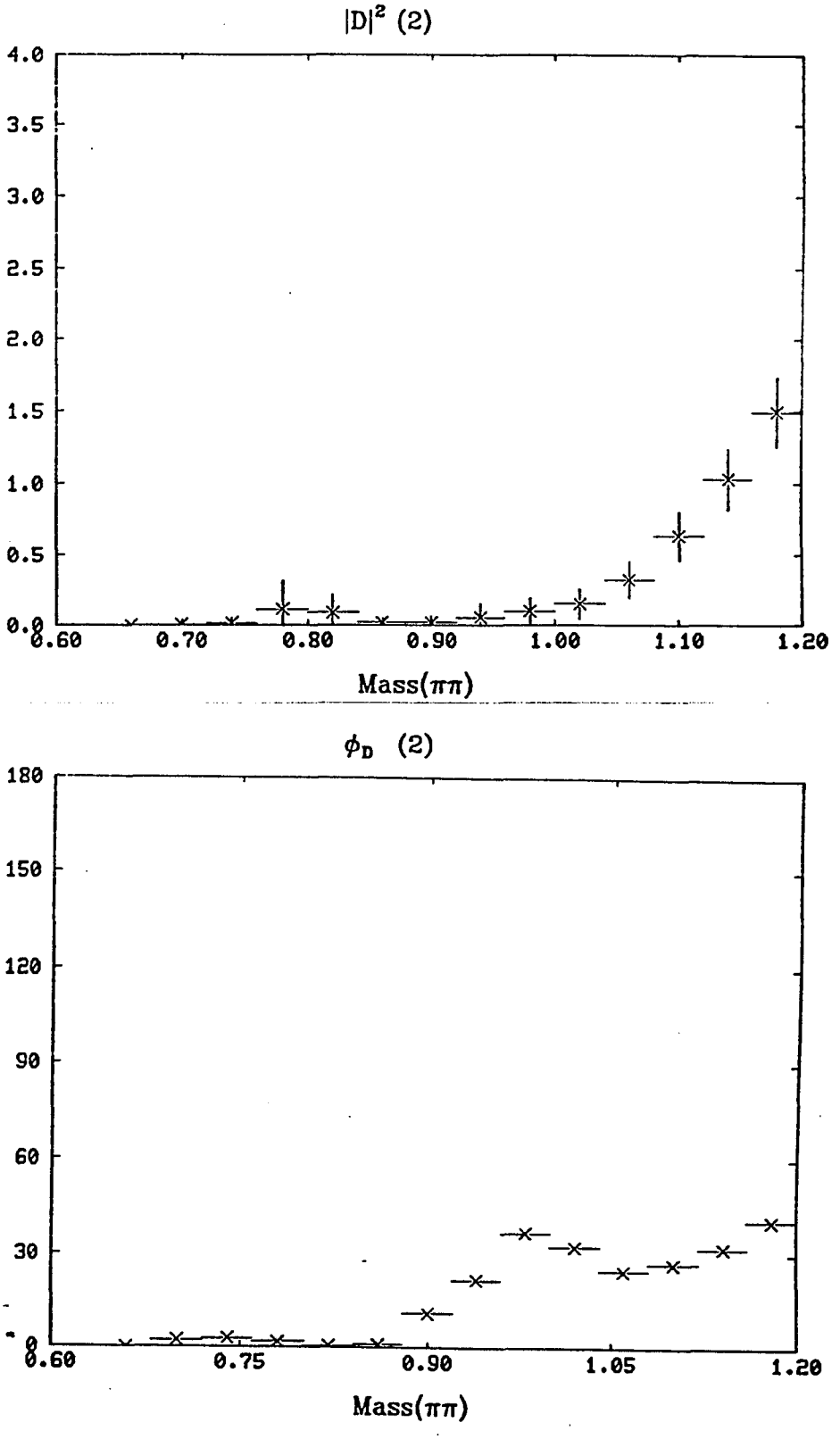

Fig. 2.9 (b) ***D*-wave amplitudes from set (2) below 1.2 Gev/c^2, phases are the same as those of (7).**

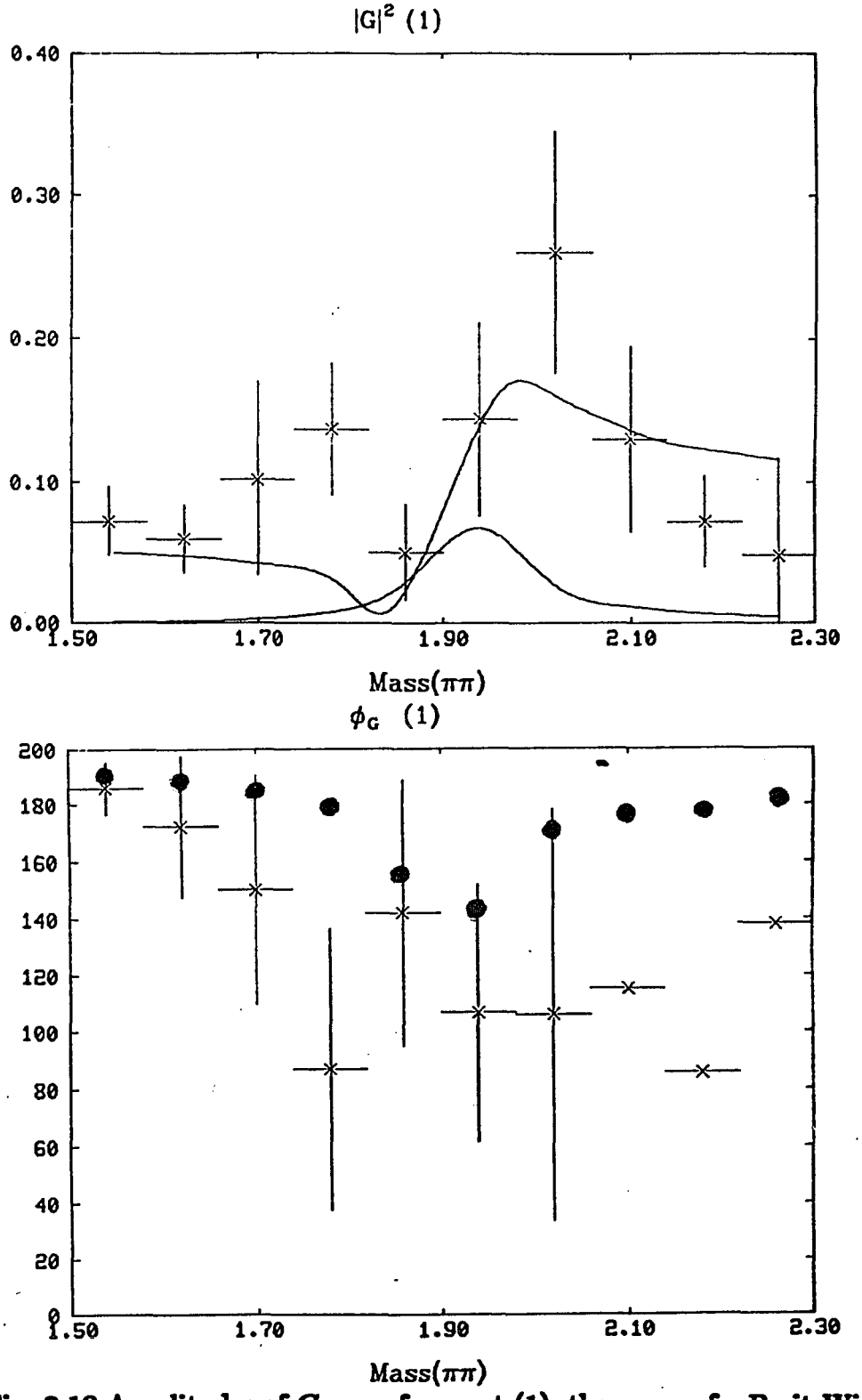

Fig. 2.10 Amplitudes of G-wave from set (1), the curve of a Breit-Wigner shape is at th level of $f_4(2030)$, the other curve is the result of the fit described in the text including the background, dots show the results of the fit for the phases, errors of the last three bins of ϕ_G are 360^0.

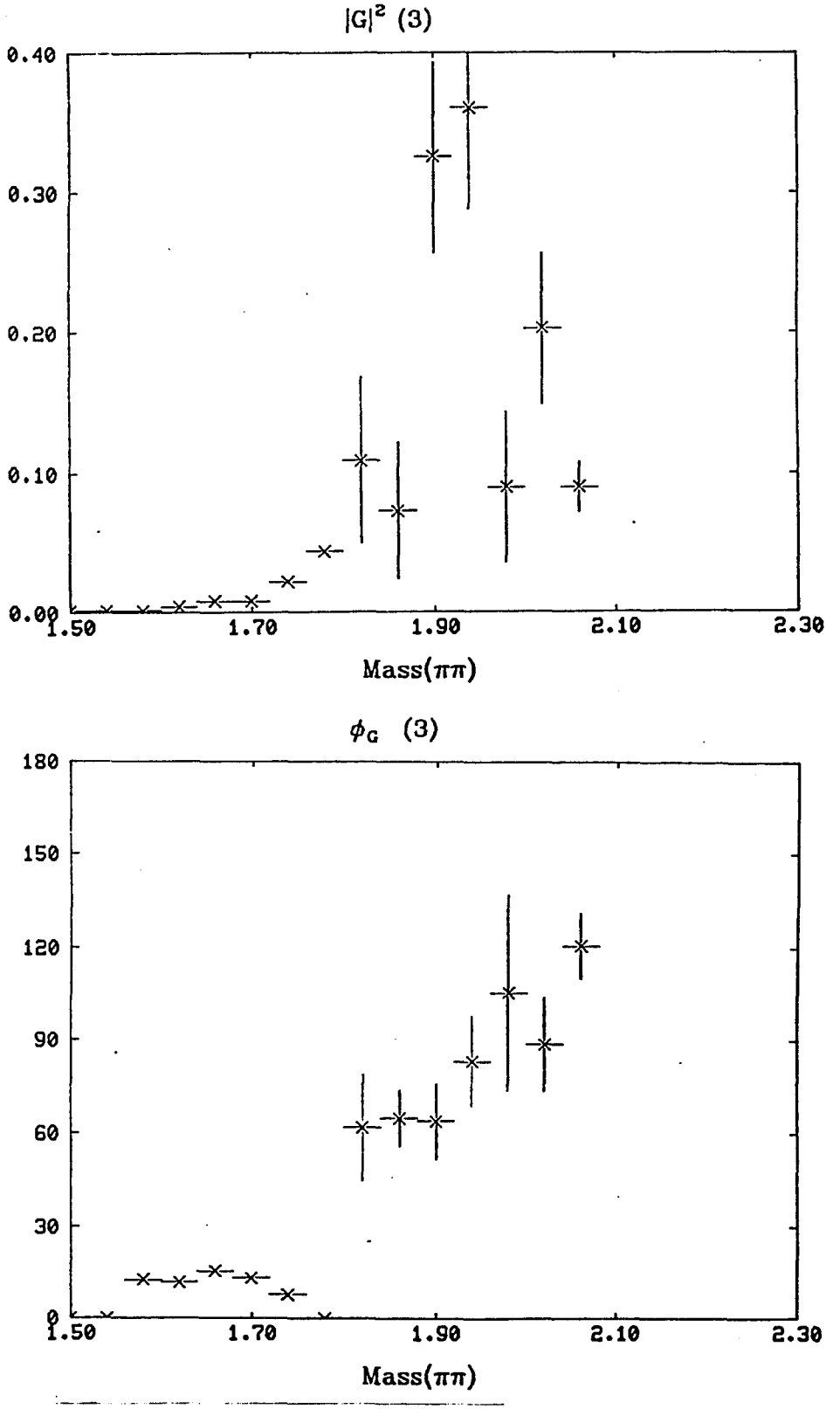

Fig. 2.11 *G*-wave amplitudes from set (3).

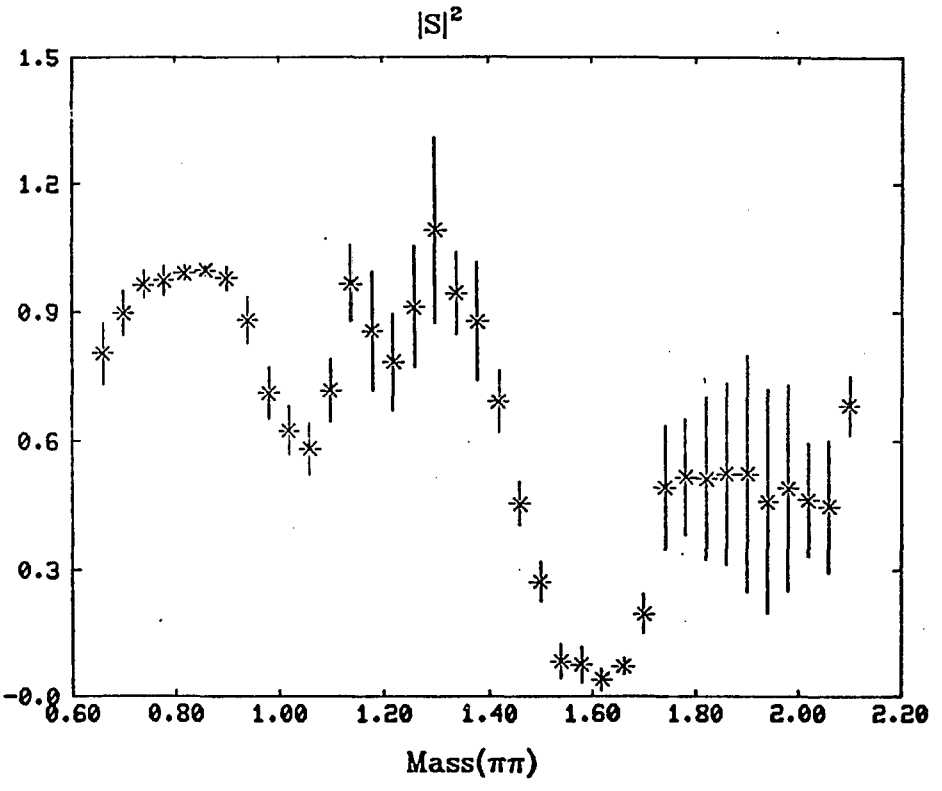

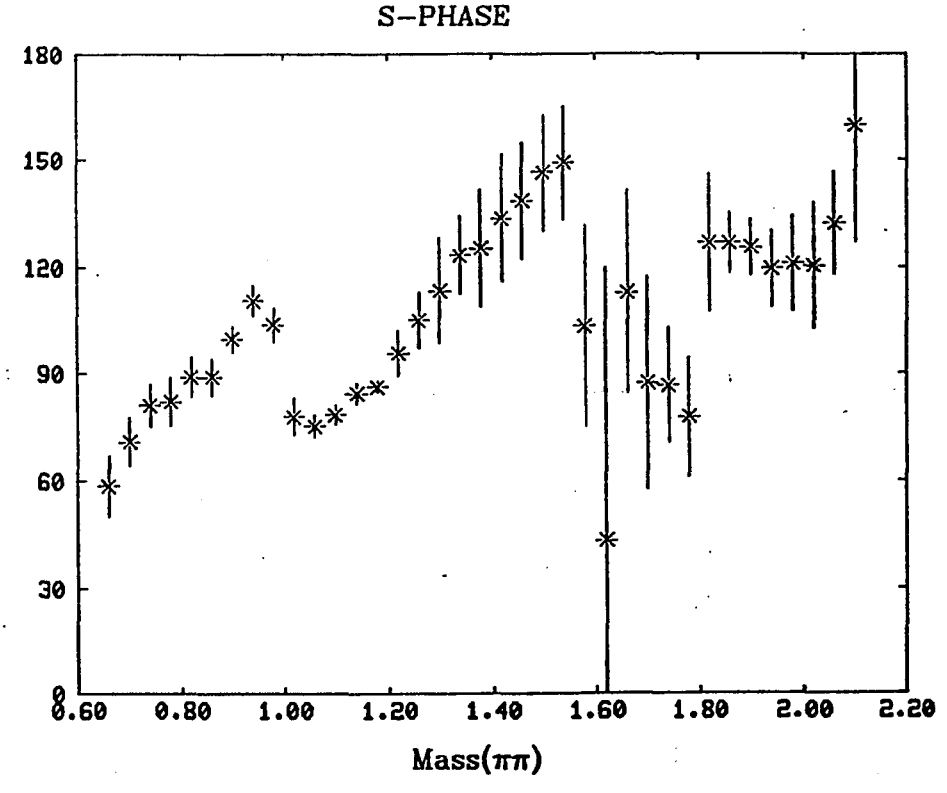

Fig. 2.12 (a) Averages of *S*-wave.

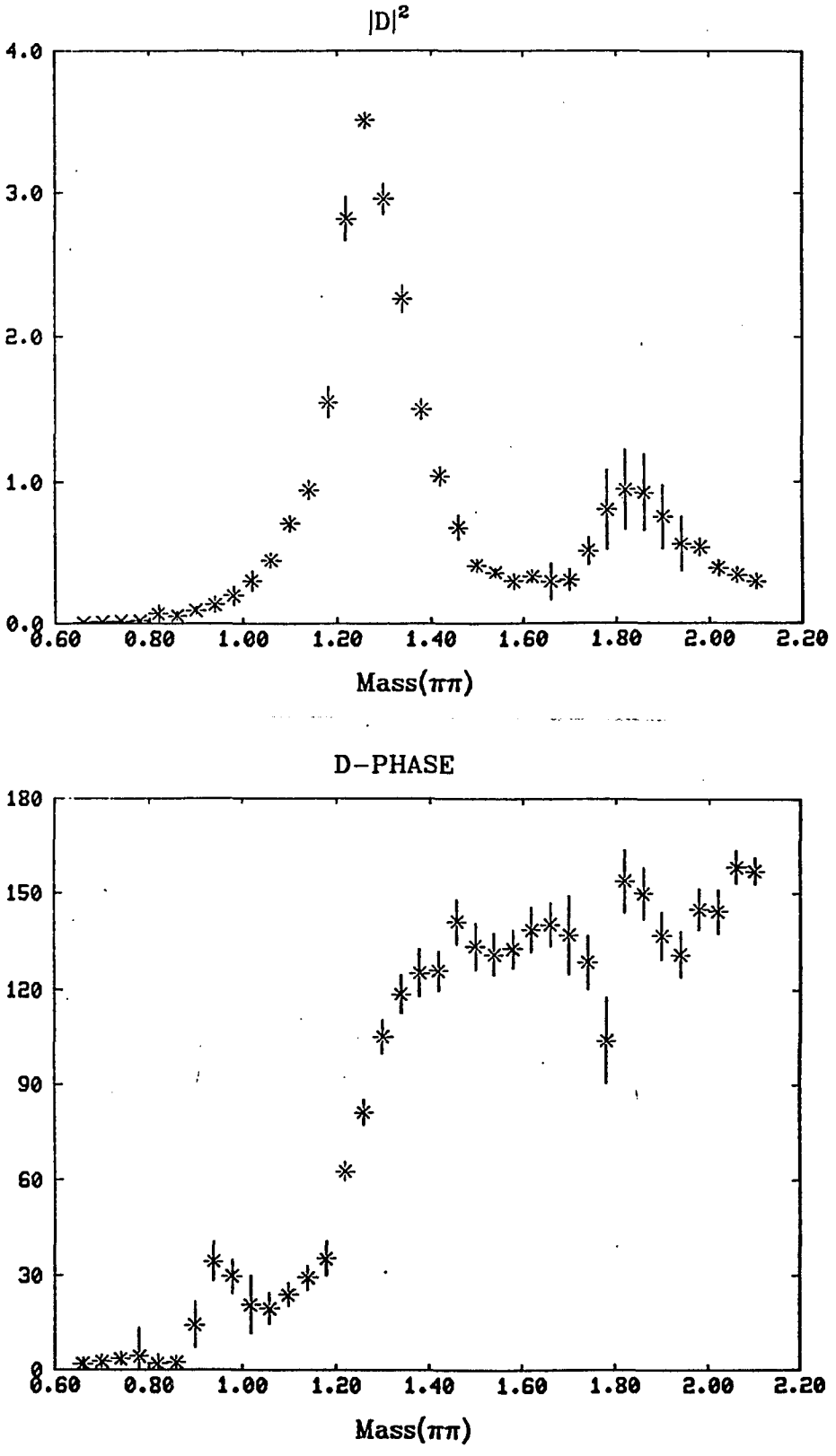

Fig. 2.12 (b) Averages of *D*-wave.

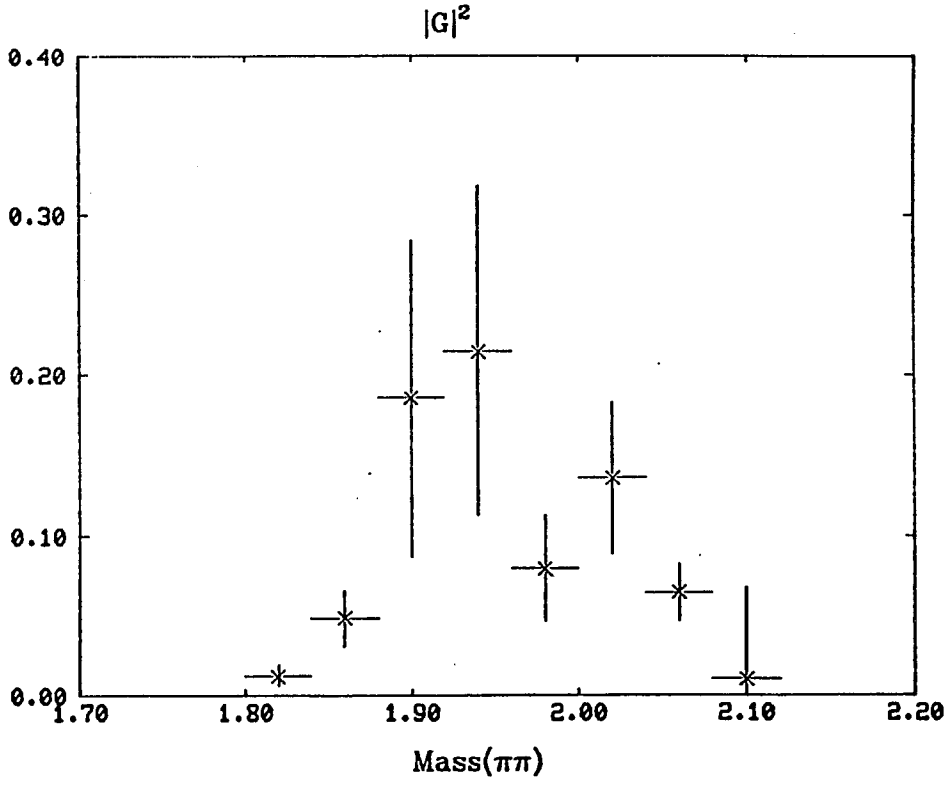

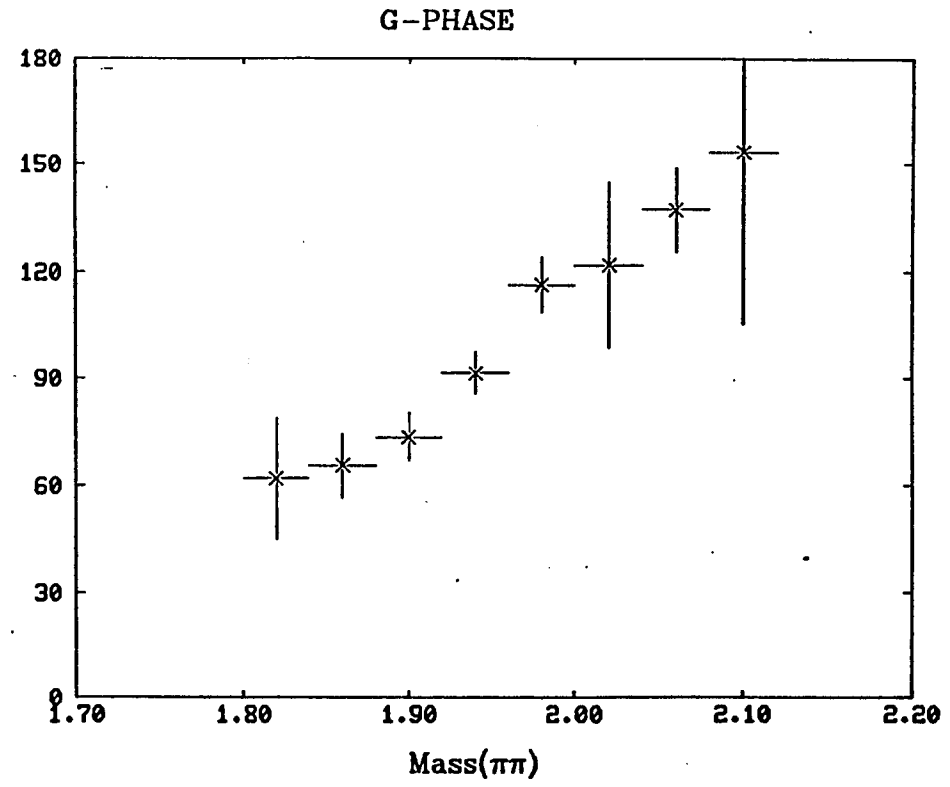

Fig. 2.13 Averages of *G*-wave.

Chapter 3 The $K\bar{K}$-Data

3.1 The π-induced $K\bar{K}$ data

The following data sets for π-induced $K\bar{K}$ production are available.

i) V. A. Polychronakos *et al.*[19]

ii) W. Wetzel *et al.*[20]

iii) D. Cohen *et al.*[21]

iv) G. Costa *et al.*[22]

v) MPS I experiment[23]

vi) MPS II experiment[24]

The amplitudes were again extracted from the raw data by assuming the one-particle-exchange mechanism.

The amplitudes to describe the following two reactions,

$$\pi^- p \rightarrow K^+ K^- n \tag{3-1}$$

$$\pi^- p \rightarrow K^0 \bar{K}^0 n \tag{3-2}$$

are denoted by $A_{K^+K^-}$ and $A_{K^0\bar{K}^0}$, these amplitudes can be decomposed,

$$A_{K^+K^-} = I_0 + I_1$$

$$A_{K^0\bar{K}^0} = I_0 - I_1$$

where I_0 and I_1 are the isospin 0 and 1 parts. By charge independence the amplitudes for the reaction,

$$\pi^+ n \rightarrow K^+ K^- p \tag{3-3}$$

is $A_{K^0\bar{K}^0}$. Consequently a comparison of the amplitudes from two reactions (3-1) and (3-3) can be made in order to determine the amplitudes with specific isospin.

Cohen *et al.* studied the isospin components measured in the two reactions. The t-distributions of the squared modulus of the partial amplitudes that are separated into these isospin channels show that the isospin 0 part indeed dominate the cross section in the low $|t|$ region if one considers the S- and D-waves. Since their analysis covers the low mass region (below $M_{K\bar{K}}$=1.6 Gev/c^2), one can not make rigorous statements about the high mass region. But one can safely assume that the partial amplitudes (S-, D-, and G-waves) in the reaction,

$$\pi^- p \rightarrow K_s^0 K_s^0 n$$

are dominated by the I=0 amplitudes.

Fig. 3.1 and Fig. 3.2, taken from the ref. 23, show the squared modulus of the S-amplitudes and the $S-D$ relative phases of these data sets i) through v) as a function of the $K\bar{K}$ invariant mass. The over-all agreement is reasonably good. The same statement can be made about the D-wave amplitudes upon a comparison of these data sets. The data sets v) and vi) cover the largest region in the $K\bar{K}$ invariant mass up to 2.40 Gev/ c^2 and the total number of events of the set v) was approximately 15000, this number is clearly enough to do any meaningful analysis. The analysis of this data set was done(ref. 23 and ref. 25). The major discrepancy among the data sets is seen in the $S-D$ relative phases around the $K\bar{K}$ threshold. In the analysis, moments $\langle Y_l^m \rangle$ with m=2 were all set equal to zero by hand in the process of extracting amplitudes from the moments. This constraint introduced systematic problems making the S-waves and D-waves develop correlations. Correlations of this kind are dangerous especially near the $K\bar{K}$ threshold where the $|D|^2$ is very small. In the analysis of new data from a high-statistics(40494 events)experiment at MPS II, the data set vi), the moments with m=2 were set free. It should be noted that the techniques employed to perform

the moment analysis were essentially the same in the new analysis. This is described in the old publication(ref. 23). The resulting $S-D$ relative phases turned out to be large (roughly 180 degrees) with large error bars. Fig. 3.3 and Fig. 3.4 show new results along with the old ones. The discrepancy is resolved now in favor of the large relative phases near the threshold. A general conclusion is that the $S-D$ phases in $K_s^0K_s^0$ production are around 180 degrees and difficult to determine with reasonable accuracy near the threshold of the $K_s^0K_s^0$ invariant mass. This high-statistics experiment at the MPS II had made use of drift chambers which gave better resolution than the old spark chambers. This fact is reflected in the smaller error bars of the data points and the finer sizes of mass bins. These features clearly constitute our taking this $K_s^0K_s^0$ data for the multi-channel K-matrix fit.

The general features of the $K_s^0K_s^0$ data v) and vi) are now discussed.

Two sets of amplitudes below $M(K_s^0K_s^0)$=1.6 Gev/c^2 and four sets of amplitudes above this mass exist due to the ambiguities inherent in the amplitudes. In our analysis, one particular set was chosen which was the same as the old set in the old analysis. Its criteria was that these amplitudes had the smallest number of resonances, also physical consistency among the mixing angles of the established resonances was confirmed in this choice of the amplitude set.

A prominent structure is seen both in the S-wave and the D wave below 1.60 Gev/c^2. In the mass-dependent fit, two resonances, the $f_0(980)$ and the $f_0(1300)$, were necessary to understand the S-phases in this region. One important result of the old study was that the statistical significance of the $f_0(980)$ was merely 0.6σ and its effect was seen only at the threshold. The modulus squared of the S-wave, $|S|^2$, around 1.30 Gev/c^2 presented substantial difficulties in the old analysis as

it is seen clearly in Fig. 3.3. In the region around the $f_0(1300)$ the fit is indeed seen to be rather inadequate. Small error bars of $|\phi_S - \phi_D|$ between 1.20 Gev/c^2 and 1.60 Gev/c^2 apparently made these relative phases more significant statistically than the amplitudes modulus squared in the fit. This was remedied later(ref. 25) by introducing another state $f_0(1240)$ (Fig. 3.3c, 3.3d), the statistical significance of this state was determined to be 7σ, the improvement is clearly seen in the $|S_0|^2$. It is clear from Fig. 3.4 that the structure in $|S_0|^2$ around 1.30 Gev/c^2 is different somewhat. This difference may be related to the above-mentioned fact that the moments with m=2 were all set free in the new moment analysis. This new state claimed in the old analysis did not change the previous understanding of the relative phases, but the statistical significance of this state $f_0(1240)$ came mainly from the fit to the $|S_0|^2$ data, its significance is illustrated by the shoulder around 1.30 Gev/c^2. The understanding of the S-wave spectrum above 1.60 Gev/c^2 required another state, $f_0(1730)$, upon a careful investigation of the relative phases $|\phi_S - \phi_D|$ which indeed showed a remarkably rapid forward motion of approximately 100 degrees in the interval of 300 Mev/c^2 . The statistical significance of this was 10σ, necessity of this state to understand the spectrum is thus highly impressive.

The region above 2.10 Gev/c^2 in the new data contains a modest enhancement peaked at around 2.20 Gev/c^2, the relative $S-D$ phase is roughly 50 degrees. This phase motion is marginal to assume a new state in this region. However this mass region is important since several resonances have been claimed, examples are the $X(2020)$ observed at SLAC and the $f_0(2240)$. An attempt was made to fit this part of the $K_s^0K_s^0$ S-wave spectrum by a relativistic Breit-Wigner form,

$$T = \frac{f}{m^2 - s - im\Gamma}$$

where m is the mass of the assumed resonance, s is the squared invariant mass and Γ is the width of the state, and f is another parameter.

The best fit gave the following values of the parameters,

$$m = 2.240 \text{Gev/c}^2$$

$$\Gamma = 0.202 \text{Gev/c}^2$$

$$f = 0.471 \times 10^{-1} (\text{Gev/c}^2)^2$$

with the total χ^2 of 2.71 for 8 bins. This is, of course, an excellent fit. The fit results show that the structure of the spectrum in this mass region is consistent with one almost purely Breit-Wigner shape, and a background is unnecessary to understand the region.

The D-wave spectrum did not create any serious difficulties, an interference between the $f_2(1270)$ and the $f_2'(1525)$ adequately described the spectrum up to 1.70 Gev/c^2. The region above 1.60 Gev/c^2 is seen to be almost structureless, one broad background of the Breit-Wigner form was sufficient. The region between 1.60 Gev/c^2 and 1.80 Gev/c^2 was extensively investigated in this analysis as we report the detailed results later. The motivation for this analysis was to see the possibilities to establish the $f_2(1720)$ in the hadronic $K_s^0 K_s^0$ production. In the old analysis the $f_2(1720)$ was not necessary, but it was thought that with smaller bin sizes due to the improved mass resolution and smaller error bars of the data points the new data might show fine structure in this mass region. The predicted phase ϕ_D was used to determine the S-wave phases ϕ_S as seen in Fig. 3.5, since only the absolute magnitude of the difference of the phases $|\phi_S - \phi_D|$ is measured in the $K_s^0 K_s^0$ production experiment.

The G-wave extends from 1.6 Gev/c^2 to 2.4 Gev/c^2. One Breit-Wigner form was used to fit the data. The fit appeared to be rather inadequate to understand

the G-wave amplitudes both in $|G_0|$ and ϕ_G. In the new moments analysis the moments with l=10 were all seen to be consistent with zero. Two spectra (new and old) are completely consistent with each other. One may naturally ask whether the G-wave contains two resonances. Several resonances with higher spin states, such as the $f_4(2300)$ and the $f_6(2510)$, have been claimed. The state $f_4(2300)$ is reported to have a $\pi\pi$ decay mode. Because of a highly stable phase motion as seen in the $|\phi_G - \phi_D|$ data, it will be difficult to build a hypothesis along this line, unless the D-wave amplitude contains a structure not seen in the $|D_0|$ but with a phase motion. This view is also supported by the fact that the acceptance of the detector decreases above 2.40 Gev/c^2, measurements of higher moments are made difficult due to this problem.

A remark should be made about the ratios of the visible cross sections of these waves above 2.0 Gev/c^2. One integrates the areas of the spectra, the ratios of these areas are directly proportional to those of the production cross sections. We obtain the following ratios,

$$\sigma_S : \sigma_D : \sigma_G = 1.0 : 7.2 : 4.1$$

Another independent determination of the ratio of the area under the $f_2(1270)$ peak to the area above 2.0 Gev/c^2 can be carried out. These numbers along with the well-known production cross section of the $f_2(1270)$ give a value of 400 nb for the cross section of the D-wave in this region.

3.2 The K-induced $K\bar{K}$ Data

K-induced $K\bar{K}$ production experiments have not been done extensively. One data set available to us comes from a CERN experiment[27]. The analysis carried out by the CERN group concentrated on the shape of the spectra. Based upon a fit to the

F-wave spectrum, a state f_3 (1850) was observed. A very important assumption they made was that waves with spin larger than 3 are negligible. Their data set extends to 2.0 Gev/c^2, clearly waves with higher spins become significant in the region above 1.8 Gev/c^2. Thus it is highly important to verify their assumption in the future by performing high-statistics experiments.

The D-wave spectra are completely dominated by the $f_2'(1525)$(figure will be seen in chapter 7). Due to the unavailability of the phase information in their publication, this data set is useful to study the width of the $f_2'(1525)$ in a consistent way, since we do not see this state as an enhancement in the $\pi\pi$ or π-induced $K\bar{K}$ data. The data from the K-induced $K\bar{K}$ production experiments yielded small statistics, the total number of events in these data vary in a range of 100 to 650. One clearly sees needs to perform high-statistics production experiments.

Finally a remark is to be made. The $\pi\pi$ data from a K-induced $\pi\pi$ production experiment should describe amplitudes for a process $K\bar{K} \rightarrow \pi\pi$, when a K-exchange is assumed through the O.P.E. mechanism. The amplitudes modules squared for this process should look the same as those for a process $\pi\pi \rightarrow K\bar{K}$, if the O.P.E. mechanism is exact. Unfortunately they do not look the same. This might invalidate our picture of the K-exchange in the reaction $K^-p \rightarrow K^+K^-\Lambda$. We can, however, consider exchanges of other particles in addition to K. It is very difficult to isolate these exchange processes from the K-exchange. We will not attempt this.

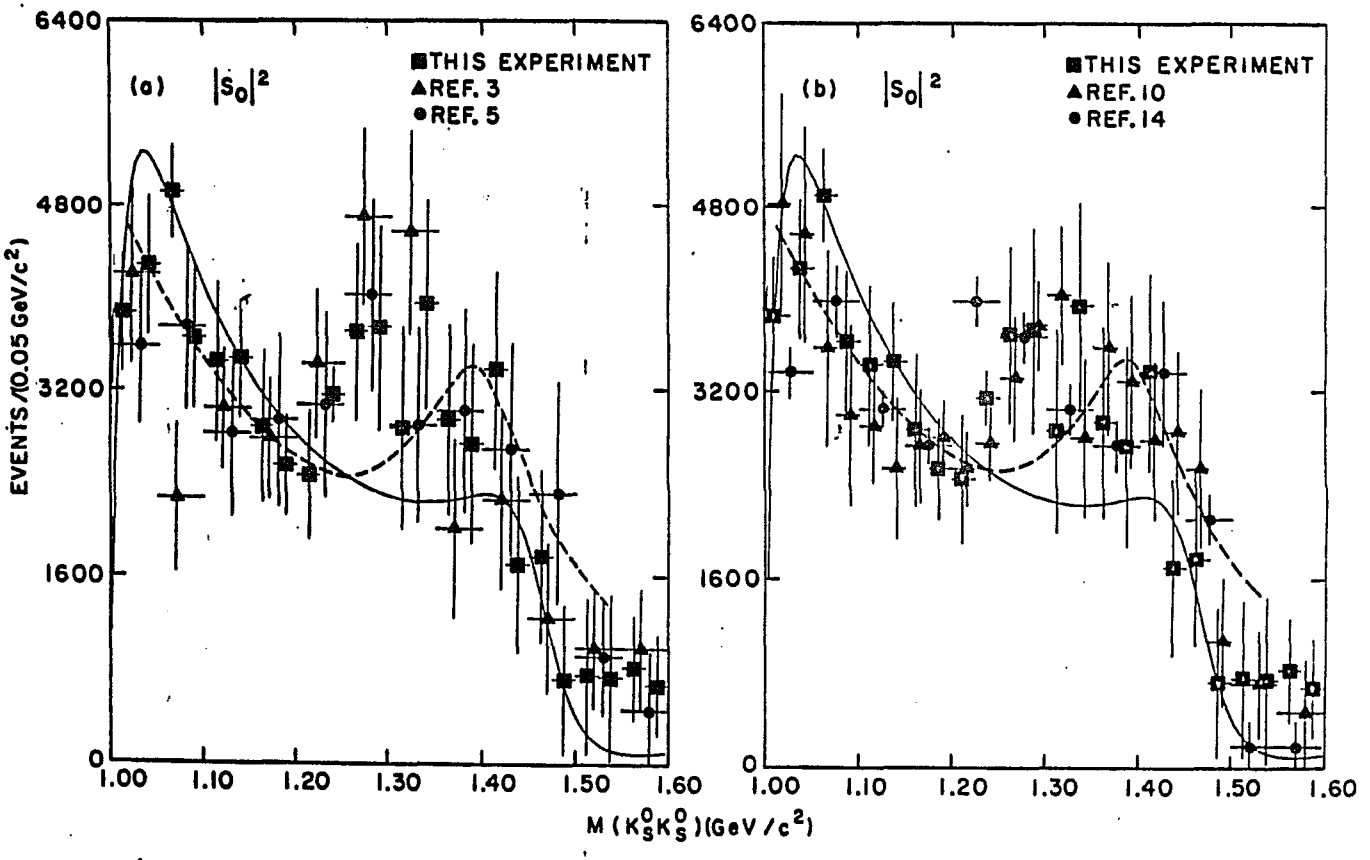

Fig. 3.1 Comparison of the squared modulus of the old S-wave solution as a function of the $K\bar{K}$ effective mass with those of Ref. 3(Ref. 19), 5(Ref. 20), 10(Ref. 21), and 14(Ref. 22). The solid curve is the result of the old mass-dependent fit(Ref. 26). The dashed curve is the fit of Irving *et al.*(Ref. 26). Some points have been displaced from the bin centers to avoid overlapping error bars.

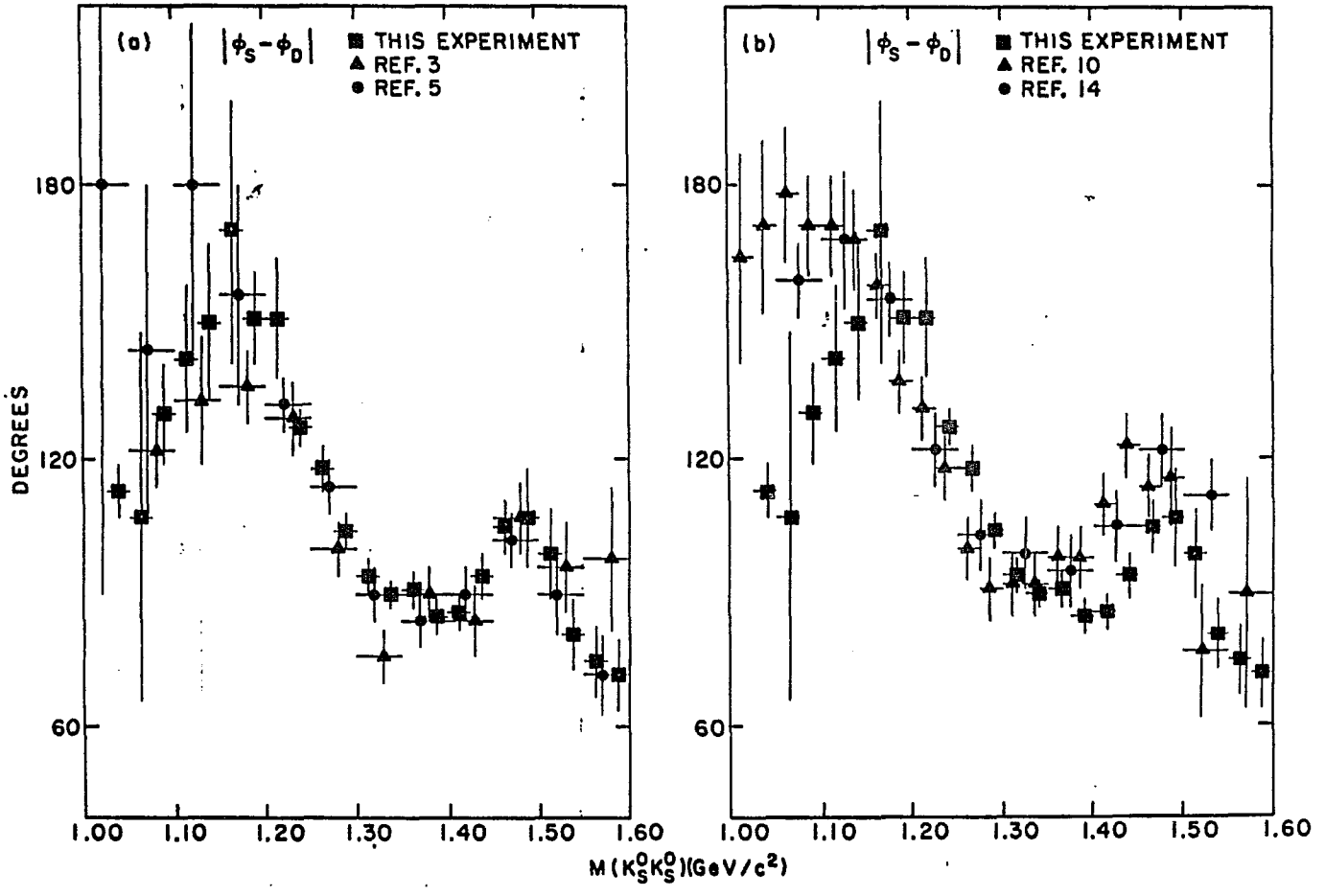

Fig. 3.2 Comparison of the old $S - D$ relative phase as a function of the $K\bar{K}$ effective mass with others. Some points are displaced from the bin centers to avoid overlapping error bars.

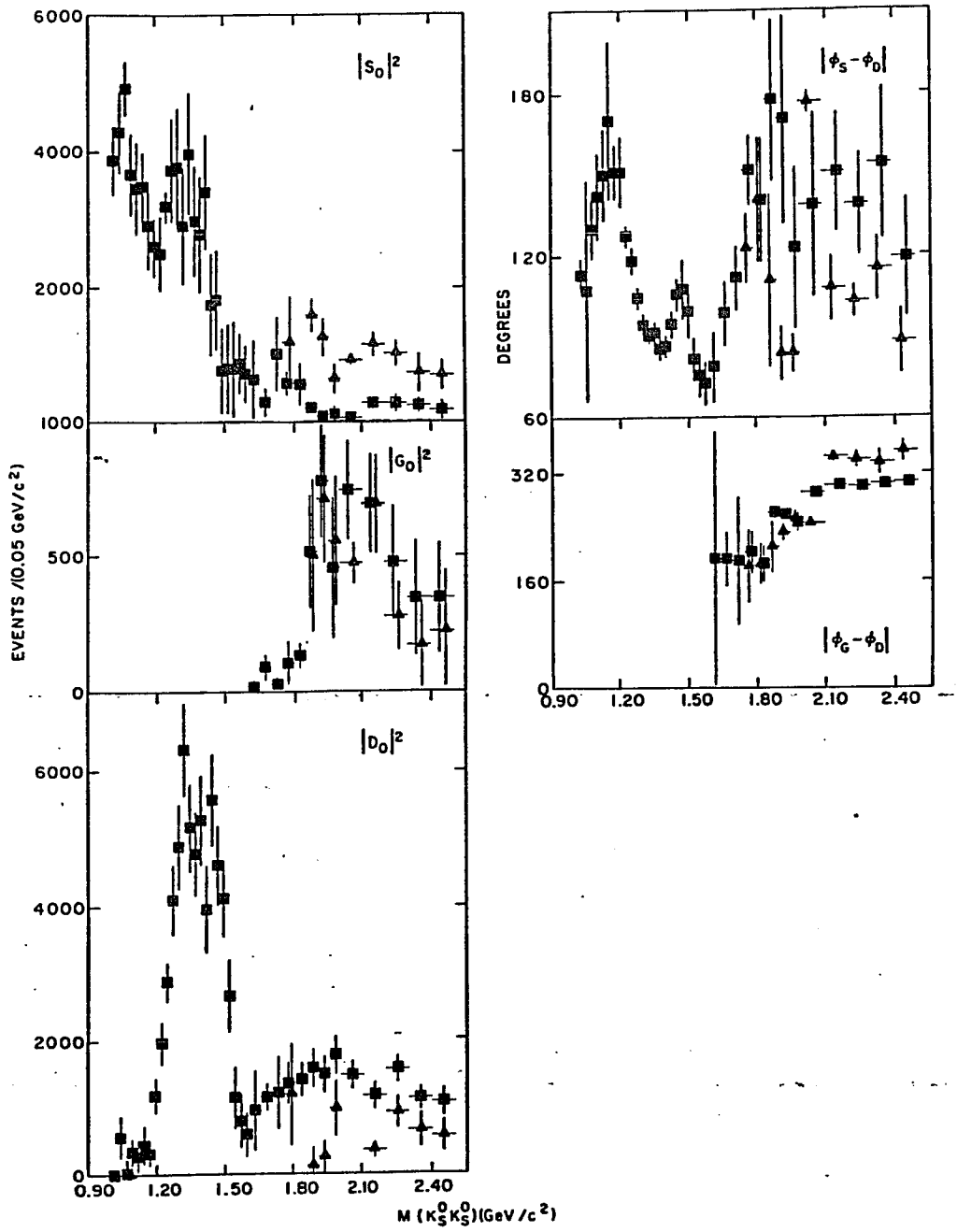

Fig. 3.3 a) The square of the moduli of the S_0, D_0, and G_0 amplitudes as a functions of $K_S^0 K_S^0$ effective mass together with the $S-D$ and $G-D$ relative phases for $|t'| \leq 0.1$ (Gev/c)^2. Above 1.6 Gev/c^2, two ambiguous solutions are shown. The errors indicated are the result of propagating the errors on the moments.

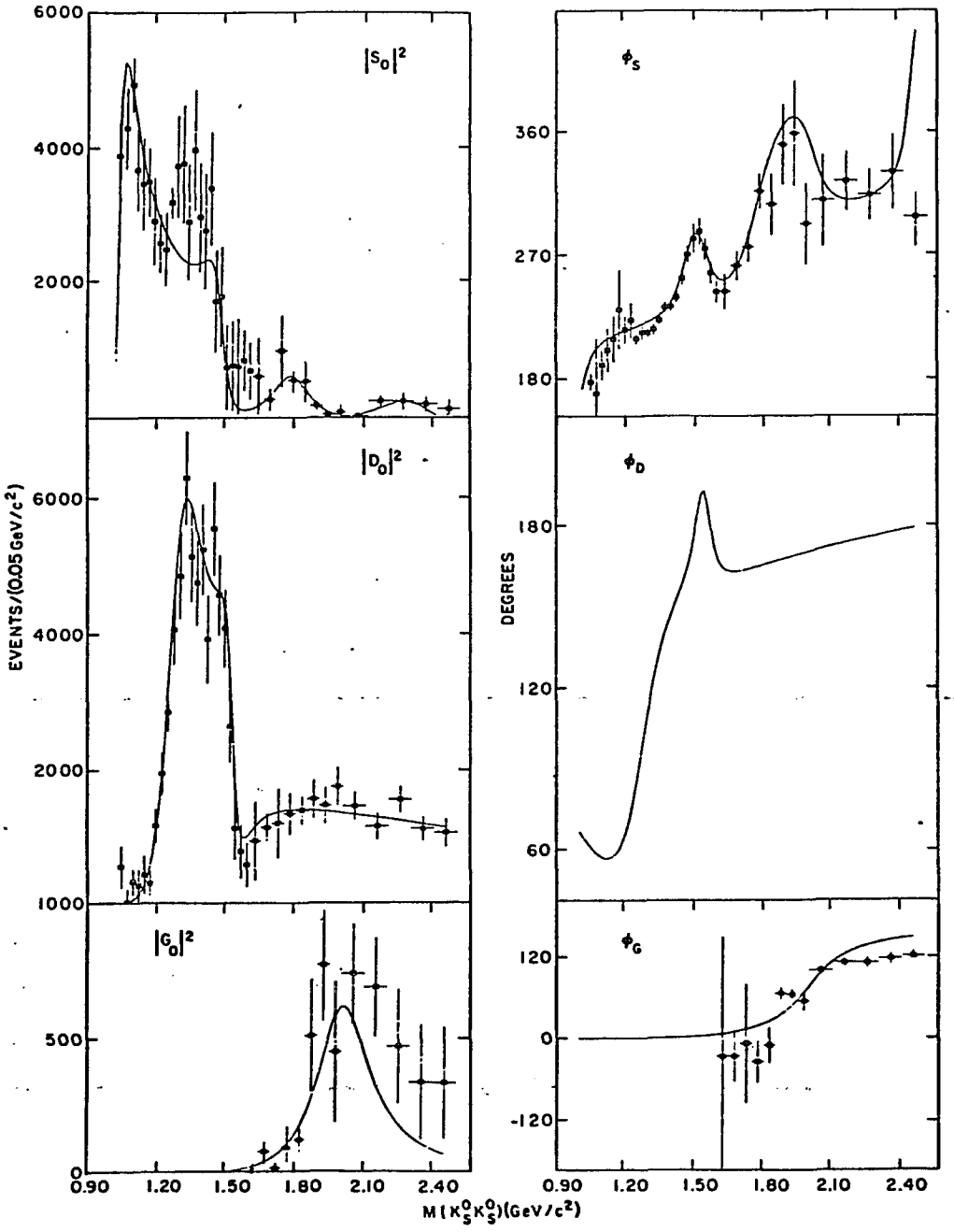

Fig. 3.3 b) The old result of the fit to the preferred solution, in the same $|t'|$ interval.

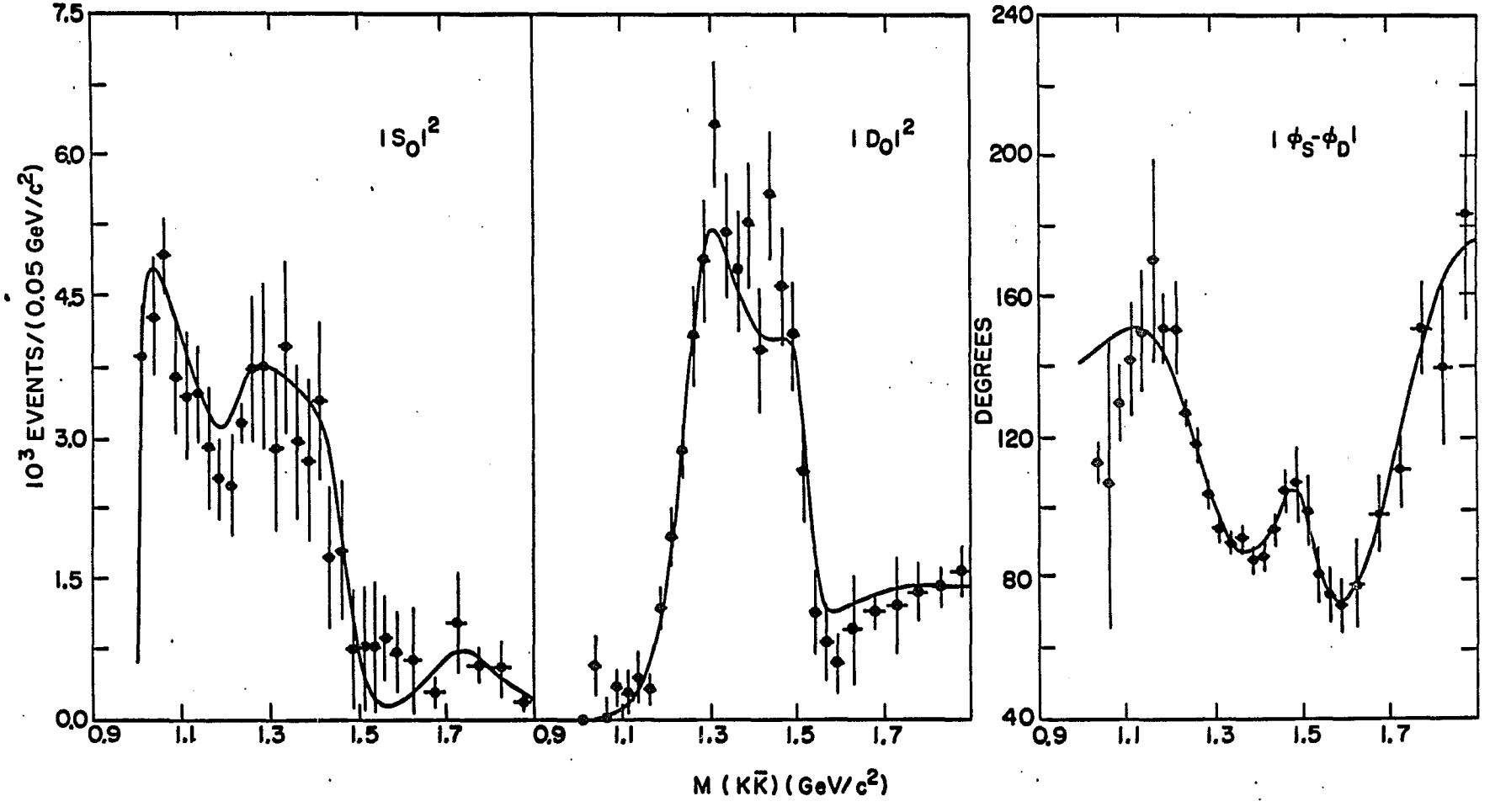

Fig. 3.3 c) The improved fit result from Ref. 25 to $|S_0|^2$ and $|\phi_S - \phi_D|$ for the same t interval.

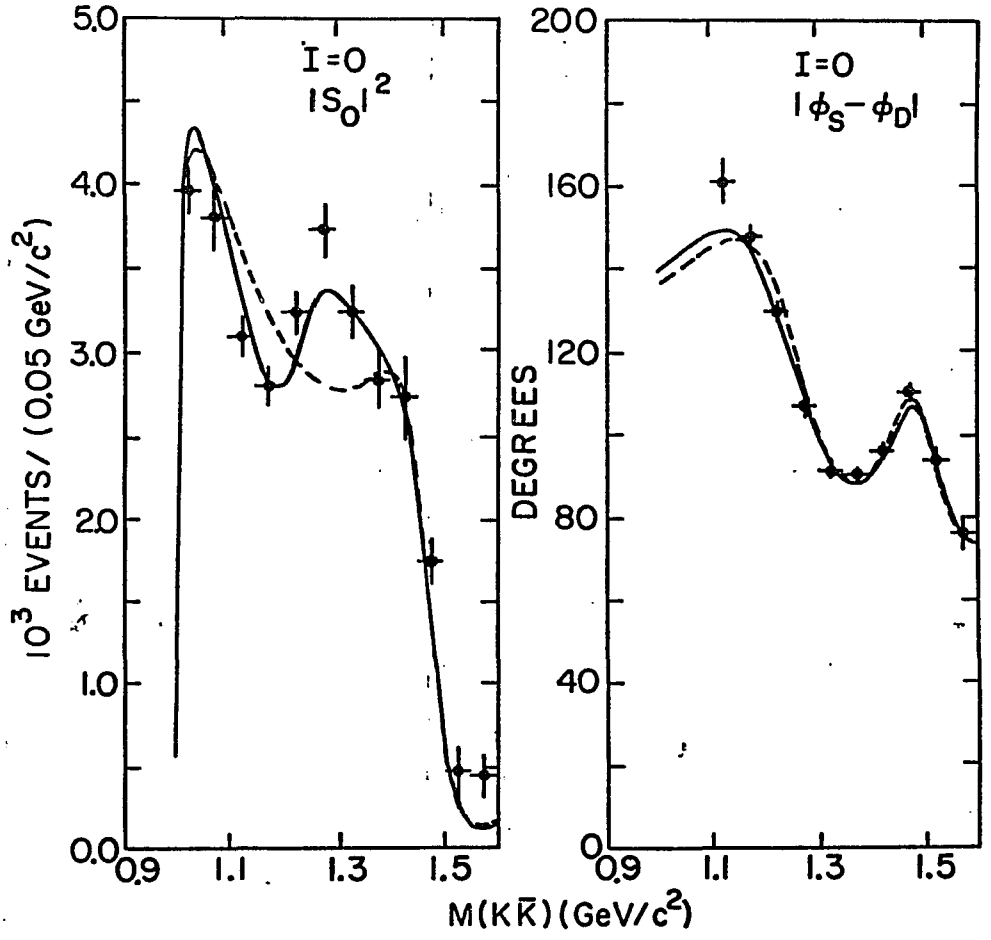

Fig. 3.3 d) Averages of the data sets i) through v). The solid (dashed) curve shows the fit with(without) $f_0(1240)$ from Ref. 25.

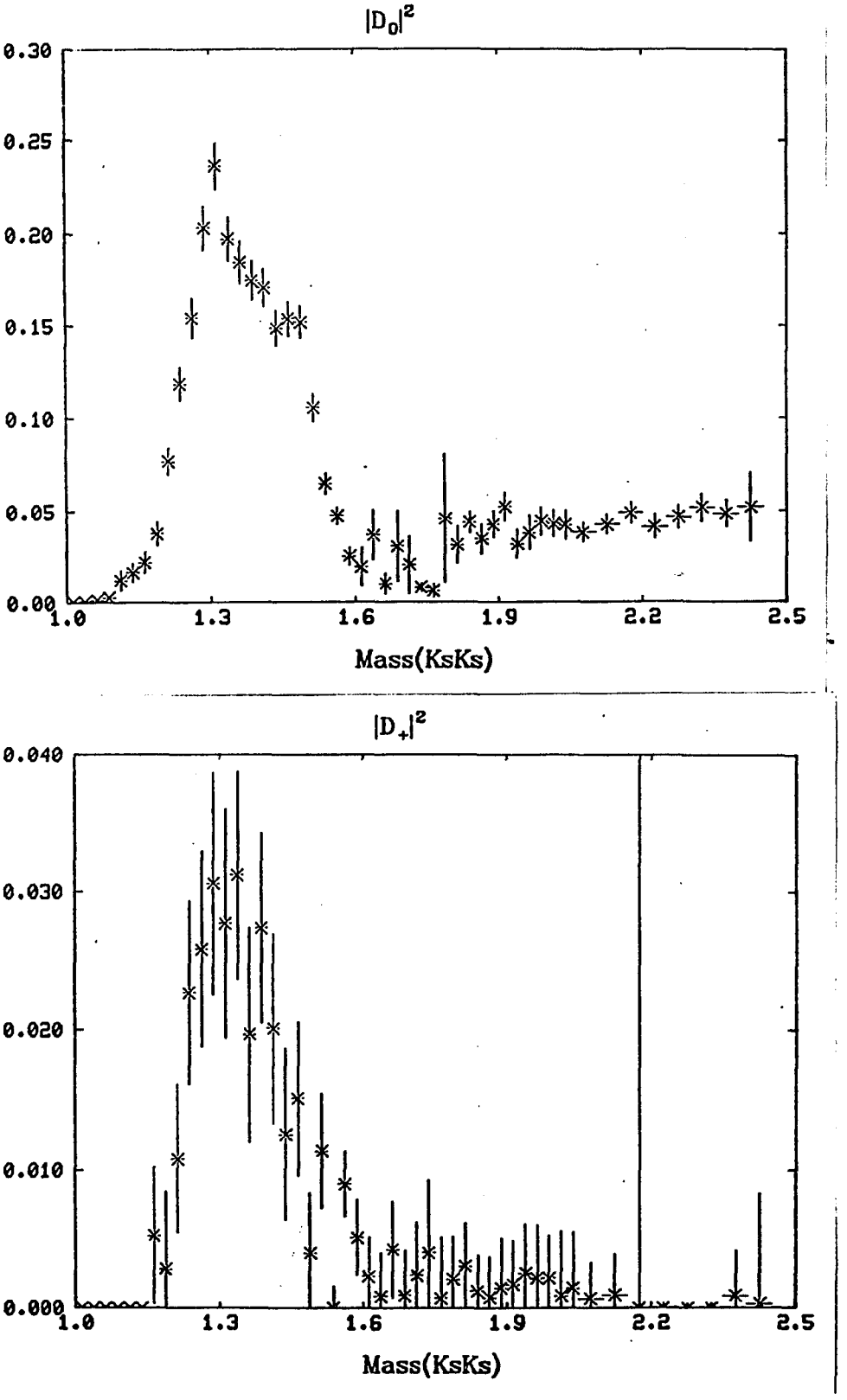

Fig. 3.4 a) The new data on absolute moduli squared of D_0 and D_+ waves as functions of $K_S^0 K_S^0$ effective mass.

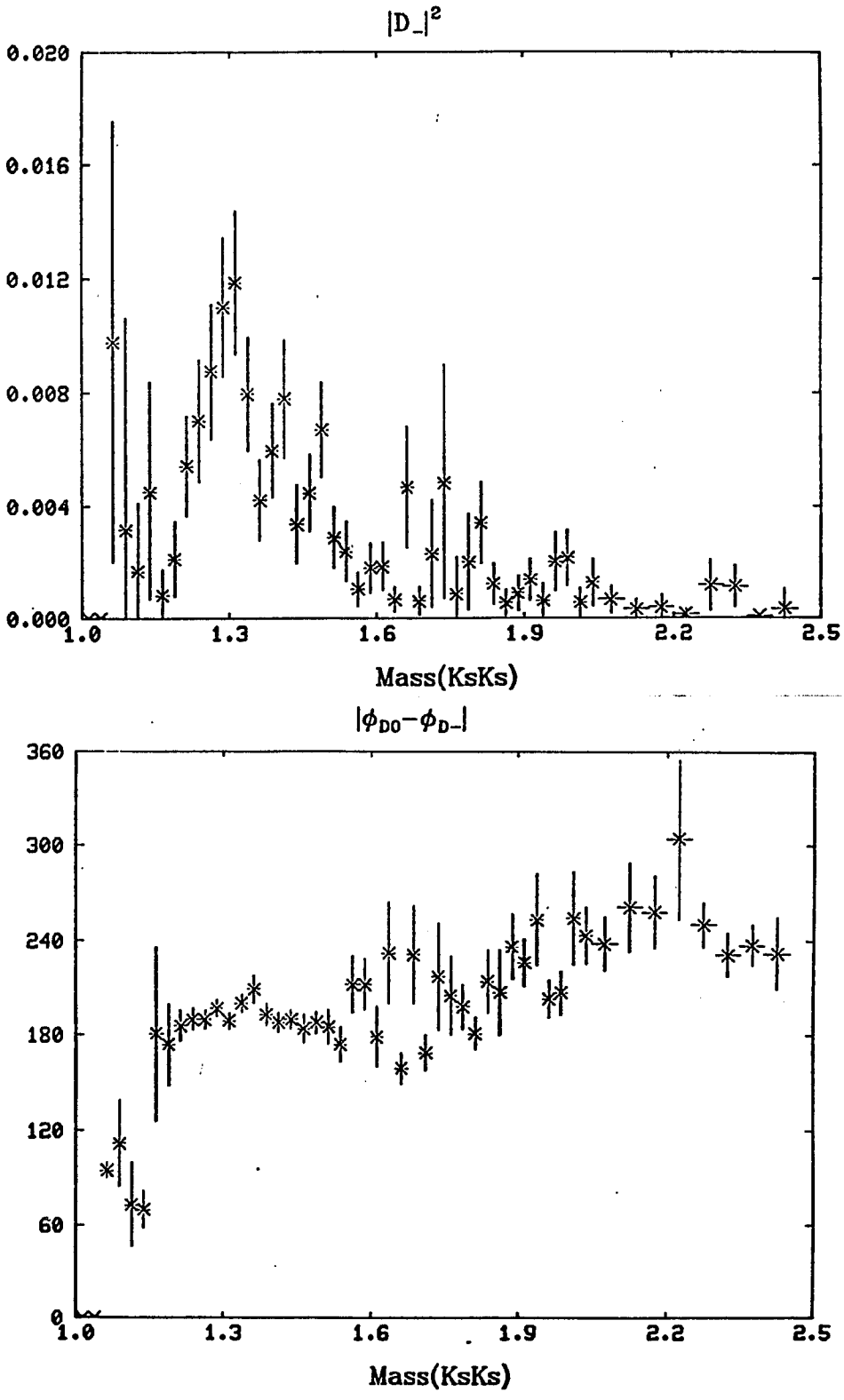

Fig. 3.4 b) The new data on absolute modulus of D_- wave and the relative phase $|\phi_{D_0} - \phi_{D_-}|$.

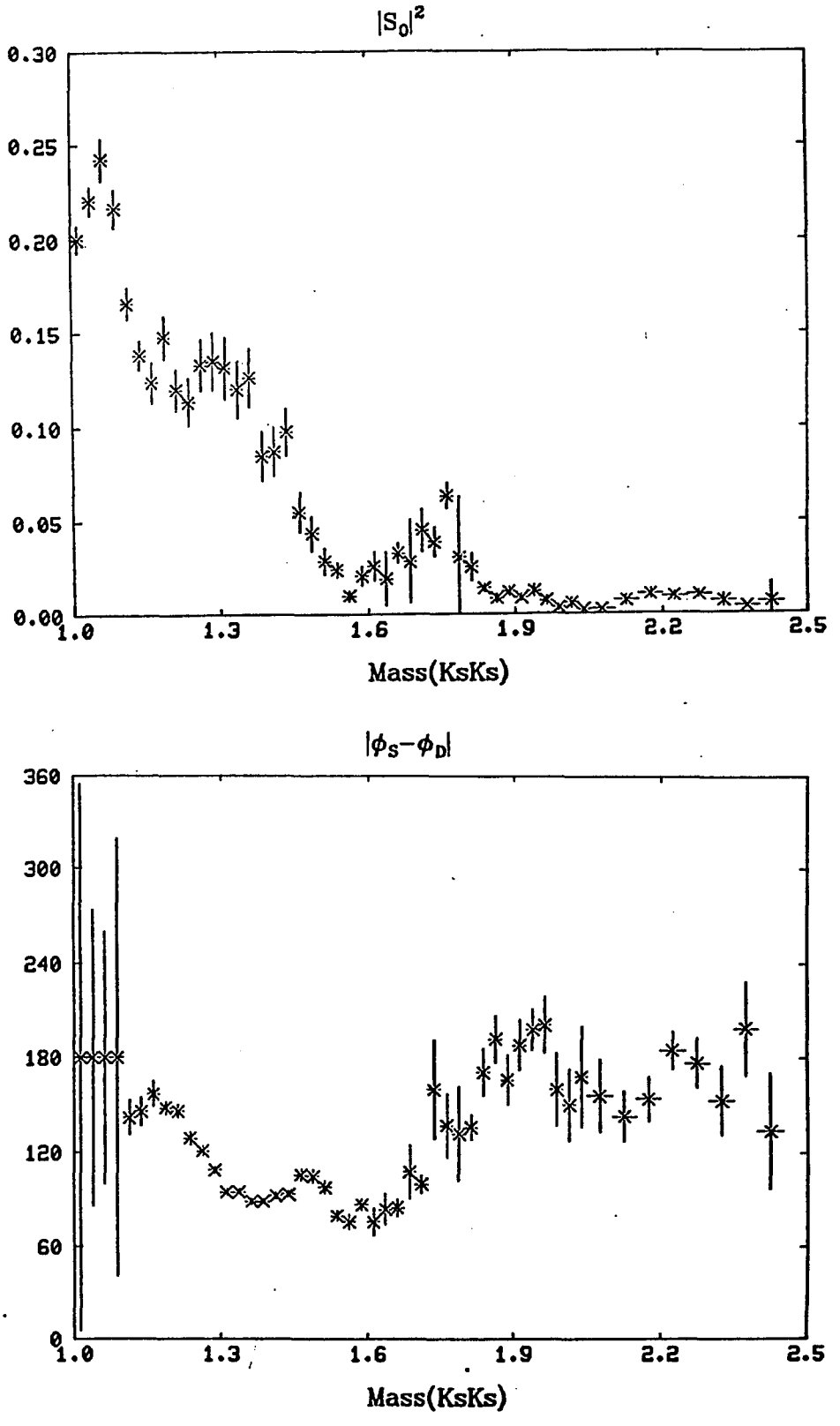

Fig. 3.4 c) The new data on absolute modulus squared of S wave and the relative phase $|\phi_D - \phi_S|$.

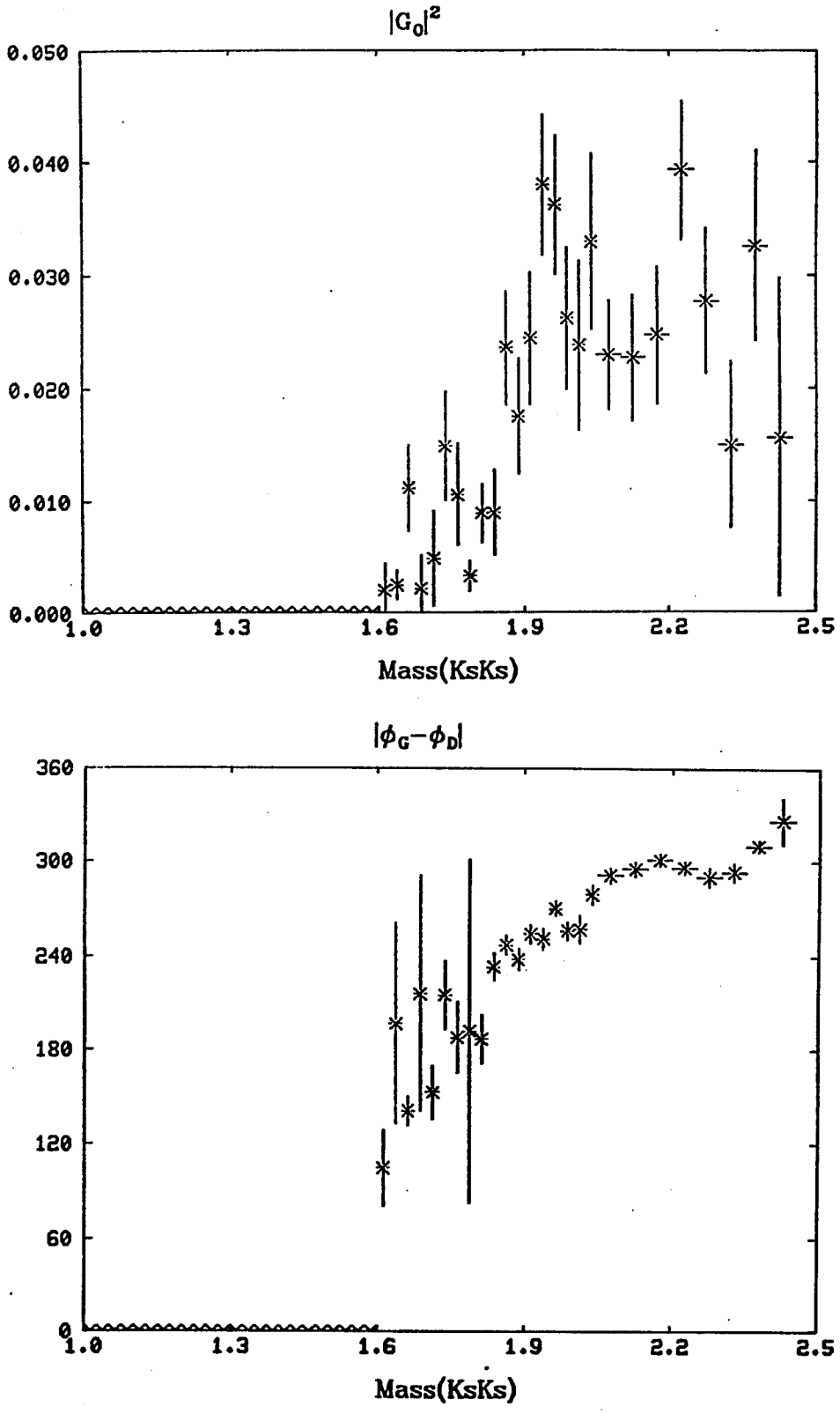

Fig. 3.4 d) The new data on absolute modulus squared of G wave and the relative phase $|\phi_G - \phi_D|$.

Chapter 4 The Experiment on $\pi^- p \to K_s^0 K_s^0 n$ and Moments Analysis

An experiment to study the reaction

$$\pi^- p \to K_s^0 K_s^0 n$$

at 22 Gev/c was performed using the MPS II detector at Brookhaven National Laboratory.

This experiment superseded the previous one[23] in various ways. The spark chambers were all replaced by drift chambers and the data acquisition system had been upgraded[28]. These resulted in over-all improvements in mass resolution and event rates. The veto counters around the hydrogen target had been improved, so that efficient detection of large-angle charged particles and photons from the target became possible. The basic configuration of the detector was otherwise similar to the previous one, and the trigger requirement for this experiment was essentially identical to the old one. The trigger rate was $\sim$ 1 trigger per 1.7×10^5 beam π's.

The total number of observed 4-prong events was 3.5×10^5. The following kinematic cuts were used for the final event selection:

i) cuts in the $\pi^+\pi^-$ effective-mass at 0.475 Gev/c^2 and 0.525 Gev/c^2, yielding 2.2×10^4 events.

ii)a MM^2(missing mass squared) cut at 1.6 (Gev/c^2)^2, with this cut 82111 events were selected.

iii) a t-cut, $t' = |t - t_{min}| \leq 0.1$, was finally applied to obtain 40494 events.

The event distribution in the Gottfried-Jackson variables $\Omega = (cos\theta, \phi)$ was expanded in terms of normalized spherical harmonics as before,

$$\frac{d^4\sigma}{dt' dM d\Omega} = N(M, t') I(\Omega)$$

where $N(M,t')$ is the number of events in a given t' and mass M bin, and the angular distribution is given by

$$I(\Omega) = \sum_l [\langle Y_l^0 \rangle_{obs} Y_l^0(\Omega) + 2 \sum_m \langle Y_l^m \rangle_{obs} Re Y_l^m(\Omega)],$$

where expansion coefficients $\langle Y_l^m \rangle_{obs}$ are the observed moments. A Monte Carlo simulation was performed to study the geometric acceptance and other systematic biases. The techniques used in this Monte Carlo study were the same and described in detail in the previous publication[23]. In this new analysis, we introduced a new procedure to determine statistical significance of each moment. This procedure is described below in details.

The geometric acceptance $A(\Omega)$ was used to calculate the acceptance moments by performing the following integral numerically over the allowed solid angle for each mass bin,

$$G_l^m = \int A(\Omega) Y_l^m(\Omega) d\Omega.$$

The acceptance-corrected moments, $\langle Y_l^m \rangle_c$, are those that minimize the negative of the log-likelihood function,

$$\ln L = \sum_i \ln I(\Omega_i) - \sum_{l,m} G_l^m \langle Y_l^m \rangle_c,$$

where the first summation is over the selected events in a given mass bin. We also computed the acceptance matrices simultaneously,

$$G_{ll_1}^{mm_1} = \int A(\Omega) Y_l^m(\Omega) Y_{l_1}^{m_1}(\Omega) d\Omega$$

These matrices are directly related to the acceptance moments,

$$G_{ll'}^{mm'} = \sum_{l''m''} T_{ll'l''}^{mm'm''} G_{l''}^{m''},$$

where

$$T^{mm'm''}_{ll'l''} = \int Y^m_l(\Omega) Y^{m'}_{l'}(\Omega) Y^{m''}_{l''}(\Omega) d\Omega.$$

The acceptance matrices in turn gave expected observed moments from the corrected moments through the following relation,

$$\langle Y^m_l \rangle_{obs(expected)} = \sum_{l'm'} G^{mm'}_{ll'} \langle Y^{m'}_{l'} \rangle_c.$$

These expected moments and the observed moments were used to perform χ^2 tests in each mass bin to see goodness of our moments determination.

In the previous moments analysis, the moments with m=2 together with $\langle Y^1_6 \rangle$ and $\langle Y^1_8 \rangle$ were all consistent with zero. With a larger event sample this was no longer the case. In this new analysis, $\langle Y^2_2 \rangle$ and $\langle Y^2_4 \rangle$ below $M(K^0_s K^0_s)$= 1.588 Gev/c^2, and $\langle Y^1_6 \rangle$ above $M(K^0_s K^0_s)$= 1.613 Gev/c^2 were introduced. The moment $\langle Y^1_8 \rangle$ was seen to be consistent with zero. By the above-mentioned χ^2 tests, statistical significance of these moments turned out to be 3σ below 1.588 Gev/c^2 and 4.5σ above 1.613 Gev/c^2. Clearly moments with m=2 are important to understand the $K^0_s K^0_s$ production. With this set of new moments we extracted amplitudes. The Barrelet-zero method[29] was used to obtain one set of amplitudes.

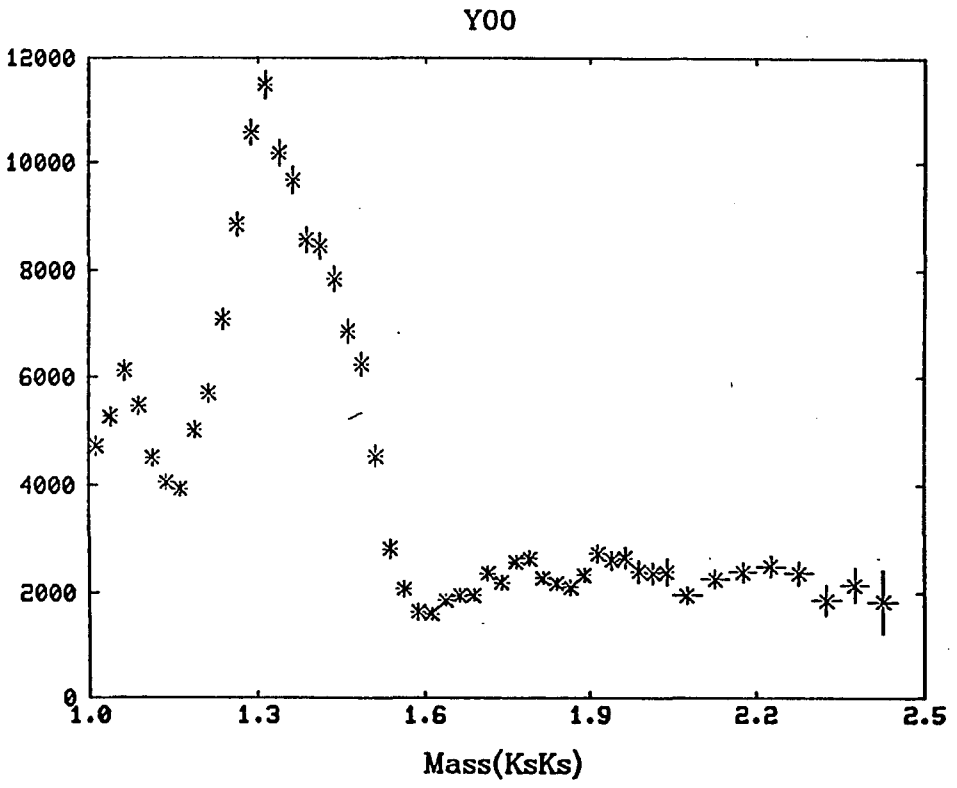

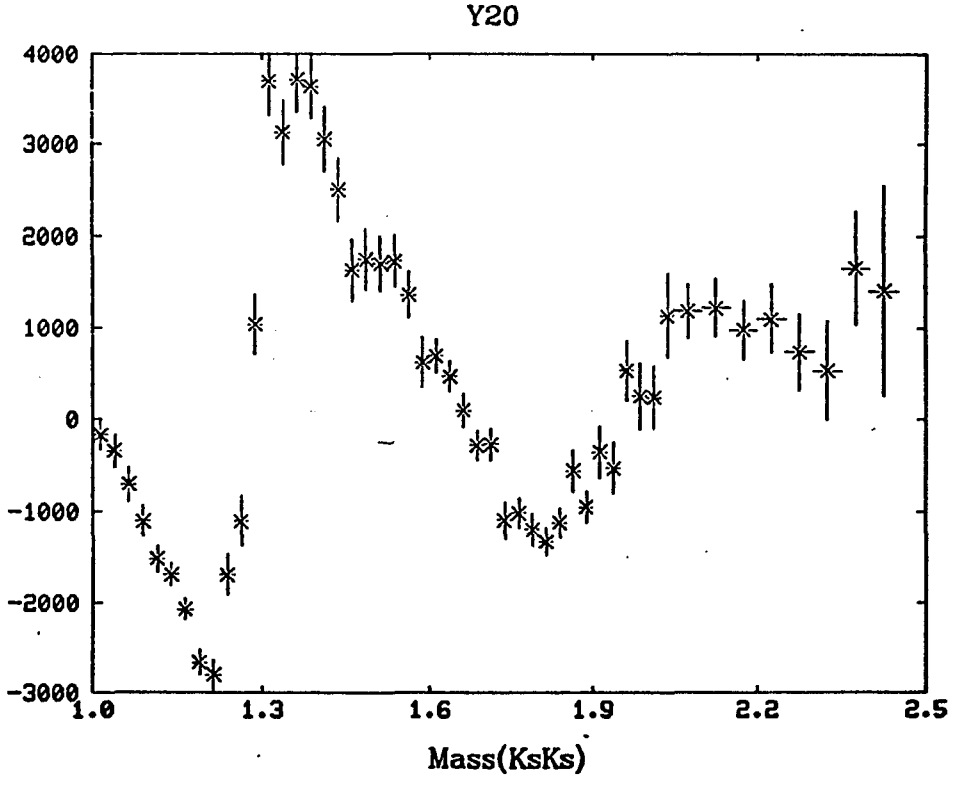

Fig. 4.1 The moments $\langle Y_{lm} \rangle$ as a function of the effective mass of $K_s^0 K_s^0$ in Gev/c^2 from the new experiment. The moments will be denoted by YLM.

Y21

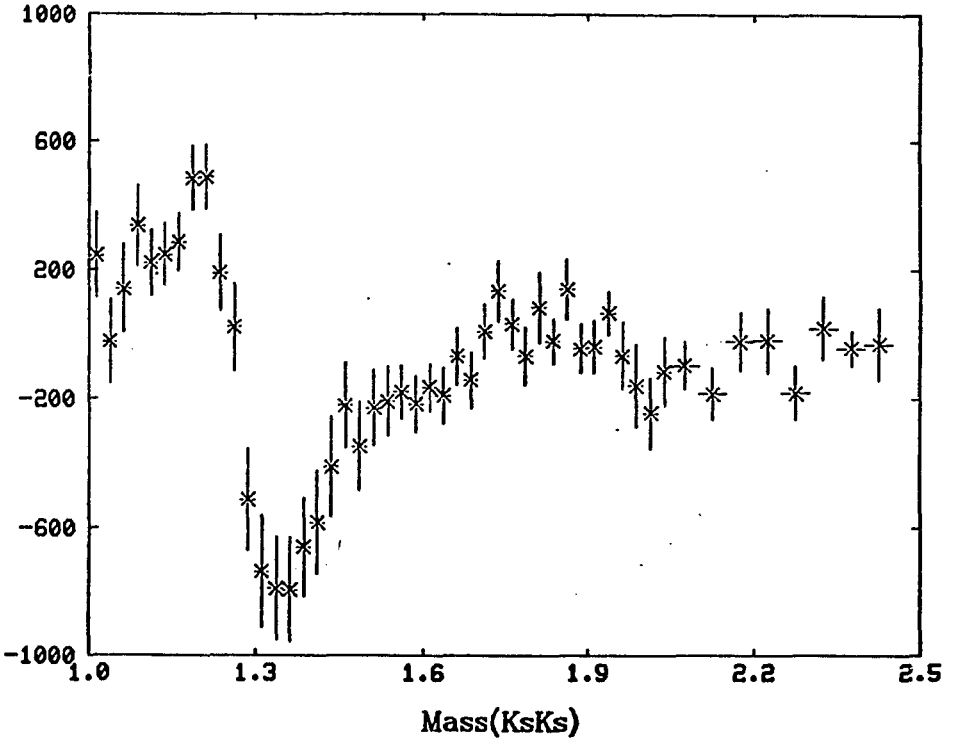
1000
600
200
-200
-600
-1000
1.0
1.3
1.6
1.9
2.2
2.5
Mass(KsKs)

Y22

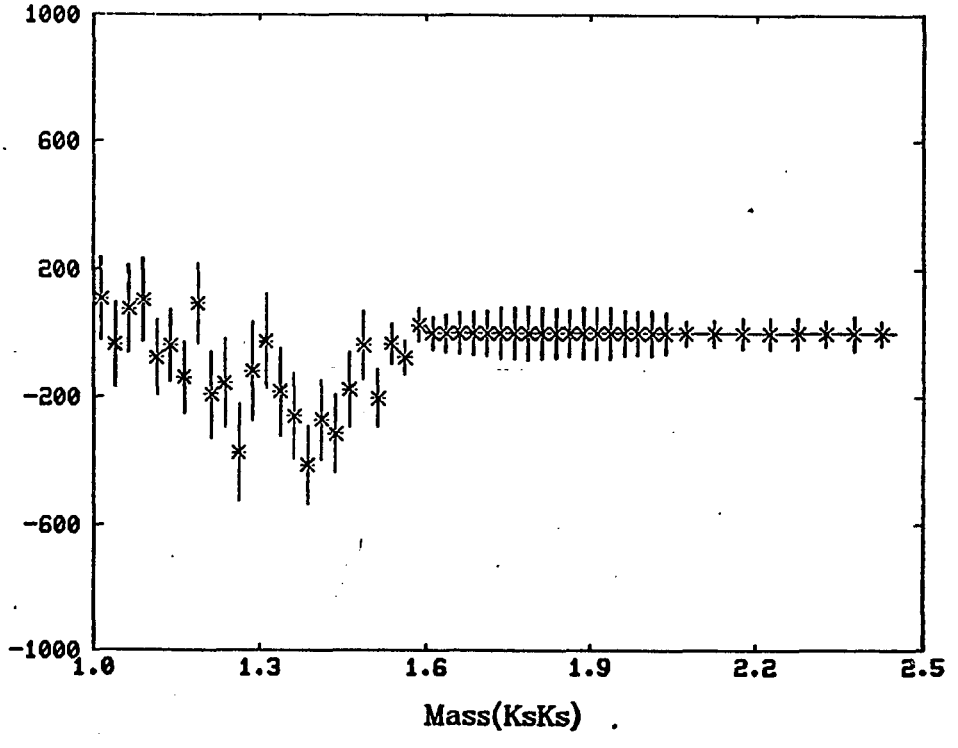
1000
600
200
-200
-600
-1000
1.0
1.3
1.6
1.9
2.2
2.5
Mass(KsKs)

Y40

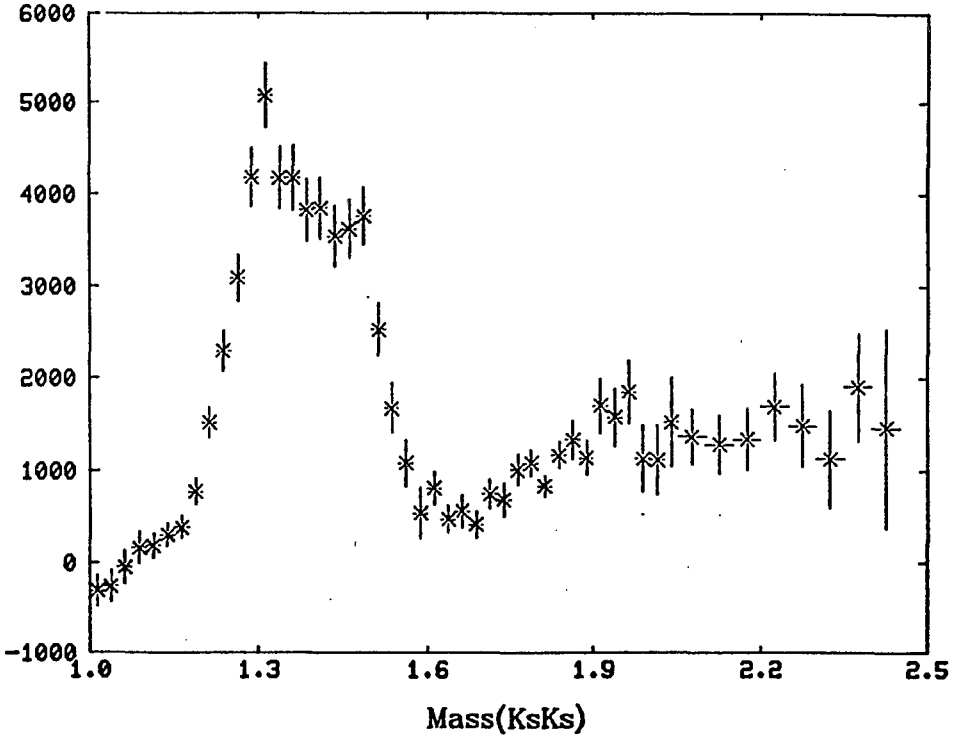
6000
5000
4000
3000
2000
1000
0
-1000
1.0
1.3
1.6
1.9
2.2
2.5
Mass(KsKs)

Y41

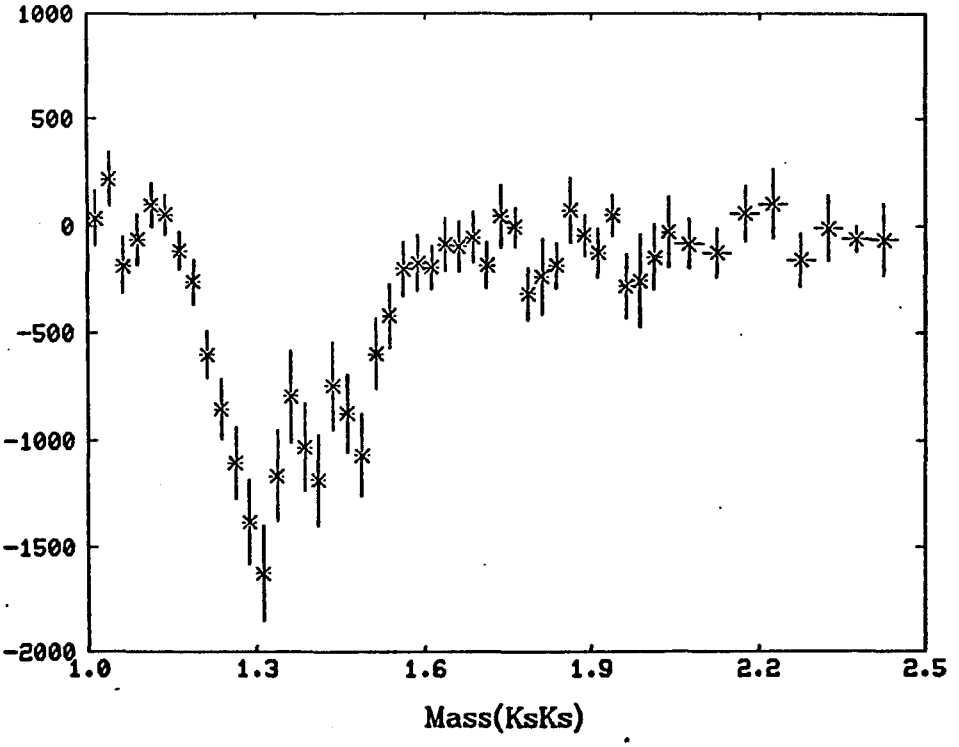
1000
500
0
-500
-1000
-1500
-2000
1.0
1.3
1.6
1.9
2.2
2.5
Mass(KsKs)

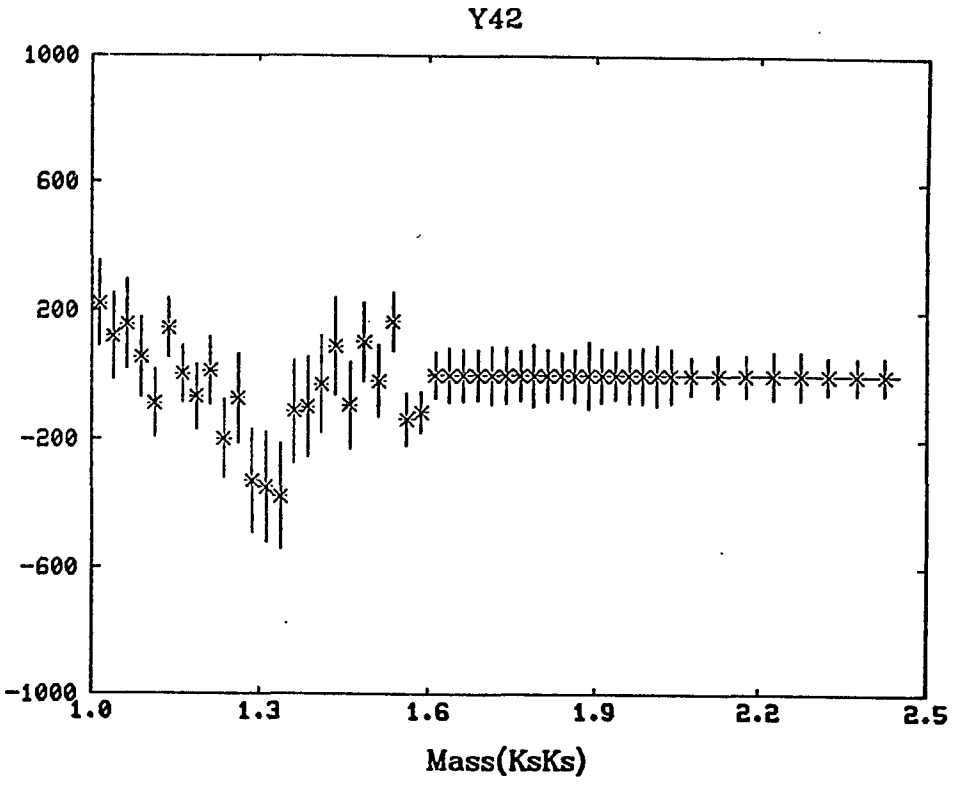
Y42
1000
600
200
-200
-600
-1000
1.0
1.3
1.6
1.9
2.2
2.5
Mass(KsKs)

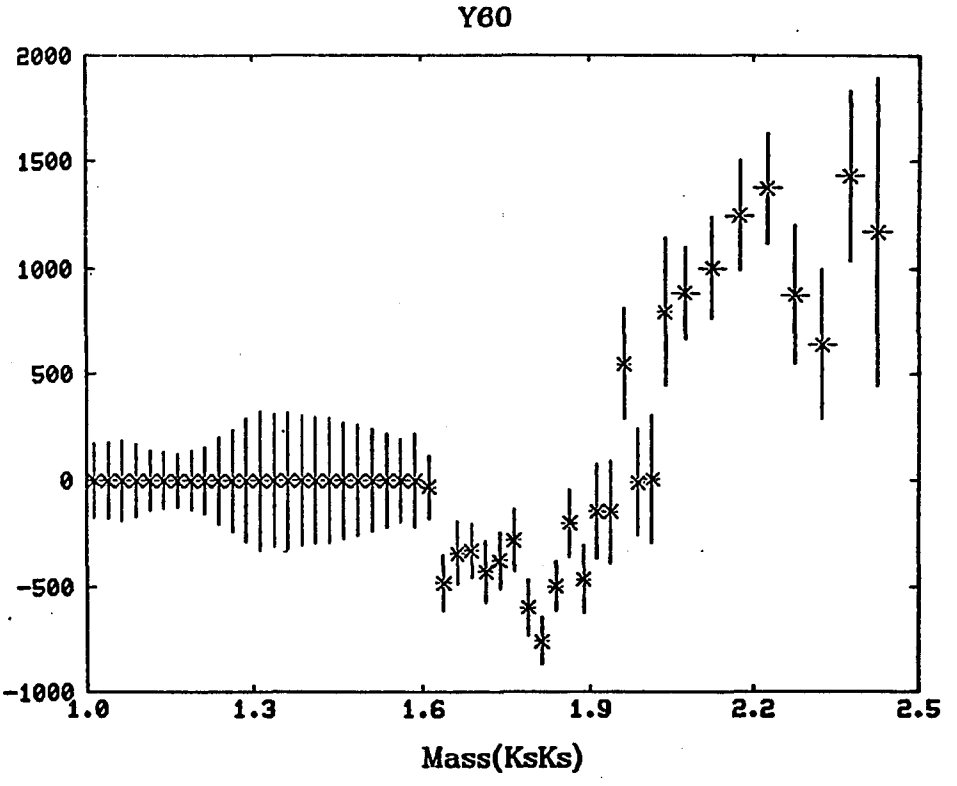
Y60
2000
1500
1000
500
0
-500
-1000
1.0
1.3
1.6
1.9
2.2
2.5
Mass(KsKs)

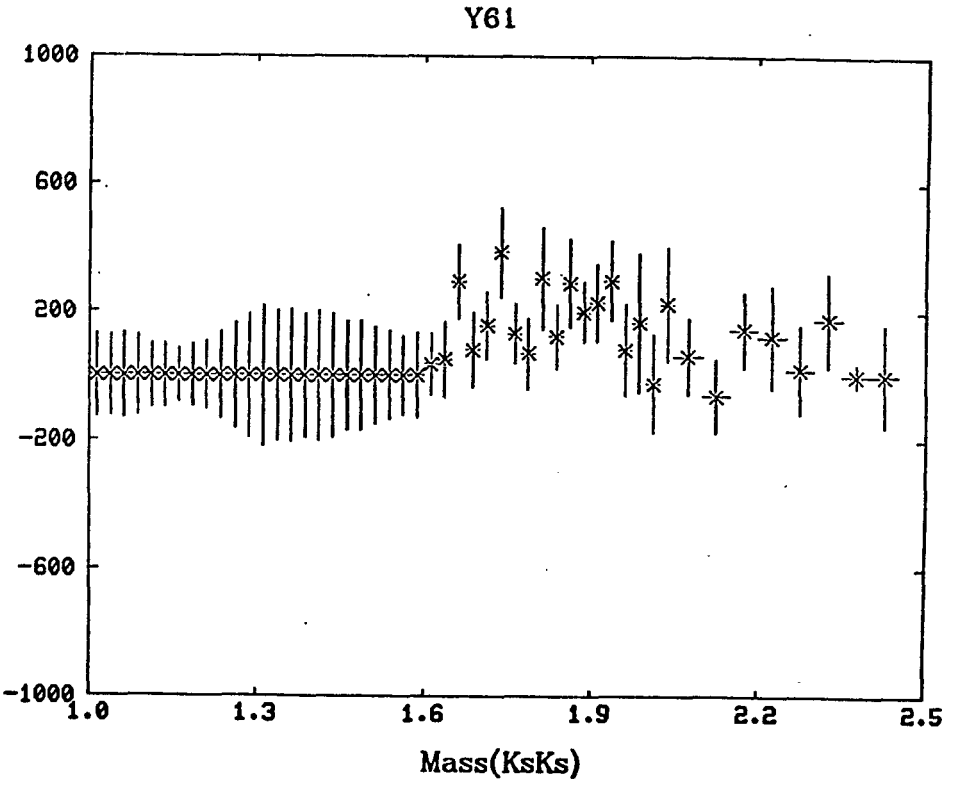
Y61
1000
600
200
-200
-600
-1000
1.0
1.3
1.6
1.9
2.2
2.5
Mass(KsKs)

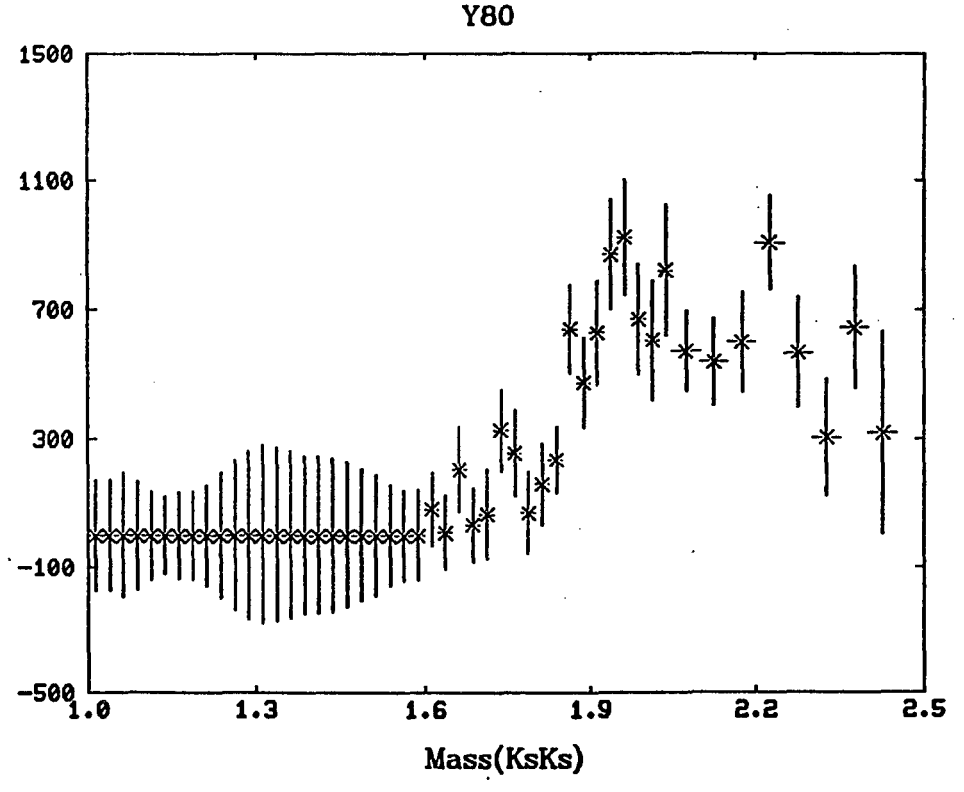
Y80
1500
1100
700
300
-100
-500
1.0
1.3
1.6
1.9
2.2
2.5
Mass(KsKs)

Chapter 5 The $\eta\eta$ Data and Other Data Sets

5.1 The Old $\eta\eta$ Data

Experiments to study the $\eta\eta$ system are difficult to perform. Indeed large fractions of events one observes in a typical experiment are,

$$\pi^- p \rightarrow \pi^0\pi^0 n,$$

and

$$\pi^- p \rightarrow \pi^0\eta n.$$

Since isospin of the $\eta\eta$ system has to be zero and its spin can be only even, analysis is relatively straightforward once data are obtained. The difficulties are to extract data by doing reliable experimental identification of good events which is technically complicated by the presence of massive combinatorial backgrounds. It is to be noted that the $\pi^0\pi^0$ production cross section is roughly 30 times larger than the $\eta\eta$ production cross section at a beam momentum of 38 Gev/c. Only recently data with reasonable statistics became available[30]. In the first phase of the present analysis this data set was used to investigate the 2^{++} sector. This experiment was performed using a 38 Gev/c π^- beam. Since other data sets discussed so far come from the experiments at lower beam momenta, we have scaled the data through the use of the O.P.E. expression along with corrections in the t-distribution. These corrections turned out to be rather small and the shapes of the spectra did not change much except by an over-all scale factor. The spectra extend up to 1.89 Gev/c^2.

The threshold region is dominated by the S-wave. Identifying the structure around the threshold with the $f_0(1300)$ might be possible, but the peak position, at 1.2 Gev/c^2, is slightly below the generally accepted value. The structure around 1.6

Gev/c^2 was fitted by a Breit-Wigner form in their analysis yielding the parameters,

$$m = 1.592 \pm 0.025 \text{Gev}/c^2$$

$$\Gamma = 0.210 \pm 0.040 \text{Gev}/c^2$$

This is the first observation of a scalar meson in this mass region with a definite isospin assignment.

The D-wave spectrum shows one peak with a width of 240 Mev/c^2 which is on top of a rising tail. This tail was interpreted as a background by the authors in the publication. This peak, the $f_2(1270)$, is shifted by about 100 Mev/c^2. They point out that this shift is due to the kinematic effect in that the Breit-Wigner form has a factor of p^5(p is the momentum of one of the η's in the rest frame of the resonance). The relative phases do indeed show a typical forward phase motion in this general region of the mass. In their publication they did not consider the presence of the $f_2'(1525)$ in their data. We have, however, allowed the $\eta\eta$ coupling of this state in the analysis.

5.2 The New $\eta\eta$ Data

The new data set came from a recent experiment performed at CERN SPS using a 100 Gev/c π^- beam[31]. By comparing the new data with the old data, one sees a remarkable consistency among these sets up to 1.9 Gev/c^2 as far as the shape of the spectra are concerned(figures will be given in Chapter 7). The event distribution in t is a typical one expected by the O.P.E. mechanism if the region of low $t(|t'| \leq 0.1)$ is selected. The data have been analyzed and two possible solutions are known. These are solutions due to the ambiguities of the amplitudes, the difference is seen only in the region above 1.8 Gev/c^2 where the G-wave begins. Clearly one of the solutions is not physical. Indeed the results of their analysis of one solution(solution

I) show that the region around 2.0 Gev/c^2 in the D-wave spectrum is not of a Breit-Wigner form. This solution(solution I) has an anomalously rapid phase motion, the relative $D-S$ phase changes by 360 degrees within the entire range of the $\eta\eta$ invariant mass. Although introducing another Breit-Wigner term in the fit might have helped improve their fit of the amplitudes modulus squared of the D-wave, it would be extremely difficult to understand the phase motion of this nature. On the other hand, the solution II does not contain any unusual structure. This solution is compatible with the particular solution obtained in the analysis of $K_s^0K_s^0$ data.

The S-wave mass spectrum below 1.8 Gev/c^2 contains two peaks. The parameters for the $f_0(1590)$ are consistent with the old ones listed in the Table 5.1. The parameters for the $f_0(1300)$ are, m=1210$\pm$30 Mev/c^2 and Γ=315$\pm$60 Mev/c^2. The mass parameter, if this identification is correct, is the lowest among those ever reported[32]. The region above 1.8 Gev/c^2 in the S-wave spectrum is clearly dominated by one structure. The phase motion is seen to be comparable to that of the $K_s^0K_s^0$ data. The visible cross section in this region is large.

The structure observed around 1.8 Gev/c^2 in the D-wave spectrum was regarded as a rising background in the analysis of the old $\eta\eta$ data. The width and the position of the peak of this structure make it possible to identify this with the $f_2(1810)$ which was previously seen only in the $\pi\pi$ channel and possibly in the 4π channel as we discussed in Chapter 2.

The G-wave spectrum show two clearly enhanced structures. The phase motion is rather difficult to understand, if one assumes presence of two resonances. They fitted the G-wave with one Breit-Wigner form.

A general remark upon comparison of the $\eta\eta$ spectrum with the $\pi\pi$ and the $K_s^0K_s^0$ spectra can be made.

The D-wave spectra do not show noteworthy difference. A peak due to the $f_2(1270)$ followed by a minimum at around 1.6 Gev/c^2 is the common feature. The spectra are compatible with each other. This sort of common feature is shared by the $\pi\pi$ and $K_s^0K_s^0$ S-wave spectra, but the S-wave $\eta\eta$ spectrum appears to be different especially in the region between 1.4 Gev/c^2 and 1.8 Gev/c^2.

Table 5.1 Parameters for the resonances in the $\eta\eta$ mass spectra(solution II) from the CERN-IHEP Joint Experiment ref. 31, numbers are in units of Gev/c^2.

state	mass	tatal width
0^{++}	1.210±0.030	0.315±0.060
	1.590±0.030	0.300±0.030
	2.090±0.040	0.215±0.030
2^{++}	1.310±0.030	0.215±0.030
	1.525	0.050
	1.890±0.040	0.250±0.030
4^{++}	2.070±0.050	0.500±0.100

5.3 The $\eta\eta'$ Data

The data set on the $\eta\eta'$ system comes from an experiment performed on the reaction,

$$\pi^- p \rightarrow \eta\eta' n$$

using the 38 Gev/c π beam[33]. One particular decay mode $\eta\eta' \rightarrow 4\gamma$ was studied. This decay mode has an extremely small decay probability, 7×10^{-3}. The presence of large combinatorial background from other processes makes the experiment exceptionally difficult to perform. The total number of events after kinematical cuts is 610, and the event distribution extends from the $\eta\eta'$ threshold to 1.8 Gev/c^2. The angular distribution of the events indicates that the entire spectrum consists of the S-wave. A fit was made to the spectrum using a Breit-Wigner form and the following parameters were obtained,

$$m = 1.568\pm0.033 Gev/c^2$$

$$\Gamma = 0.260\pm0.060 Gev/c^2$$

The values of these parameters are consistent with assuming that this state is the $f_0(1590)$. With this identification they derive the following ratio of the branchings,

$$\frac{BR(f_0 \rightarrow \eta'\eta)}{BR(f_0 \rightarrow \eta\eta)} = 2.7\pm0.8.$$

This ratio is consistent with the predicted value of 3 based upon an assumption of a scalar bound state of gluons decaying to $\eta\eta'$(Ref. 33). However this state has not been observed in the radiative decay modes of the J/ψ.

5.4 The $\pi\pi$ and $K\bar{K}$ Data from the Radiative Decays of the J/ψ

The literature on the subject of experimental and theoretical studies of the J/ψ has grown enormous. Among those we see that studies on the radiative decays of this state have been extensively done. If one considers all of the possible modes of the radiative decays of the J/ψ, one finds that the total of the branching ratios is around 0.04[34]. This is a rather small number, studies of each of the radiative decay modes are made rather difficult due to this over-all rarity.

Among these channels we are particularly interested in the following:

$$J/\psi \rightarrow \gamma\pi\pi,$$

$$J/\psi \rightarrow \gamma K\bar{K}.$$

In the mass spectra[35] of the $\pi\pi$ and $K\bar{K}$ the $f_2(1270)$ and the $f_2'(1525)$ are unmistakable. The presence of these states in the spectra was indeed the main reason for us to consider these data in our global analysis.

Only the regions below 1.9 Gev/c^2 in the $\pi\pi$ and $K\bar{K}$ spectra were taken for the fits in the present analysis since it is not known if the spectra above 1.9 Gev/c^2 are also dominated by the D-wave. Also a background estimated by the SLAC group has been subtracted from the raw spectra.

During the fit it was always checked to see if the following important ratio,

$$R = \frac{\Gamma(\psi \rightarrow \gamma f_2'(1525))}{\Gamma(\psi \rightarrow \gamma f_2(1270))}$$

was in the vicinity of the reported value of 0.54$\pm$0.19.

5.5 The $\pi\pi$ data from $pp \rightarrow pp\pi^+\pi^-$

The centrally produced π's in a reaction[36],

$$pp \rightarrow pp\pi^+\pi^-$$

are the example of the $\pi\pi$ production through double pomeron exchange. Here "central" means that two protons are scattered by typically 5 mrad and its kinematics is characterized by $0.01 \leq |t| \leq 0.06$ Gev/c^2, $x_F \geq 0.95$, and $|y|$(rapidity) $\sim$ 4.2. This kind of special production mechanism has been extensively studied theoretically. It has been pointed out that the pomeron exchange can be regarded as multiple gluon exchange[36], since π's are produced in this gluon-rich environment, it has been argued that one may expect to see a bound state of gluons in the data. This particular $\pi\pi$ data will be called the Pomeron $\pi\pi$ data.

The $\pi^+\pi^-$ data are dominated by the S-wave, up to 1 Gev/c^2 where the D-wave becomes significant.

As a preliminary study, an attempt was made to fit the Pomeron $\pi\pi$ data with one K-matrix pole and an arbitrary production amplitude of the form,

$$|T|^2 = \frac{|(1 - iK)^{-1}P|^2}{M_{\pi\pi}^2},$$

where the production amplitude is defined as,

$$P = \frac{a\gamma}{m^2 - M_{\pi\pi}^2}.$$

One-pole K-matrix is simply given by

$$K = \frac{\gamma^2}{m^2 - M_{\pi\pi}^2},$$

m is the mass of the pole, $M_{\pi\pi}$ is the invariant mass of the $\pi\pi$ system and a is an arbitrary parameter. For the parameter set, m=0.767 Gev/c^2 together with γ=1.292 Gev/c^2 and a=3.296 Gev/c^2, the total χ^2 was 48 for 29 bins. Large

contributions in χ^2 came from 0.937 Gev/c^2 and 1.0125 Gev/c^2 bins(χ^2=10 and 11 respectively), the quality of the fit was good otherwise.

Here we conclude our study of the data. We now go on to describe the tools of the analysis.

Chapter 6 K-Matrix and Parameter Determination

6.1 K-Matrix

A representation of the following form,

$$S = (1 - iK)^{-1}(1 + iK)$$
$$= 1 + 2i(1 - iK)^{-1}K \quad ,$$

guarantees unitarity of the S-matrix. The matrix elements of a transition matrix

$$T = \frac{S - 1}{2i},$$

are specified by the channel indices, i=initial meson-meson state, f=final meson-meson state. In our study the channel index (1,2,3,4,5,6,7) corresponds to ($\pi\pi$, $K\bar{K}$, $\eta\eta$, $\epsilon\epsilon$, $\rho\rho$, $\omega\omega$, $\eta\eta'$) respectively. This correspondence is according to the order of the increasing threshold energies of these meson-meson systems. Thus a matrix element T_{11} is for the interaction $\pi\pi \rightarrow \pi\pi$, T_{12} is for the interaction $\pi\pi \rightarrow K\bar{K}$, and so on.

A real symmetric matrix is defined as,

$$K_{ij} = \sum_{l=1,n} \frac{U_{li}U_{lj}}{m_l^2 - s}$$

where s is the energy of the center of mass of a meson-meson system squared, m_l is the mass parameter which we call the l-th K-matrix pole, and U's are the coupling constants to be discussed shortly. This definition is almost unique since a one-channel single resonance case shows that the K-matrix will lead to a form of the Breit-Wigner amplitude.

6.2 Methods for Parameter Determination

One defines a K-matrix,

$$K = \frac{U^2}{D + iU^2},$$

by identifying $D = m^2 - s - iU^2$ we obtain a relativistic Breit-Wigner amplitude,

$$T = \frac{U^2}{D}.$$

The width of the resonance is formally defined as,

$$\Gamma = \frac{m^2 - s}{m} K,$$

this is equivalent to U^2/m. The width is evidently a function of $\sqrt{s}$, the full width of this resonance is the value of Γ evaluated at $\sqrt{s} = m$.

The K-matrix now takes the following form if the case of two poles is considered,

$$K = \frac{U_1^2}{D_1 + iU_1^2} + \frac{U_2^2}{D_1 + iU_2^2},$$

then the T-matrix will become,

$$T = \frac{U_1 D_2 U_1 + U_2 D_1 U_1 - 2U_1 D_{12} U_2}{D_1 D_2 - D_{12}^2}. \tag{5-1}$$

Here we defined,

$$D_{12} = -iU_1 U_2,$$

and $D_l = m_l^2 - s - iU_i^2, (l = 1, 2)$. The equation(5-1) can be expressed compactly in the following form,

$$T = U^T D^{-1} U,$$

where,

$$D = \begin{pmatrix} D_1 & D_{12} \\ D_{12} & D_2 \end{pmatrix}, \tag{5-2}$$

and,

$$U = \begin{pmatrix} U_1 \\ U_2 \end{pmatrix}.$$

The equation (5-1) is already rather complicated. This expression, however, can be separated into two terms,

$$T = U_1 D_1^{-1} U_1 + \frac{\det W}{D_1} \frac{D_1}{\det D} \frac{\det W}{D_1}, \tag{5-3}$$

with,

$$W = \begin{pmatrix} D_1 & U_1 \\ D_2 & U_2 \end{pmatrix}. \tag{5-4}$$

The first term and the second term in the equation (5-3) are both of a Breit-Wigner form, the second term carries an over-all phase which is a function of energy. Indeed with the following identification,

$$\begin{aligned} m^2 - s - im\Gamma &= \frac{\det D}{D_1} \\ m\Gamma &= |\det W/D_1|^2 \\ &= |\alpha|^2, \\ e^{i\theta} &= \alpha^2/|\alpha|^2, \end{aligned} \tag{5-5}$$

we obtain the amplitude,

$$T = \frac{m_1\Gamma_1}{m_1^2 - s - im_1\Gamma_1} + \frac{m\Gamma e^{i\theta}}{m^2 - s - im\Gamma},$$

where we set $U_1^2 = m_1\Gamma_1$. The identification of the second term in the above expression for the amplitude with a Breit-Wigner form is purely formal since a complicated functional dependence of the phase θ on $\sqrt{s}$ might distort its shape. This procedure is based upon the ideas introduced by Goebel and McVoy[37]. Notice the mass of the second resonance is not the same as the mass parameter m_2 that appears in the original expression for the K-matrix. The resonance mass m computed from the equation (5-5) is a function of $\sqrt{s}$, $m = m(\sqrt{s})$. We formally define the mass of the second resonance,

$$m(\sqrt{s_0}) = \sqrt{s_0},$$

the particular value at which $m(\sqrt{s})$ and $\sqrt{s}$ are equal to each other.

The generalization of the above procedure to the case of M channels and N poles is exceedingly complicated, but the following ansatz formula for the T-matrix elements$(a, b = 1, \ldots, M)$ can be derived based upon equation (5-3),

$$T_{ab} = U_a'^T d^{-1} U_b' + \frac{\det W_a}{\det d} \frac{\det d}{\det D} \frac{\det W_b}{\det d}. \tag{5-6}$$

Here D is an N by N symmetric matrix similar to equation (5-2), d is a sub-matrix constructed from D by removing the N-th column and the N-th row, W_a is a matrix essentially the same as D except the last column(N-th column) is replaced by a column vector U_a similar to equation (5-4), U_a' is a column vector the same as U_a except the last component is removed, therefore it is a vector of dimension $(N-1)$. The last part of the equation (5-6) is of a Breit-Wigner form if one makes identification,

$$\begin{aligned} m^2 - s - im\Gamma &= \frac{\det D}{\det d}, \\ m\Gamma_a &= |\det W_a / \det d|^2 \\ &= |\alpha|^2, \\ e^{i\theta} &= \alpha^2/|\alpha|^2. \end{aligned} \tag{5-7}$$

Since the first two leading terms in the first line of equations (5-7) are $m_N^2 - s$, we will define the mass of the N-th resonance to be,

$$\left(\text{Real}(\frac{\det D}{\det d}) + s\right)^{1/2}.$$

The value evaluated by the method discussed already, *i.e.* through the condition $m(\sqrt{s}) = \sqrt{s}$, is used in the equations (5-7) to compute the partial widths and total width of this resonance. In particular the imaginary part of the first line of equations (5-7) gives the total width of the resonance, the partial widths are

computed from the second line. Masses and widths of all the remaining resonances are computed by following the algorithms through cyclic permutations,

$$1,2,\ldots,N \rightarrow N,1,2,\ldots,N-1 \rightarrow 2,3,\ldots,1.$$

This method has been used in a study of the $\phi\phi$ system[38].

Formally a resonance is defined as a complex pole in the S-matrix. As one sees the definition of the S-matrix through the K-matrix, a complex pole is inside the matrix $(1-iK)^{-1}$. If one calculates, $(m^2-s)(1-iK)$, one obtains the expression denoted by Δ which is the inverse of a complex pole,

$$\Delta = m^2 - s - iU^2$$

For the general case of M channels and N poles, one defines the following expression for Δ corresponding to the N-th resonance,

$$\Delta = \frac{\Pi_i(m_i^2-s)\det(1-iK)}{\Pi_{i,i\neq N}(m_i^2-s)\det(1-iK_N)}$$

where K is the M-channel(M by M) K-matrix with N poles, K_N is the same M-channel K-matrix with the N-th pole removed. The appropriateness of this definition can be seen if one studies simple cases. A major difference between this method and the first method is that one is concerned with only one M by M matrix in this method no matter how many poles one introduces in the fit. Again the mass of the N-th resonance is close to the mass parameter m_N of the N-th pole but dependent on the energy $\sqrt{s}$,

$$m = (\mathrm{Real}\Delta + s)^{1/2},$$

$$\Gamma = -\mathrm{Imag}(\frac{\Delta}{m}).$$

The partial widths of the resonance is defined to be,

$$\Gamma_a = |\frac{\Delta}{m}(T_{aa} - T'_{aa})|,$$

where T_{aa} is the (a,a) element of the T-matrix computed from K, and T'_{aa} is the (a,a) element of the T-matrix computed from K_N.

6.3 Auxiliary Data Sets

As we discussed previously, we do not have detailed information concerning the unitarity limits of these data sets. We can not use the K-matrix representation of T-matrix. We can write the production amplitude

$$T = (1 - iK)^{-1}P,$$

where P is given through the use of arbitrary complex parameters C_j,

$$P_\beta = \sum_j \frac{C_j U_{j\beta}}{m_j^2 - s}.$$

This parameterization follows the generalization considered by Aitchison[39] and has been successfully applied to the analysis of the 3π data[40]. The central observation from which this generalization was considered was that in the definition of the T-matrix the $(1 - iK)^{-1}$ term describes the propagation of two-body intermediate states and the additional factor K is for the formation and decay of these states. Thus replacing one of the coupling constants with arbitrary complex parameters to form the P-vector is equivalent to introducing arbitrariness in the formation and decay of resonances, the result of this is to relax the unitarity constraints.

6.4 Kinematics

The coupling constant U_{li} for the l-th K-matrix pole and the i-th channel is of the following form,

$$U_{li} = \gamma_{li} B(rq_i),$$

where γ_{li} is a free parameter to be determined by fit, $B(rq_i)$ is the Blatt-Weisskopf barrier factor which is a function of the effective momentum of the meson-meson system in the i-th channel and another free parameter r of dimension length. This parameter was 5.0 in our fits. For the S-wave this factor is equal to q_i. For the higher waves they are of the following forms,

$$B(rq) = q\frac{(rq)^4}{(rq)^4 + 3(rq)^2 + 9},$$

for the D-wave, and

$$B(rq) = q\frac{(rq)^8}{(rq)^8 + 10(rq)^6 + 135(rq)^4 + 1575(rq)^2 + 11025},$$

for the G-wave.

Among seven different channels, the $\epsilon\epsilon$ and the $\rho\rho$ channels are different from the others, since the ϵ(the old ϵ at around 720 Mev/c^2) and the ρ both have non-negligible widths. These channels represent that of a broad 4 π continuum background rather than a real 2 meson decay channel. The phase space integral is defined on a 4-body phase space (2 pions versus 2 pions), and it requires Monte Carlo computations to perform this integral. Instead, we used the standard formula from the 2-body kinematics,

$$q^2 = \frac{(s - (m_1 + m_2)^2)(s - (m_1 - m_2)^2)}{4s},$$

modified by introducing complex masses, m_1 and m_2, and with use of a parameter θ to adjust the threshold,

$$q'^2 = q^2 + \frac{\theta}{4s}.$$

The values of the effective momenta used in the fit are obtained from the real part of q' defined above. The parameters, the imaginary parts of m_1 and m_2 and θ were chosen so that the effective momenta calculated are approximately identical to those obtained by the Monte Carlo calculations. The values which we obtained were,

$$m_\epsilon = 0.720 + 0.0401i \mathrm{Gev/c^2}$$

$$\theta_\epsilon = 0.0127 (\mathrm{Gev/c^2})^2$$

$$m_\rho = 0.770 + 0.023i \mathrm{Gev/c^2}$$

$$\theta_\rho = 0.0053 (\mathrm{Gev/c^2})^2.$$

Chapter 7 Fits to the Data

7.1 Mesons with $J^{PC}=2^{++}$ and 4^{++}

The fact that the $\pi\pi$ and K_sK_s data are both dominated by the $f_2(1270)$ below 1.6 Gev/c^2 made the first part of the fit relatively smooth. A K-matrix pole was introduced at 1.2 Gev/c^2 and the $\pi\pi$ and $K\bar{K}$ couplings were opened to fit these two data sets below 1.6 Gev/c^2. When the phases of the $\pi\pi$ were fitted and the convergence was reached, the second K-matrix pole was introduced at 1.5 Gev/c^2 with the $\pi\pi$ and $K\bar{K}$ couplings. This second pole improved the total χ^2 dramatically. Then we introduced the K-induced $K\bar{K}$ data to the fit, in order to constrain the total width of the second pole as well as the $K\bar{K}$ partial width of the first pole. Clear improvements in the widths of these poles were seen. The $\eta\eta$ couplings of these poles were then opened at this stage to avoid unnecessary constraints among the parameters. The widths and masses of the states were always computed at each mass bin every time a fit was performed. The third pole was then introduced at 1.6 Gev/c^2 with three couplings($\pi\pi$, $K\bar{K}$, and $\eta\eta$), while the range of the fit was extended to 1.8 Gev/c^2. When the convergence was reached, the $\eta\eta$ data were introduced. The $\eta\eta$ and $\rho\rho$ channels needed to be opened to achieve unitarity. The fit was constrained by the total and partial widths of these poles. We then introduced the SLAC $\pi\pi$ and K^+K^- data sets with the helicities separated explicitly according to the claims made by the SLAC group. The entire range of the $\pi\pi$ and K_sK_s data were fitted with the $\omega\omega$ couplings turned on.

A reasonable fit was found using 5 poles. This fit, which we called Fit I, has a χ^2 of 273 for 225 degrees of freedom. The parameters were listed in the Table 7.3. By

the χ^2 test described in the Ref. 23, this is a 2.3 σ fit. The large χ^2 contributions come from three different regions:

a)the region around 1.7 Gev/c^2 in the SLAC $\pi\pi$ data especially in the helicity 2 part of the spectrum.

b)the region around 1.6 Gev/c^2 in the K-induced K^+K^- data.

c)the $\pi\pi$ phases between 1.5 Gev/c^2 and 1.9 Gev/c^2.

The contribution a) is the largest. The over-all quality of the fit was otherwise satisfactory as seen in the Fig. 7.1 through Fig. 7.3. The parameters in the Table 7.3 show that these poles can be identified with $f_2(1270)$, $f_2'(1525)$, $f_2(1720)$, and $f_2(1810)$. This fit and the all other fits to be described below required a broad pole located at higher masses shown in the Table 7.9. The most noteworthy aspect of this fit result is seen in the total and the partial widths of the $f_2(1270)$ and the $f_2'(1525)$.

Upon comparing these parameters with the published values, we found that the branching ratios of the $f_2(1720)$ were rather inconsistent. In particular the $\pi\pi$ branching ratio of this state appeared to be too small,

$$\frac{\Gamma_{\pi\pi}}{\Gamma_{total}} = 0.036.$$

this number is almost half the published value. Also noteworthy is the substantial inelasticity seen in the ratio,

$$\frac{\Gamma_{\epsilon\epsilon} + \Gamma_{\rho\rho} + \Gamma_{\omega\omega}}{\Gamma_{total}} = 0.72$$

this number has never been measured since decays of the $f_2(1720)$ into these channels have not been seen.

We then attempted a constrained fit to see compatibility of the branching ratios of the $f_2(1720)$ with the reported values. The resulting fit is called Fit II, the parameters are listed in the Table 7.4. The total width of the $f_2(1720)$ is substantially smaller.

Though the helicity separation we used was done according to the assumption made by the SLAC group, it is clear that their assumption had never been verified explicitly. We have also considered the possibility that this helicity component separation of the SLAC $\pi\pi$ data around the $f_2(1720)$ region relied on a wrong assumption. To see if this possibility was reasonable we attempted another fit in which the helicity 2 part of the SLAC $\pi\pi$ data was dropped. The resulting parameters are given in the Table 7.5. This fit(Fit III) is not different from the Fit II except that the total width of the fourth pole is larger by roughly 100 Mev/c^2. The χ^2 per degrees of freedom of the Fit II and Fit III are also similar. In both cases extra contributions to the total χ^2 comes from the above-mentioned region b). The conclusion we draw from this result is that the assumption of the helicity separation is not significant in understanding the smallness of the $\pi\pi$ branching ratio of the $f_2(1720)$.

We have attempted three more different fits. The first fit(Fit A) was done without including the SLAC data. This fit was a 1.26σ fit.

The second fit(Fit B) had a highly important purpose to see the general significance of the $f_2(1720)$ in the hadronic data. The SLAC data sets were dropped and the pole at 1.7 Gev/c^2 was removed. The quality of the fit did not change except in the region b). The fit basically failed to describe this region because in this fit we have only one pole strongly coupled to the K^+K^-. This is a 2.9σ fit.

The third fit(Fit C) was a study of the significance of the pole at 1.8 Gev/c^2. In this fit this pole was removed but the third pole located at 1.7 Gev/c^2 in the Fit A was retained. This fit could not describe the $\pi\pi$ data, both the phases and the amplitudes modulus squared, in the region between 1.5 Gev/c^2 and 1.9 Gev/c^2.

Two important conclusions emerged from these fits. One of them is that the $f_2(1720)$ is not seen in the hadronic channels. High-statistics data from the K-induced $K\bar{K}$ production experiment in the future could shed light on this point. The $f_2(1810)$ is definitely established in the hadronic $\pi\pi$ channel by 7.8σ.

During these fits, the G-wave amplitudes were also studied. Since the old $\eta\eta$ data sets do not contain the G-wave, we only used three couplings(the $\pi\pi$, $K\bar{K}$, and the $\rho\rho$ channels). All six fits(I, II, III, A, B, and C) gave similar results for the $f_4(2030)$,

$$m = 1.980^{+0.008}_{-0.007}$$

$$\Gamma_{total} = 0.330^{+0.009}_{-0.041},$$

with the following branching ratios,

$$x_{\pi\pi} = 0.079^{+0.004}_{-0.002}, x_{K\bar{K}} = 0.044^{+0.001}_{-0.001}.$$

The phases of the $K^0_S K^0_S$ above 1.85 Gev/c^2 were exceptionally influential in determining these parameters mainly because of their small error bars. Also these phases made it extremely difficult to introduce another state above 2.0 Gev/c^2, although it is evident that the fits to the $|G|^2$ of both the $\pi\pi$ and the $K^0_S K^0_S$ data require another state which may be a background.

Tables of the fit results

Table 7.1 The fits with description. h=2 means helicity component 2.

fit	description
I	the best global fit
II	fit with SLAC branching ratios
III	fit without SLAC $\pi\pi$ (h=2)
A	the best global fit without SLAC data
B	fit without $f_2(1720)$
C	fit without $f_2(1810)$

Table 7.2 The channel labels and the processes.

channel	process
1	$\pi\pi \rightarrow \pi\pi$
2	$\pi\pi \rightarrow K\bar{K}$
3	$\pi\pi \rightarrow \eta\eta$
4	$\pi\pi \rightarrow \epsilon\epsilon$
5	$\pi\pi \rightarrow \rho\rho$
6	$\pi\pi \rightarrow \omega\omega$

Table 7.3 The parameters of the Fit I. The numbers in the first row are channel labels from the Table 2. The numbers are all in the units of Gev/c^2. Those in the parentheses are the K-matrix pole positions.

state	mass	width	1	2	3	4	5	6
$f_2(1.281)$	1.283	0.185	0.156	0.009	0.001	0.000	0.019	0.000
$f_2'(1.537)$	1.548	0.114	0.001	0.065	0.025	0.014	0.010	0.000
$f_2(1.728)$	1.725	0.194	0.007	0.037	0.010	0.018	0.014	0.108
$f_2(1.887)$	1.856	0.406	0.082	0.002	0.003	0.010	0.253	0.056

χ^2/d.f.=273/225=1.21

Table 7.4 The parameters of the Fit II.

state	mass	width	1	2	3	4	5	6
$f_2(1.283)$	1.286	0.192	0.162	0.009	0.001	0.000	0.020	0.000
$f_2'(1.541)$	1.553	0.114	0.001	0.062	0.028	0.011	0.014	0.000
$f_2(1.740)$	1.729	0.119	0.005	0.047	0.024	0.020	0.023	0.010
$f_2(1.801)$	1.787	0.183	0.041	0.004	0.007	0.017	0.050	0.065

χ^2/d.f.=307/225=1.36

Table 7.5 The parameters of the Fit III.

state	mass	width	1	2	3	4	5	6
$f_2(1.283)$	1.286	0.191	0.160	0.009	0.001	0.000	0.019	0.000
$f_2'(1.541)$	1.557	0.110	0.001	0.059	0.026	0.011	0.013	0.000
$f_2(1.717)$	1.718	0.115	0.002	0.053	0.024	0.013	0.013	0.010
$f_2(1.811)$	1.806	0.276	0.054	0.004	0.008	0.083	0.084	0.056

χ^2/d.f.=310/225=1.378

Table 7.6 The parameters of the Fit A

state	mass	width	1	2	3	4	5	6
$f_2(1.287)$	1.289	0.184	0.156	0.009	0.001	0.000	0.019	0.000
$f_2'(1.543)$	1.556	0.111	0.001	0.062	0.025	0.014	0.009	0.000
$f_2(1.700)$	1.697	0.212	0.003	0.058	0.014	0.019	0.011	0.107
$f_2(1.905)$	1.876	0.458	0.082	0.001	0.001	0.014	0.297	0.063

χ^2/d.f.=189.4/167=1.13

Table 7.7 The parameters of the Fit B

state	mass	width	1	2	3	4	5	6
$f_2(1.282)$	1.284	0.189	0.168	0.011	0.001	0.000	0.025	0.000
$f_2'(1.526)$	1.533	0.101	0.002	0.062	0.002	0.008	0.009	0.000
$f_2(1.880)$	1.838	0.429	0.075	0.002	0.000	0.113	0.238	0.000

χ^2/d.f.=241.6/173=1.40

Table 7.8 The parameters of the Fit C

state	mass	width	1	2	3	4	5	6
$f_2(1.277)$	1.278	0.185	0.157	0.009	0.001	0.000	0.019	0.000
$f_2'(1.541)$	1.551	0.112	0.001	0.063	0.025	0.013	0.009	0.000
$f_2(1.719)$	1.731	0.175	0.005	0.029	0.014	0.030	0.024	0.088

χ^2/d.f.=329/173=1.84

Table 7.9 The K-matrix pole mass parameters for the background pole.

Fit	pole position
I	6.000
II	6.387
III	6.402
A	6.071
B	5.974
C	5.962

Table 7.10 The masses and widths of the $f_2(1270)$ and $f_2'(1525)$ with errors in the units of Mev/c^2 from the Fit I.

state	mass	Γ_{tot}	$\Gamma_{\pi\pi}$	$\Gamma_{K\bar{K}}$	$\Gamma_{\eta\eta}$
$f_2(1270)$	1283^{+6}_{-5}	186^{+9}_{-2}	157^{+6}_{-1}	$9.0^{+0.7}_{-0.3}$	$1.0^{+0.1}_{-0.1}$
$f_2'(1525)$	1547^{+10}_{-2}	108^{+5}_{-8}	$1.4^{+1.0}_{-0.5}$	63^{+6}_{-5}	24^{+3}_{-1}

Table 7.11 The parameters for the $f_2(1810)$ and the $f_2(1720)$ from the Fit I. The fourth raw are the parameters for the $f_2(1720)$ from the Fit II for comparison.

state	mass	width	$X_{\pi\pi}$	$X_{K\bar{K}}$	$X_{\eta\eta}$	X_{other}
$f_2(1810)$	1858^{+18}_{-71}	388^{+15}_{-21}	$0.21^{+0.02}_{-0.03}$	$0.003^{+0.019}_{-0.002}$	$0.008\ ^{+0.028}_{-0.003}$	$0.77^{+0.03}_{-0.07}$
$f_2(1720)$	1725^{+4}_{-7}	196^{+2}_{-81}	$0.035\ ^{+0.004}_{-0.020}$	$0.19^{+0.27}_{-0.01}$	$0.05^{+0.16}_{-0.01}$	$0.73^{+0.01}_{-0.41}$
$f_2(1720)$	1730^{+2}_{-10}	122^{+74}_{-15}	$0.039^{+0.002}_{-0.024}$	$0.38^{+0.09}_{-0.19}$	$0.18^{+0.03}_{-0.13}$	$0.41^{+0.33}_{-0.11}$

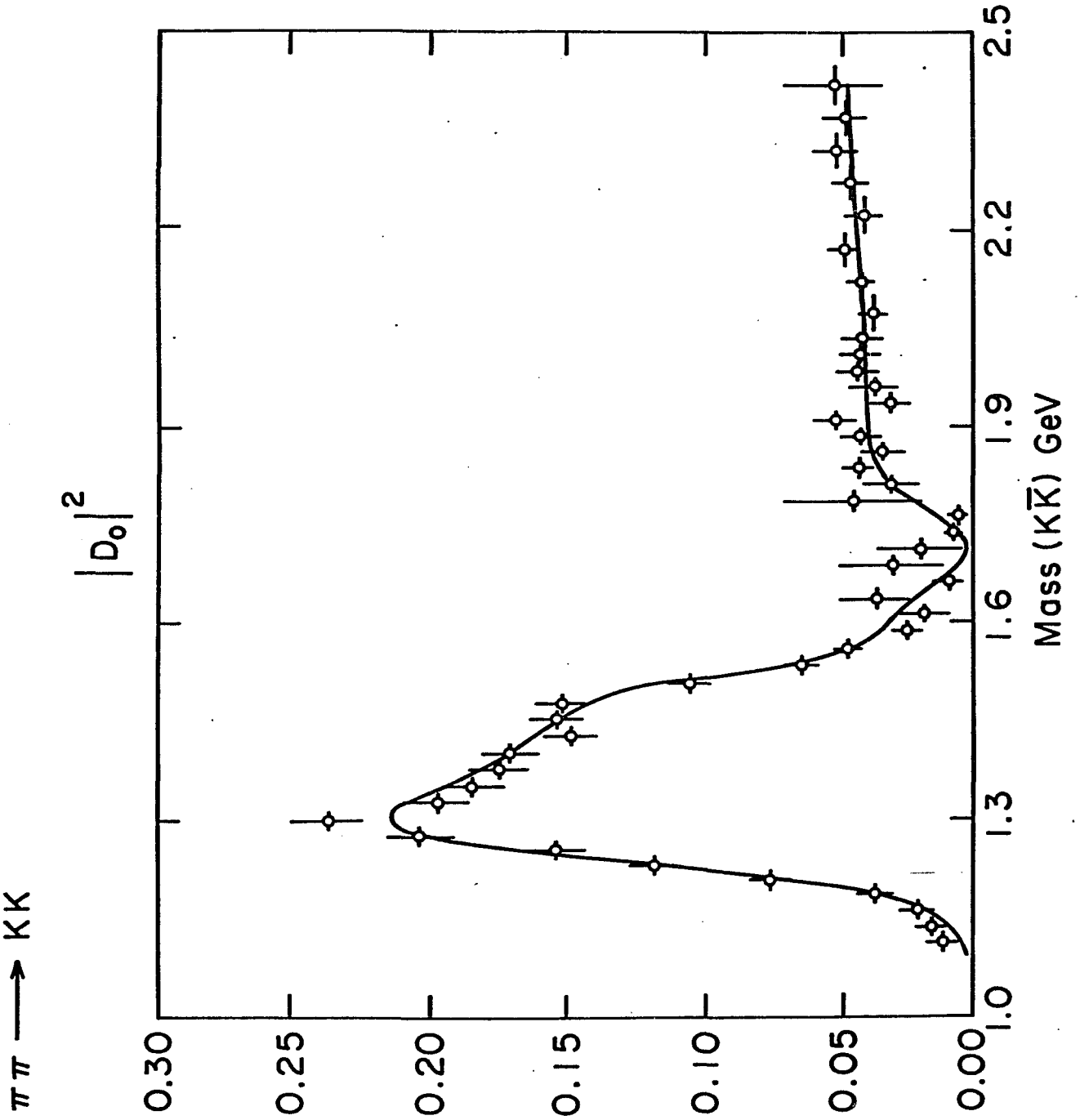

Fig. 7.1 The modulus square of the D-wave amplitude as a function of $K\bar{K}$ invariant mass(Gev/c^2). The solid curve is the Fit L

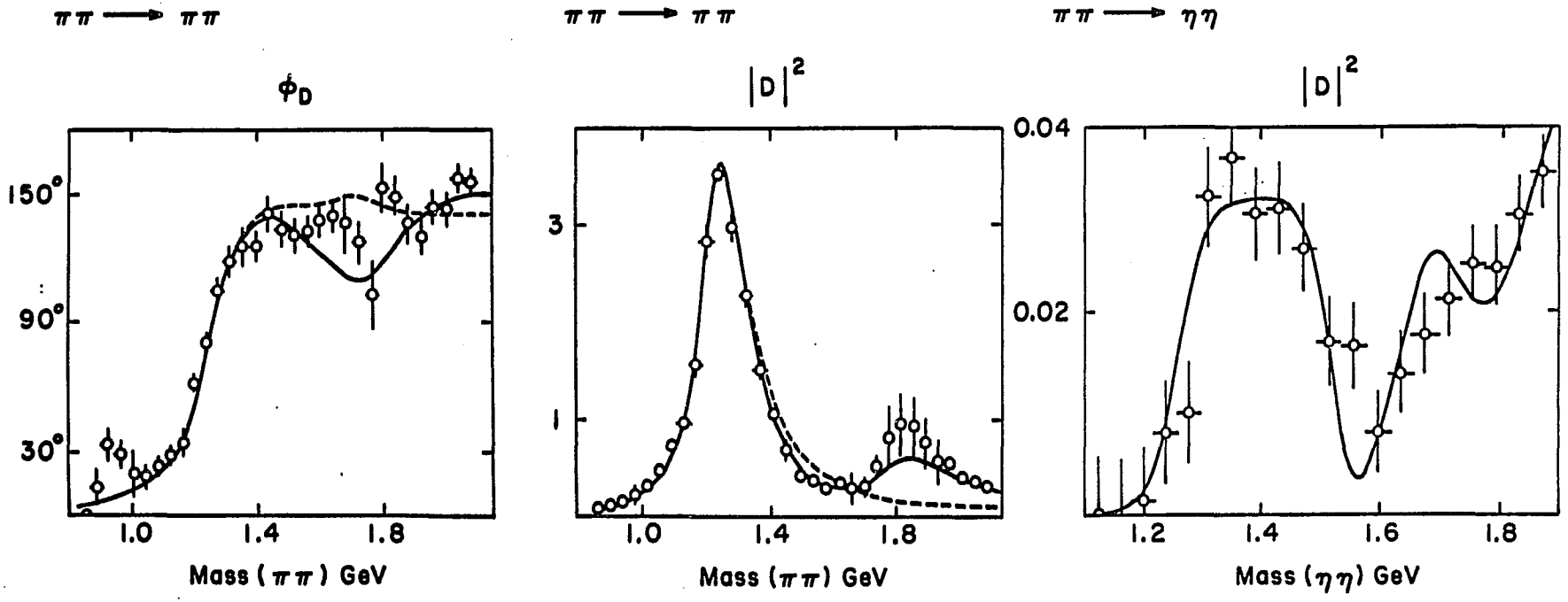

Fig. 7.2 a) The D-wave phase in degrees; b) The modulus square of the D-wave from chapter 2; c) The modulus square of the D-wave OPE amplitude for the $\eta\eta$ as a function of $\eta\eta$ invariant mass(Gev/c^2). The solid and dashed curves came from Fit I and Fit C.

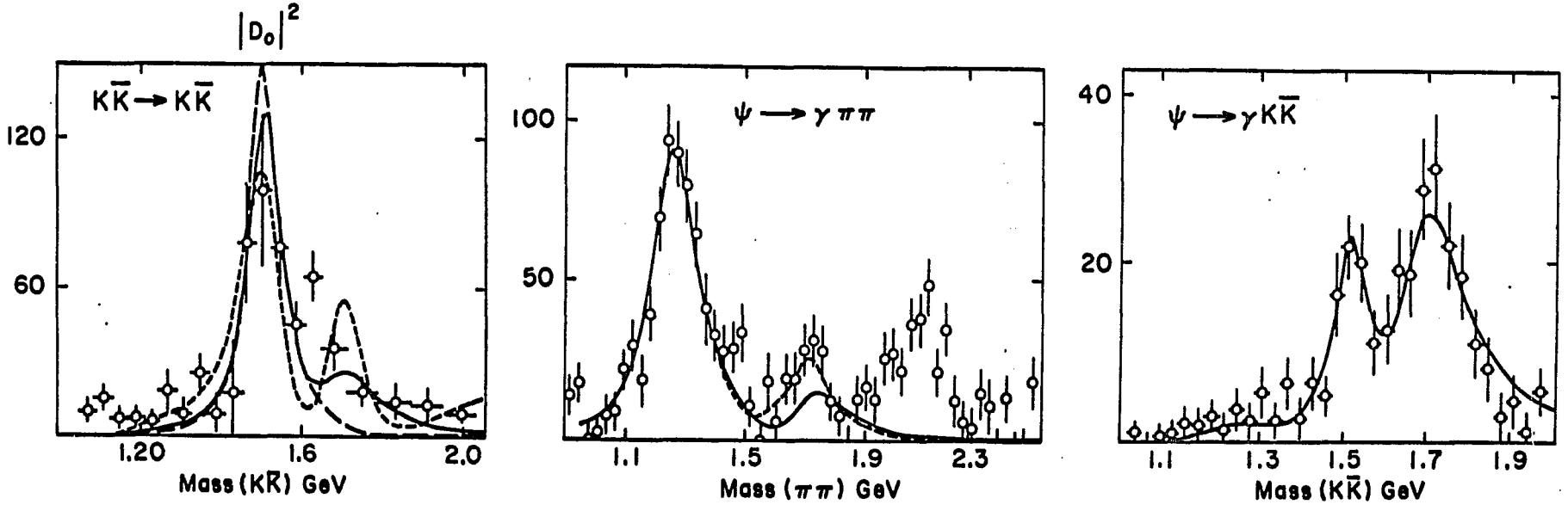

Fig. 7.3 a) The modulus square of the *D*-wave amplitude from Ref. 27 in events as a function of K^+K^- invariant mass(Gev/c^2); b) The $\pi^+\pi^-$ spectrum from the radiative decay of J/ψ in events as a function of $\pi^+\pi^-$ invariant mass(Gev/c^2); c)The K^+K^- mass spectrum from the radiative decay of J/ψ in events as a function of K^+K^- invariant mass(Gev/c^2). The solid curve is the Fit I; the short dashed curve is the Fit II; the long dashes are Fit B.

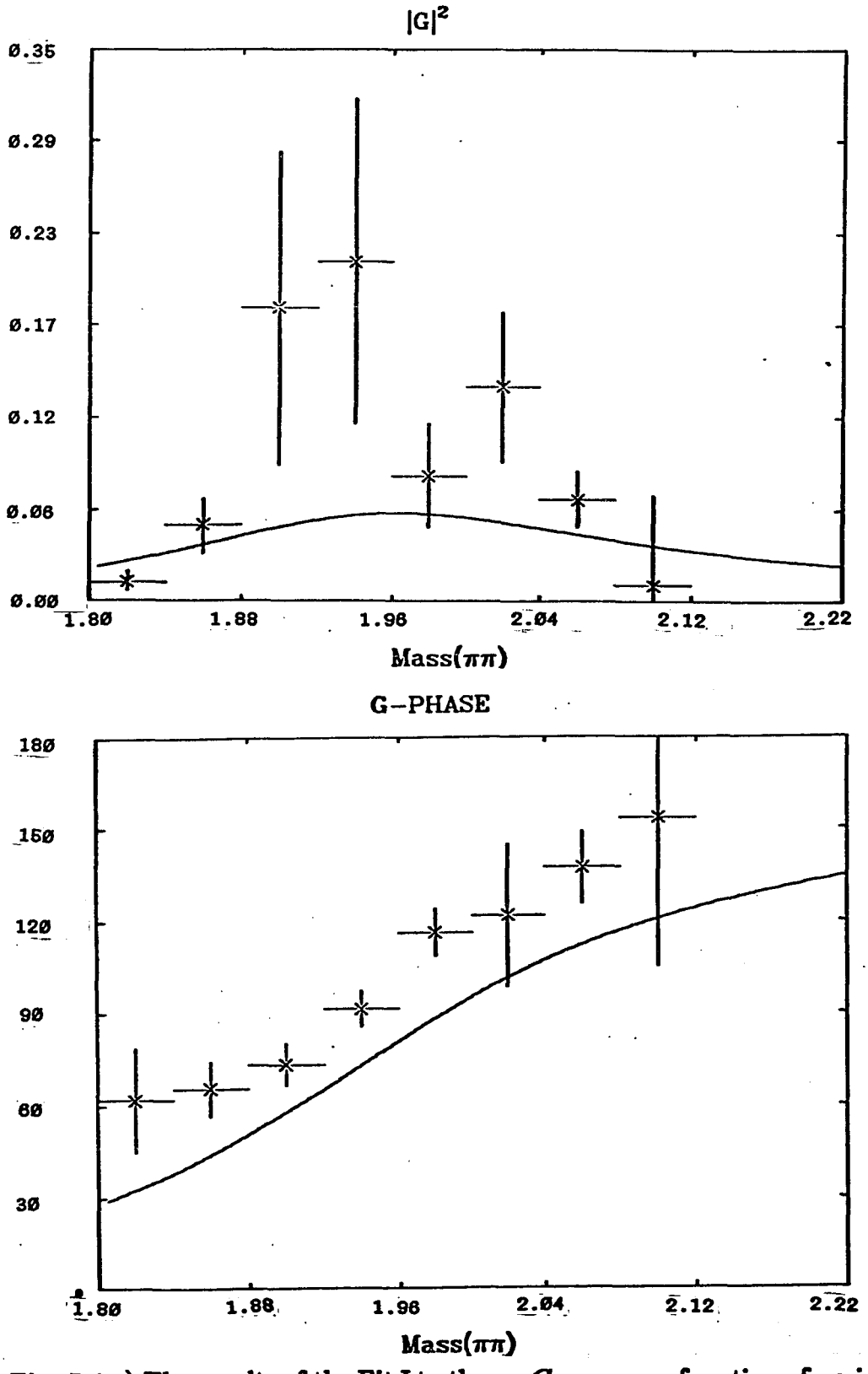

Fig. 7.4 a) The results of the Fit I to the $\pi\pi$ G-wave as a function of $\pi\pi$ invariant mass(Gev/c^2); a) The modulus square of G-wave world averages from chapter 2; b) The G-wave phase in degrees.

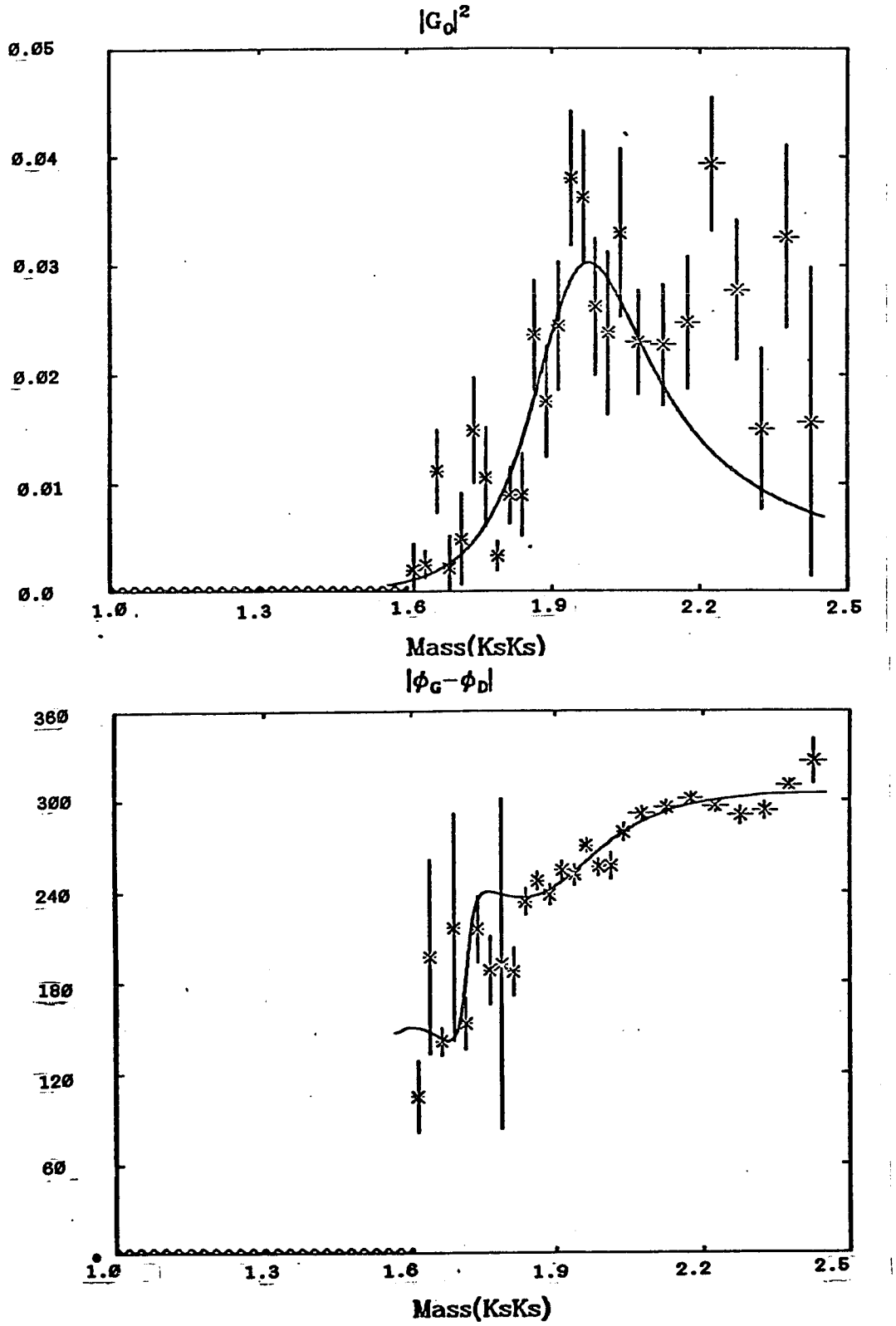

Fig. 7.5 The results of the Fit I to the $K\bar{K}$ G-wave as a function of $K\bar{K}$ invariant mass(Gev/c^2); a) The modulus square of G-wave amplitude; b) The relative phase $|\phi_G - \phi_D|$ in degrees.

7.2 Preliminary Investigation of Mesons with $J^{PC} = 0^{++}$

We recall the general strategy in the fit of the D-wave data sets. The parts of the spectra around the $f_2(1270)$ and the $f_2'(1525)$ made the beginning of the fit very smooth. The data points around the $f_2(1270)$ were even used to "calibrate" the phase motion. Upon making a qualitative comparison of the $|S|^2$ of the $\pi\pi$, $K\bar{K}$, and the $\eta\eta$ data, one finds that they do not share similarities(the kinds of similarities that we observed in the $|D|^2$ simply do not exist). The most outstanding difference in the $|S|^2$ is seen in the region around 1.6 Gev/c^2 in the $\eta\eta$ data. This along with the total absence of narrow structure in the S-waves makes the fit extremely difficult. In this section, some of the results of the fits that are still in progress are presented and discussed.

We have taken the Fit I and fixed all the parameters for the D-waves and G-waves, we proceeded according to the following order:

1) fit the $|S|^2$ of the $\pi\pi$ data up to 1 Gev/c^2.

2) the $|S|^2$ of the $K_S^0K_S^0$ data added and the $\pi\pi$ data extended to 1.5 Gev/c^2.

3) the $|S|^2$ of the $\eta\eta$ data added to 1.5 Gev/c^2.

4) the Pomeron $\pi\pi$ data added.

5) the phases of the $\pi\pi$, $K_S^0K_S^0$, and $\eta\eta$ added.

6) the $\eta\eta'$ data added.

7) the steps 1) through 5) were repeated with data points extended to 2.5 Gev/c^2.

At present fit results based upon 7 K-matrix poles indicate that this fit is possible except in the region between the threshold and 1.8 Gev/c^2 of the $|S|^2$ in

the $\eta\eta$ data. These fit results had been presented already. The masses and widths of these resonances are:

a) the low mass region(below 1.0 Gev/c^2),

$$\begin{aligned} m_1 &= 0.99\text{Gev}/c^2 \\ \Gamma_1 &= 0.03\text{Gev}/c^2 \\ m_2 &= 0.96\text{Gev}/c^2 \\ \Gamma_2 &= 0.17\text{Gev}/c^2. \end{aligned} \tag{7-1}$$

b) the medium mass region(1.0 Gev/c^2 to 1.60 Gev/c^2),

$$\begin{aligned} m_3 &= 1.32\text{Gev}/c^2 \\ \Gamma_3 &= 0.59\text{Gev}/c^2 \\ m_4 &= 1.51\text{Gev}/c^2 \\ \Gamma_4 &= 0.29\text{Gev}/c^2. \end{aligned} \tag{7-2}$$

c) the high mass region(1.60 Gev/c^2 to 2.0 Gev/c^2),

$$\begin{aligned} m_5 &= 1.74\text{Gev}/c^2 \\ \Gamma_5 &= 0.33\text{Gev}/c^2 \\ m_6 &= 1.75\text{Gev}/c^2 \\ \Gamma_6 &= 0.34\text{Gev}/c^2. \end{aligned} \tag{7-3}$$

d) the region above 2.0 Gev/c^2,

$$\begin{aligned} m_7 &= 2.30\text{Gev}/c^2 \\ \Gamma_7 &= 0.27\text{Gev}/c^2. \end{aligned} \tag{7-4}$$

The following Table shows the branching ratios of these seven states.

Table 7.12 Branching Ratios of the Scalar resonances.

state	$x_{\pi\pi}$	$x_{K\bar{K}}$	$x_{\eta\eta}$
m_1	1.0	0.0	0.0
m_2	1.0	0.0	0.0
m_3	0.55	0.35	0.02
m_4	0.13	0.00	0.52
m_5	0.25	0.05	0.07
m_6	0.57	0.01	0.00
m_7	0.10	0.01	0.47

In addition to these, we obtained $x_{\eta\eta'}$=0.25, 0.23 for the fifth and the sixth states respectively.

The $\pi\pi$ world averages presented in Chapter 2 are extremely close to the data set obtained by Hyam *et al.* in the CERN-Munich experiment(Ref. 10). The data set 7) taken from their experiment dominated in the averaging process. This is due to the fact that their data points have very small error bars. Their data set also has smaller bin sizes. With this data we made efforts to understand the $\pi\pi$ data below 1 Gev/c^2 independent of other data sets. This is possible since the elasticity of the $\pi\pi$ amplitudes is 1 up to the $K\bar{K}$ threshold, simple fits to the δ_0^0(the isospin=0 S-wave phases) were attempted using various ways of parametrization. The most important conclusion of these independent fits is that two resonances are definitely necessary to understand the $\pi\pi$ data below the $K\bar{K}$ threshold. These resonances are one extremely narrow and one extremely wide ones,

$$\begin{aligned} m_1 &= 1.017\text{Gev/c}^2 \\ \Gamma_1 &= 0.067\text{Gev/c}^2, \\ m_2 &= 1.038\text{Gev/c}^2 \\ \Gamma_2 &= 1.710\text{Gev/c}^2. \end{aligned} \tag{7-5}$$

The second resonance may be regarded as a background because of its extreme width. These parameter values (7-5) become the values (7-1) when other channels

are introduced, also the qualitative feature(one narrow state and one wide background) change dramatically. This necessity of two poles can be seen most clearly if one considers the $\cot\delta_0^0$ as a function of the invariant mass of the $\pi\pi$ system. Recall that the elastic scattering amplitude can be written as,

$$f = \frac{1}{\cot\delta_0^0 - i}$$

and usually the $\cot\delta_0^0$ is expanded as a Taylor series in terms of $m_{\pi\pi}$ to obtain a classical Breit-Wigner form. One can see that the data points of $\cot\delta_0^0$ can not be approximated by a linear function of $m_{\pi\pi}$, neither can they be represented as a cubic function of $m_{\pi\pi}$, whereas the data points around the ρ region can be sufficiently represented by a linear function up to 0.85 Gev/c^2. The same observation based on the relativistic Breit-Wigner is possible.

The fit result in Fig. 7.6 shows that the pomeron $\pi\pi$ data can be reasonably understood by two K-matrix poles below 1 Gev/c^2.

The resonances in the medium mass region(7-2) are consistent with what we had known already. These resonances are the $f_0(1300)$ and the $f_0(1590)$. The resonances in the high mass region(7-3) are rather puzzling to us, but the inadequacy of the present fit to describe the $\eta\eta$ spectrum from the threshold to 1.8 Gev/c^2 will be the key to improve the results.

The necessity of the seventh K-matrix pole appears to be overwhelming, since the region of the $K_S^0K_S^0$ and the $\eta\eta$ data above 2.0 Gev/c^2 can not be described without this pole.

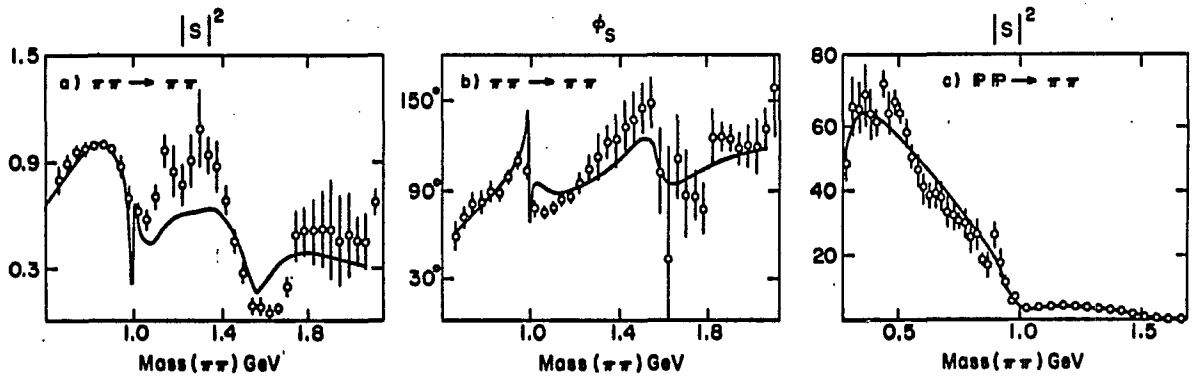

Fig. 7.6 The results of the fit to the S-wave as a function of $\pi\pi$ invariant mass(Gev/c^2); a) The modulus square of the S-wave amplitude; b) The S-wave phase in degrees; c) The $\pi\pi$ mass spectrum in events from the Pomeron $\pi\pi$ data.

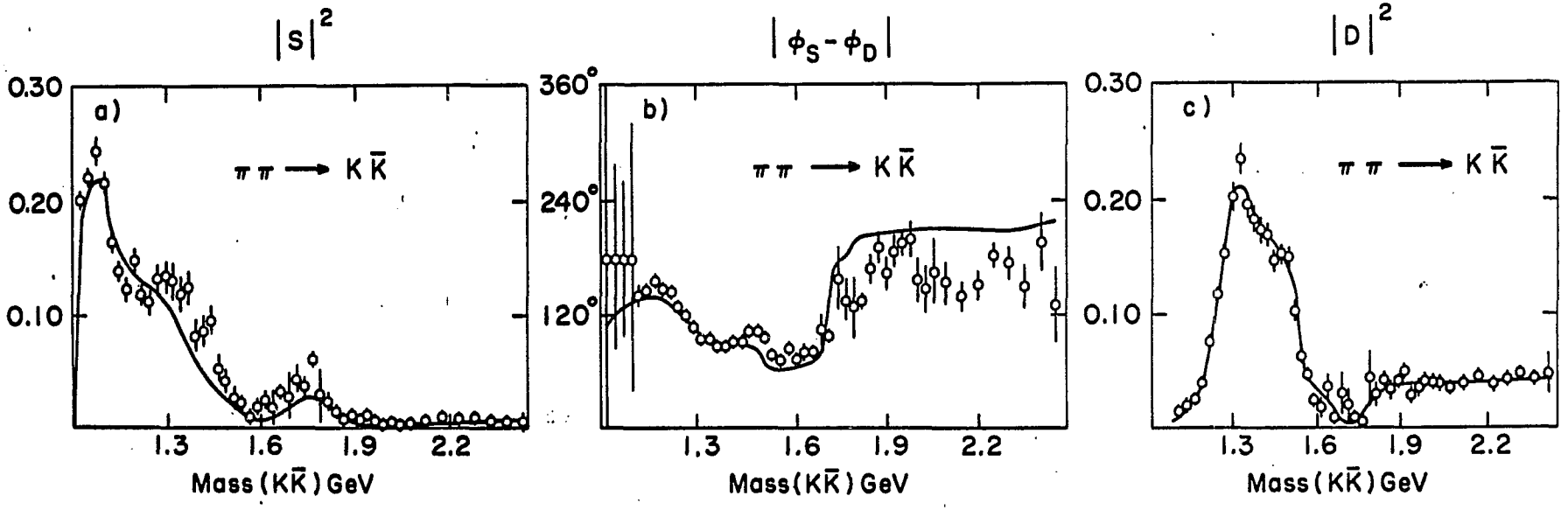

Fig. 7.7 The results of the fit to the $K\bar{K}$ S-wave as a function of $K\bar{K}$ invariant mass(Gev/c^2); a) The modulus square of the S-wave amplitude; b) The relative phase $|\phi_S - \phi_D|$.

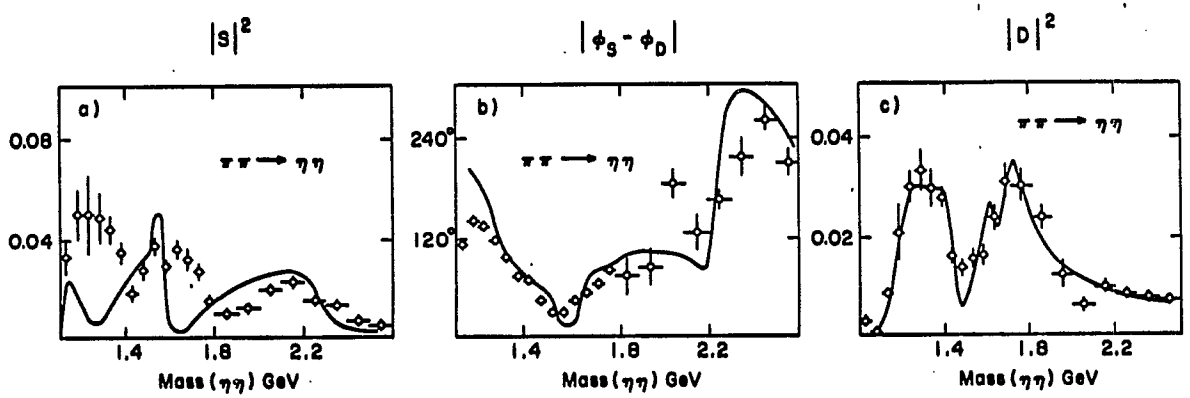

Fig. 7.8 The results of the fit to the $\eta\eta$ S-wave and D-wave(new data); a) The modulus square of the OPE extrapolated S-wave amplitude; b) The relative phase $|\phi_S - \phi_D|$ in degrees; c) The modulus square of the OPE extrapolated D-wave amplitude.

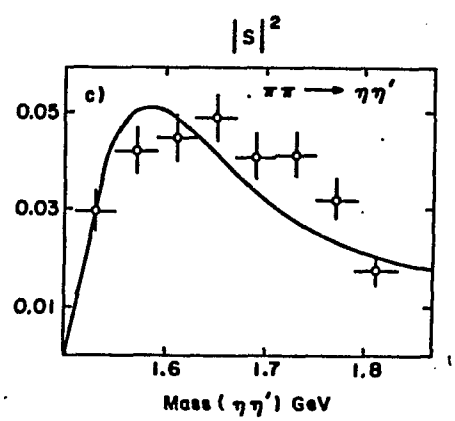

Fig. 7.9 The result of the fit to the OPE extrapolated $\eta\eta'$ S-wave amplitude modulus squared as a function of $\eta\eta'$ invariant mass(Gev/c^2).

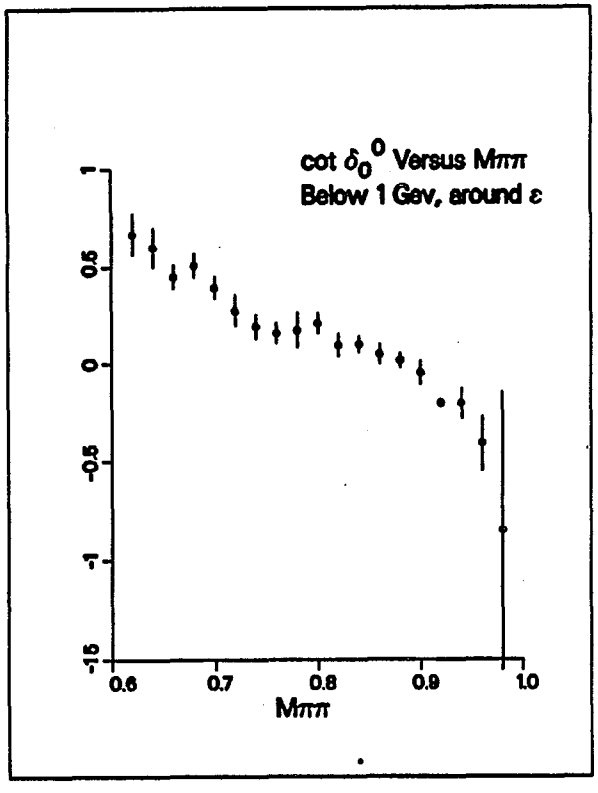

Fig. 7.10 $\cot \delta_0^0$ as a function of $\pi\pi$ invariant mass(Gev/c^2).

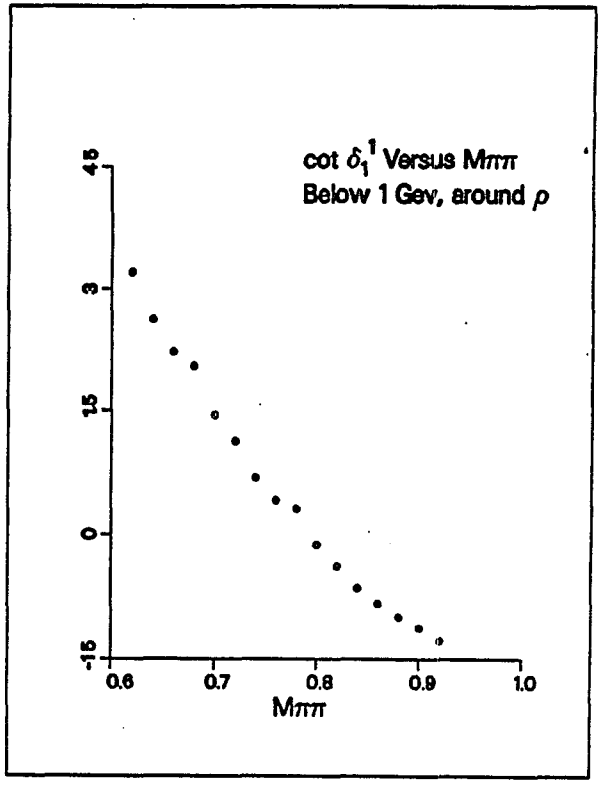

Fig. 7.11 $\cot \delta_1^1$ as a function of $\pi\pi$ invariant mass(Gev/c^2).

Chapter 8 Generalities and Summary

8.1 Low Energy QCD and Light-quark Spectroscopy

In this chapter we discuss some of the available results from theoretical studies of light-quark spectroscopy. There are three totally different approaches: 1) potential model approach, 2) bag model approach, and 3) lattice gauge theory approach. At present none of these is free from problems.

Studies of light-quark mesons in the lattice field theory have not reached full maturity yet. Most of the available results are for baryons and low-lying mesons, mesons with 0^{-+} and 1^{--}. The ratios of proton mass to those of the ρ and the Δ have been calculated on larger lattices with dynamical quark loops explicitly included[41]. Things are rather encouraging.

The potential models are now capable of giving realistic results for light-quark spectroscopy. Among the potential models, the one recently developed by Godfrey and Isgur[42] appears to be reasonably successful in describing spectra of $q\bar{q}$ mesons.

They use a relativistic Hamiltonian,

$$H_0 = (P_q^2 + m^2)^{1/2} + (P_{\bar{q}}^2 + m^2)^{1/2}$$

together with a potential of the form,

$$V = -\frac{4}{3}(\frac{\alpha_s(r)}{r} + br + c) + H^{spin-spin} + H^{spin-orbit} + H_a$$

to solve a Schrödinger equation. The last term in the potential, H_a, is for the annihilation processes of $q\bar{q}$ and is important for isoscalar mesons. The large-distance behavior of the running coupling constant $\alpha_s(r)$ was controlled by a smearing function with an important assumption that α_s saturates at some value $\alpha_s^{critical}$=0.7. Even if this assumption makes sense, we really do not know if the coupling constant

is definable at very low energies, neither do we know how to measure its value below 2 Gev. Totally 14 free parameters were employed to calculate the meson spectra of light and heavy quarks. The masses of u- and d-quarks turned out to be around 220 Mev/c^2, while the mass of s-quark was 419 Mev/c^2.

Table 8.1 Light isoscalar mesons from the potential model of Godfrey and Isgur, masses are in Gev/c^2.

state	name	J^{PC}	predicted mass
1^3P_2	f	2^{++}	1.28
	f'		1.53
2^3P_2	f'_R		1.82
	f_R		2.04
1^3F_2	f_F		2.05
	f'_F		2.24
1^3P_0	ϵ	0^{++}	1.09
	ϵ'		1.36
2^3P_0	ϵ_R		1.78
	ϵ'_R		1.99
1^3F_4	h	4^{++}	2.01
	h'		2.20

Some of the predicted states are listed in Table 8.1. States with $J^{PC}=2^{++}$, and 4^{++} are in agreement. There are three 2^{++} states above 2.0 Gev/c^2, since these states are expected to be wide they are difficult to look for in the data. The continuum structure in the $K^0_sK^0_s$ D-wave above 1.60 Gev/c^2 may contain these states, one background pole was used to describe this region. The region above 2.0 Gev/c^2 in the D-wave $\eta\eta$ data is also structureless. The most noteworthy feature of this predicted spectrum of tensor mesons is the absence of a state that would correspond to the $f_2(1720)$. A phenomenological scheme in which states above 2 Gev/c^2 together with a gluon-bound state are mixed would be possible, by a proper choice of mixing parameters one of these states could have its mass at 1.72 Gev/c^2. But even with such a scheme one can not necessarily explain why the $f_2(1720)$ is not observed in the hadronic two-meson final states.

As to the spectroscopic assignment of the $f_0(975)$ and $a_0(980)$, two closely related possibilities[43] are available:

a) $f_0(975)$ and $a_0(980)$ are $K\bar{K}$ bound states,

b) $f_0(975)$ and $a_0(980)$ are two members of the low-lying "cryptoexotic" $qq\bar{q}\bar{q}$ nonet.

The $qq\bar{q}\bar{q}$ wave function in the potential model appears to describe two weakly bound color-singlet mesons, and the potential model predicts that probably only the $K\bar{K}$ system binds suppressing other members of the nonet. The narrow widths of these scalars follow from the fact that the $K\bar{K}$ wave function is large enough to make the $\pi\pi$-production improbable. This line of observation naturally suggests that the above-mentioned possibilities are both reasonable description of these scalars.

Turning to other scalar states, the potential model gives the following predictions where x_{MM} stands for the branching ratio:

a) $\epsilon(1090)$ has $\Gamma \simeq 850$ Mev, $x_{\pi\pi} \simeq 0.86$, and $x_{K\bar{K}} \simeq 0.14$.

b) $\epsilon'(1360)$ has $\Gamma \simeq 600$ Mev, $x_{\pi\pi} \simeq 0$, $x_{K\bar{K}} \simeq 0.8$, and $x_{\eta\eta} \simeq 0.2$.

c) $\epsilon_r(1780)$ has $\Gamma \simeq 1000$ Mev, $x_{\pi\pi} \simeq 3x_{K\bar{K}} \ll 1$.

None of the reported values for the mass and width of the $f_0(1300)$ comes close to those of the $\epsilon(1090)$ or of the $\epsilon'(1360)$. Our fit to the scalar amplitudes gave entirely different results. Although we can not reject these predicted scalars until we thoroughly explore possibilities, it is likely that we will continue to see discrepancies.

8.2 Summary

The analysis of the available $\pi\pi$ data sets show several outstanding discrepancies in the S-wave and the G-wave amplitudes. Attempts were made to derive the averages using the adiabatic averaging method with weights.

The data sets on the $K\bar{K}$ systems from the fixed target experiments with π beams are consistent with each other as the results of a recent experiment on $\pi^- p \rightarrow K_S^0 K_S^0 n$ at 22 Gev/c indicate.

With these amplitudes sets along with the $\eta\eta$ and other available data, a coupled-channel analysis was carried out using the K-matrix formalism.

The results of the fits to the D-wave amplitudes were very successful. The fit results gave consistent parameter values for three states, $f_2(1270)$, $f_2'(1525)$, and $f_2(1810)$. The necessity of the $f_2(1720)$ was seen only with respect to the data from SLAC experiments on the J/ψ radiative decays. The evidence seen in the available data indicates that this state is not formed in the hadronic meson-meson channel.

The S-wave amplitudes need further work. At least seven states are necessary to describe the spectra from 0.6 Gev to 2.4 Gev.

Appendix

Given two hypotheses, we would like to know which hypothesis is better than the other and by how much. The number of σ's by which two hypotheses differentiate themselves is given by,

$$n_{\sigma} = y_2 - y_1,$$

where

$$y_k = (2\chi_k^2)^{1/2} - (2N_{D_k} - 1)^{1/2},$$

for the k-th hypothesis and χ_k^2 and N_{D_k} are the χ^2 and number of degrees of freedom for the

fit to the same data based upon the k-th hypothesis. These definitions come from the standard χ^2 distribution in the limit of the number of degrees of freedom, N_D, being large enough to make the χ^2 normally distributed about N_D with standard deviation σ of 1. Let χ_1^2 and N_{D_1} represent the best fit with the ratio of approximately 1. With the assumptions that $\delta\chi^2/\chi_1^2$ and n/N_{D_1} are small where,

$$\chi_2^2 = \chi_1^2 + \delta\chi^2$$

and

$$N_{D_2} = N_{D_1} + n,$$

we obtain,

$$n_{\sigma} \approx (2\chi_1^2)^{1/2}(\delta\chi^2/2\chi_1^2 - n/(2N_{D_1} - 1)).$$

Further neglecting the last term in the above equation, we obtain the following simple formula.

$$n_{\sigma} \approx \delta\chi^2/(2\chi_1^2)^{1/2}.$$

References

1 J. Steinberger, Phys. Rev. 76, 1180 (1949).

2 D. J. Gross and R. Jackiw, Phys. Rev. D6,477(1972); H. Georgi and S. L. Glashow, Phys. Rev. D6,429 (1972).

3 S. W. Otto and John D. Stack, Phys. Rev. Lett. 52, No. 26, 2328 (1984).

4 C. Lovelace, Phys. Lett. 28B, 264 (1968); J. P. Shapiro, Phys. Rev. 179, 1345 (1969).

5 N. M. Cason *et al.*, D28, 1586 (1983).

6 W. D. Apel *et al.*, Phys. Lett. 57B, 403 (1975).

7 M. J. Corden *et al.*, Nucl. Phys. B157, 250 (1979).

8 A. D. Martin and M. R. Pennington, Ann. Phys. (N. Y.)114, 1 (1978).

9 P. Estabrooks and A. D. Martin, Nucl. Phys. B95, 322 (1975).

10 B. Hyams *et al.*, Nucl. Phys. B100, 205 (1975).

11 F. A. DiBianca *et al.*, Phys. Rev. D23, No. 3, 595 (1981); T. J. Killian *et al.*, Phy. Rev. D21, 3005 (1980).

12 C. Bromberg *et al.*, Caltech Report CALT-68-1070.

13 K. Abe *et al.*, Phys. Rev. Lett. 53, 751 (1984).

14 G. Grayer *et al.*, Nucl. Phys. B69, 266 (1974).

15 G. F. Chew and F. E. Low, Phys. Rev., 113, 1640 (1959).

16 R. M. Baltrusaitis *et al.*, Phys. Rev. Lett. 55, 1723 (1985); J. D. Richman, Catech Report CALT-68-1136; S. Cooper, SLAC Report SLAC-PUB-3819 Oct. 1985.

17 A. Skuja *et al.*, Phys. Rev. Lett. 31, 653 (1973).

18 Particle Data Group, *Review of Particle Properties*, Phys. Lett. 170B, (1986) 7.

19 V. A. Polychronakos *et al.*, Phys. Rev. D19, 1317 (1979).

20 W. Wetzel *et al.*, Nucl. Phys. B115,208 (1976).

21 D. Cohen *et al.*, Phys. Rev. D22, 2595 (1980).

22 G. Costa *et al.*, Nucl. Phys. B175, 402 (1980).

23 A. Etkin *et al.*, Phys. Rev. D25, 1786 (1982).

24 A. Etkin *et al.*, in preparation.

25 A. Etkin *et al.*, Phys. Rev. D25, No. 9, 2446 (1982).

26 A. C. Irving, A. D. Martin, and P. J. Done, Z. Phys. C 10, 45 (1981).

27 T. Armstrong *et al.*, CERN/EP83-60 (1983).

28 S. Eisman *et al*, Nucl. Instrum. Methods 217, 140(1983).

29 E. Barrelet, Nuovo Cimento 8A, 331(1972).

30 F. Binon *et al.*, Nuovo Cimento A78 313 (1983).

31 D. Alde *et al.*, Nucl. Phys. B269 485 (1986).

32 page 194, *Review of Particle Properties.*

33 F. Binon *et al.*, Nuovo Cimento A80 363 (1984).

34 G. S. Abrams *et al.*, Phy. Rev. Lett. 44, No. 3, 114 (1980).

35 K. F. Einsweiler, *Thesis*, SLAC-272, May 1984.

36 D. Robson, Nucl. Phys. B130, 328(1977).

37 C. J. Goebel and K. W. McVoy, Phys. Rev. 164, 1932 (1967).

38 A. Etkin *et al.*, Phys. Lett. 165B (1985) 217.

39 I. J. R. Aitchison, Nucl. Phys. A189, 417 (1972).

40 R. S. Longacre, Phys. Rev. D26, No. 1, 82 (1982).

41 M. Fukugita, Y. Oyanagi, and A. Ukawa, Phys. Rev. Lett. *57*, No. 8, 953 (1986).

42 S. Godfrey and N. Isgur, Phys. Rev. D32,189 (1985).

43 J. Weinstein and N. Isgur, Phys. Rev. Lett. 48, 659 (1982); Phys. Rev. D27, 588 (1983); R. L. Jaffe, Phys. Rev. D15, 267 (1977); D15,281 (1977).